A SPECTROSCOPIC INVESTIGATION
OF
FOUR O-TYPE SUBDWARFS

Thesis by

Arsine Victoria Peterson

In Partial Fulfillment of the Requirements
For the Degree of
Doctor of Philosophy

California Institute of Technology
Pasadena, California

1970

(Submitted September 24, 1969)

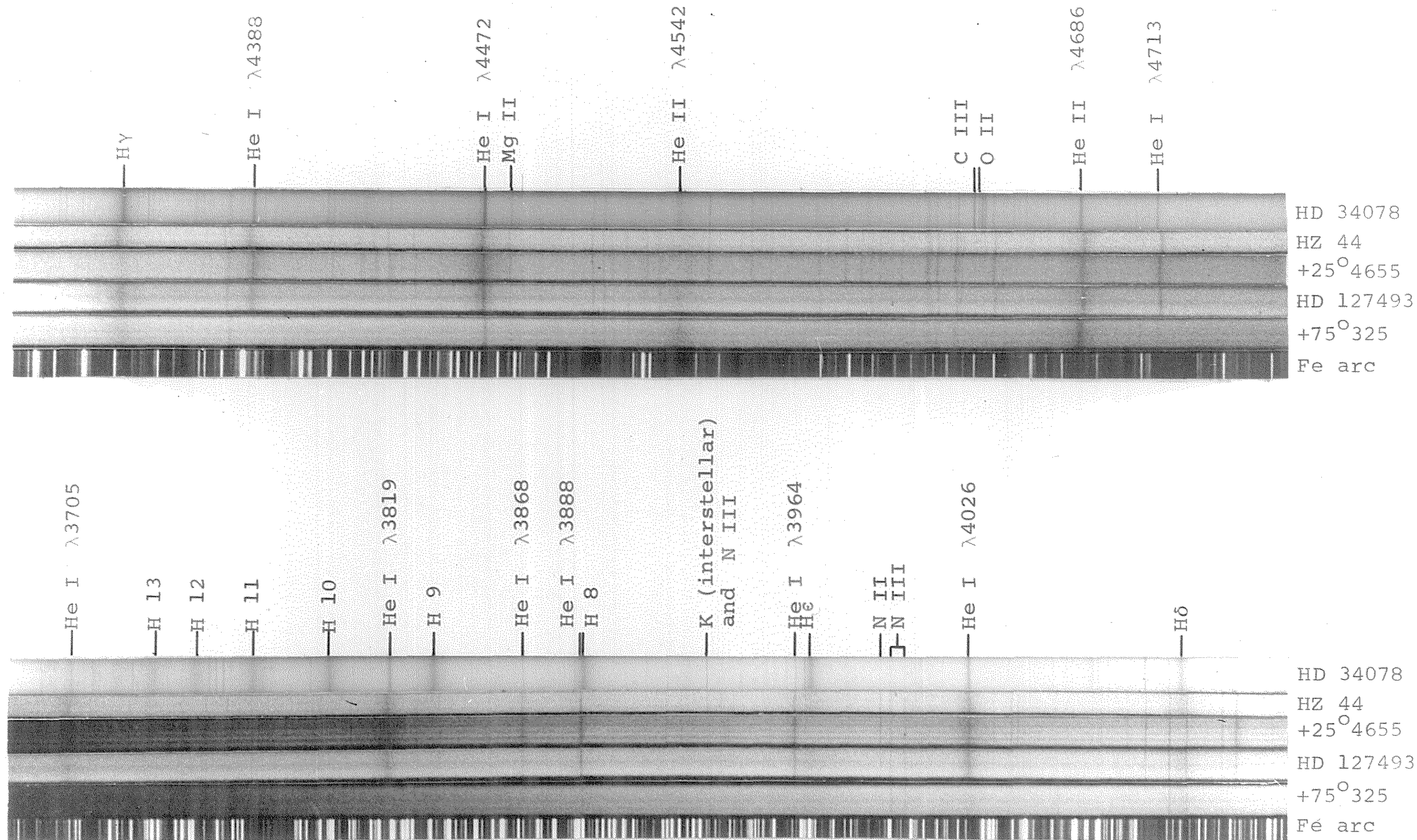

Plate I. Spectra of HD 34078 (O9.5 V) and four hot subdwarfs, HZ 44, +25°4655, HD 127493, and +75°325

ACKNOWLEDGEMENTS

It would be impossible for me to thank individually all the people who have directly and indirectly provided stimulation and guidance in this work. Discussions with many of the faculty, research fellows, and graduate students have been provocative and illuminating, and in some cases have materially affected the course of this investigation.

Particular thanks are due to Dr. G. Münch and Dr. J. L. Greenstein for suggesting the topic and making available the many fine spectra taken by them, as well as for guiding my work at various stages along the way. I am grateful to Dr. Münch for patiently reading and commenting on the manuscript as soon as it came to him - in pieces and out of order. I thank Dr. J. B. Oke for supplying unpublished photoelectric scans for some of the stars. Conversations with Dr. W. A. Fowler, Dr. W. D. Arnett, and others involved in nuclear astrophysics have been most helpful and have shed considerable light on the problem.

The analysis of the spectra included much computing; I am most grateful to the people who wrote the complex programs and made them available to me, thus freeing me from the very digressive task of computer programming. Dr. S. E. Strom provided the model atmosphere program, which he and others of the Harvard-Smithsonian group have developed-and are still developing. I thank Dr. D. M. Peterson for help in the use of this program and for keeping me up to date on the various changes and additions made by him and others.

The line analysis program was made available by Dr. M. Scholz, who not only supplied in suitable form most of the atomic data needed for its use, but also went out of his way to program a number of line profile theories in time for me to be able to use them in this investigation. It is not possible to thank him enough for all the help he has given me with one question after another relating to the problems of analyzing spectra.

To my husband, Dr. Bruce A. Peterson, I owe many thanks for many things. In particular, during the last year while he was waiting patiently(?) for me to finish, he helped me with many computing problems, both minor and major. Some of the multidinous drawings were done by him.

Finally, I wish to thank the Astronomy Dept. and the Institute for financial support in the forms of scholarships, assistantships, and fellowships.

ABSTRACT

The spectra of four O-type subdwarfs, of the class with strong nitrogen lines and very weak carbon and oxygen lines, have been studied in some detail. Model atmospheres have been constructed for the stars HZ 44, +25°4655, and HD 127493, and the computed profiles of selected hydrogen and helium lines have been compared with the observed profiles. The effective temperatures of the model atmospheres are $T_e \geq 40\ 000\ ^{\circ}K$ and the surface gravities are $g \geq 5 \times 10^5$ (cgs). A mass of approximately $0.5\ \mathcal{M}_{\odot}$ and an absolute visual magnitude of about +4 for the stars HZ 44 and HD 127493 is found to be consistent with the available data. The star +25°4655 is probably less luminous.

High helium abundances have been inferred for these stars - from $Y \approx 0.4$ for HZ 44 to $Y \approx 0.9$ for +25°4655. Chemical abundances have been derived for heavier elements in a fine analysis. The nitrogen to carbon, and nitrogen to oxygen ratios derived for these stars are two orders of magnitude greater than is observed in the sun and in other main sequence stars. The high helium abundance and the observed CNO ratios are consistent with abundances predicted for material which has undergone hydrogen-burning in the CNO cycle.

TABLE OF CONTENTS

I. INTRODUCTION

In this investigation four O-type subdwarfs have been studied in some detail. The spectra of three other stars classified as O subdwarfs have been examined qualitatively. Table I-1 gives a list of these stars with some of their properties. The magnitudes and colors are from Greenstein and Eggen (1966) except for those of +25°4655 which are by Peterson (1968). The radial velocities for HZ 44, +25°4655, HD 127493, and +75°325 are derived from wavelength measurements of selected lines made by Greenstein and Münch (1967). The proper motions for the Humason-Zwicky stars are from Luyten (1964), and those for the BD and HD stars are from the SAO Star Catalogue (1966) which compares positions from star catalogues of different epochs to derive proper motions. Except in the cases of HZ 44 and +25°4655 the quoted proper motions are not significantly larger than the errors.

The spectra of the O-type subdwarfs are characterized by broad lines of hydrogen and helium, and narrow, high excitation lines of other elements such as carbon, nitrogen, oxygen, neon, silicon, sulphur, aluminum, and iron. The broadening of the hydrogen and helium lines is intermediate to that found in main sequence stars and in the white dwarfs indicating an intermediate surface gravity. The

TABLE I-1 Some O-Type Subdwarfs

Star	$\alpha(1950)$	$\delta(1950)$	V	B-V	U-B	v_{rad}	μ_α	μ_δ
HZ 44	$13^h21^m.3$	+36°24'	11.68	-0.29	-1.19	-11.7 ±1.0	-0".062 ±.010	+0".031 ±.010
+25°4655	$21^h57^m.4$	+26°12'	9.67	-0.27	-1.20	-30.5 ±0.8	-0".019 ±.011	-0".040 ±.008
HD 127493	$14^h29^m.5$	-22°26'	9.5	-0.28		-16.0 ±1.5	-0".015 ±.018	-0".004 ±.018
+75°325	$8^h04^m.7$	+75°07'	8.9			(-44)*	-0".005 ±.006	-0".011 ±.010
HZ 1	$4^h47^m.3$	+17°37'	12.7				+0".004 ±.010	-0".018 ±.010
HZ 3	$3^h50^m.8$	+10°35'	12.86	-0.14	-1.10		+0".012 ±.007	+0".001 ±.007
GD 298	$9^h29^m.9$	+48°20'						

*derived from one plate

narrow lines of heavier elements imply very low rotational velocities. Plate I shows the spectra of HZ 44, +25°4655, and +75°325. The spectrum of the sharp-lined 09.5V star AE Aur* (=HD 34078) is shown for comparison.

The first descriptions of O-type subdwarfs were given by Greenstein and Münch (1955) and Münch (1956). The original members of this class were HZ 1, HZ 3, HZ 44, HD 127493, and +25°4655. The star +75°325 has been described by Gould et al (1957) and by Elvius and Sinnerstad (1958). Münch (1958) has discussed the formation of hydrogen and ionized helium lines in HZ 44, and on the basis of these lines and the NII/NIII equilibrium has derived atmospheric parameters for HZ 44 of T_e = 34000°K, log g = 5.7, and Y = 0.23 (helium fraction by number). These values of the temperature and gravity imply an absolute visual magnitude $M_V = +3.7$ for a mass of $1\mathcal{M}_\odot$.

Since then the spectra of a number of other hot subdwarfs have been described in the literature. Some of these are apparently quite similar to the original hot subdwarfs, while others show spectroscopic differences which may be of importance in their evolutionary implications. This investigation is primarily concerned with the subclass of O subdwarfs whose spectra show strong

*Courtesy of Dr. M. Scholz

lines of nitrogen and very weak or no lines of carbon and oxygen. The six O subdwarfs already mentioned fall into this subclass. The star GD 298 (last entry in Table I-1) does not. Since the heavy element lines are very narrow, fairly highly dispersion is needed in order to detect them. In some cases stars have been classified as O subdwarf from low dispersion plates where narrow lines were undetectable.

Of particular interest are stars for which distances can be determined. Wallerstein and Spinrad (1960) have observed the close visual binary ADS 8734 (=HD 113001) and have identified the composite spectrum as being due to a main sequence F star and a late O subdwarf. An absolute magnitude of $M_V \approx +3.6$ was derived for the O subdwarf. From the description given of the spectrum, it can be inferred that this star belongs to the same class of O subdwarfs as the four stars being analyzed in this paper.

The spectroscopic binary HD 128220 has been observed by Wallerstein et al. (1963) and Wallerstein and Wolff (1966). The two components, a G0 giant and an O9 subdwarf, are of approximately equal masses, $\mathcal{M}_G \approx \mathcal{M}_O \approx 3\mathcal{M}_\odot$, and equal magnitudes, $M_V \approx 0$. In this star the lines of OIII are the strongest among lines due to elements heavier than helium; thus the star is not included in the subclass under consideration.

Searle and Rodgers (1966) have described a very hot subdwarf occurring in the globular cluster NGC 6397. With a distance modulus for NGC 6397 of about 12.0 magnitudes, the subdwarf has an absolute visual magnitude of about +1.0. At the dispersion used only lines of hydrogen and helium could definitely be identified.

Among other hot subdwarfs which are likely to belong to the subclass described earlier, are GS 259-8 (Münch and Slettebak, 1959) and HD 49798 (Jaschek and Jaschek, 1963). It seems probable that the four Feige stars, F 34, F 67, F 80, and F 110, classified as subdwarf O from 48 A/mm plates by Sargent and Searle (1968), do not belong to this subclass, since at the dispersion used, the strong nitrogen lines would have been more easily detectable than the SiII lines reported.

The spectrum of HZ 44 shows very strong, broad hydrogen and neutral helium lines. The hydrogen lines can be seen only to about H 10 and the Balmer jump is imperceptible. The $2\,^1P - n\,^1D$ and $2\,^3P - n\,^3D$ transitions of He I are strongly affected by pressure broadening, while the $2\,^{1,3}S - n\,^{1,3}P$ and $2\,^{1,3}P - n\,^{1,3}S$ lines remain much narrower. The $n = 3$ to $n = 4$ transition of HeII at λ4686 is also much stronger and broader than in main sequence stars and it has a narrow core. In comparison the HeII lines of the Pickering series arising from the n = 4 level are very broad, shallow features. In HZ 44 the Pickering line at λ4542 is very difficult to measure because of its very extended wings and many superimposed lines of nitrogen, but it may have a total strength nearly that of λ4686 despite its much smaller central depth. The star has a very strong nitrogen spectrum with NII and NIII well represented. In contrast the carbon and oxygen lines, which are more prominent in main sequence stars, are weakened to the extent of being undetectable in HZ 44. There are strong lines of SiIII and SiIV and lines of NeII, AlIII, SIII, and FeIII. The MgII line at 4481 is moderately strong. The K line of CaII, which is almost certainly interstellar, is quite weak.

The star +25°4655 shows a level of excitation quite similar to that of HZ 44. The HeI lines are stronger; Hγ is very much weakened and Hδ is the last Balmer line visible. The HeII line at λ4686 is like that in HZ 44, but the Pickering line at λ4542 is even shallower than in HZ 44. As in HZ 44, there are numerous narrow lines. The same elements in the same ionization states occur in +25°4655 as in HZ 44.

The level of excitation in HD 127493 is higher than in HZ 44 and +25°4655. The NIII lines are stronger than the NII lines and the SiIV lines are stronger than the SiIII lines. The HeI lines are still strong, although not quite so strong as in the two preceding stars. The HeII line at λ4686 is about the same, but the Pickering lines are deeper and stronger than in HZ 44 or +25°4655, and constitute an important contribution to the Balmer series of hydrogen. The hydrogen lines (blended with HeII) can be seen to H 10 or H 11. HD 127493 has only a few lines due to heavy elements other than nitrogen and silicon. The MgII line at λ4481 persists in this star.

In +75°325 the level of ionization and excitation is considerably higher than in the other stars. The HeI lines are very much weaker. The ionized helium line at λ4686 is only a little stronger than in the other three stars, but the Pickering lines are considerably stronger and deeper, the profile of λ4542 being quite similar to that of λ4686 except at the very core where λ4686 is deeper. From the alternating strength of the Pickering lines and the shift in wavelength for the even numbered lines, it can be seen that the hydrogen lines still persist. The Pickering lines can be seen to about $n = 17$. The only prominent lines besides those of hydrogen and helium are the lines of doubly and triply ionized nitrogen. Among other weaker lines is λ4481 of MgII.

On plates of lower dispersion HZ 1 appears somewhat like +25°4655. The neutral helium lines are extremely strong and the hydrogen lines are even weaker than in +25°4655. Hγ is probably the last Balmer line visible. The spectrum of HZ 3, again on lower dispersion plates, looks approximately like that of HD 127493. The star GD 298 is apparently nearly as hot as +75°325 with very strong HeII lines and weakened HeI lines. Hydrogen does not appear to contribute significantly to the even-numbered Pickering lines. In this star the lines of CIII and CIV are considerably stronger than the nitrogen lines; thus it does not belong in the same subclass as the others.

In Part II the observational material and procedures of measurement are described. Part III contains a list of lines certainly present and their equivalent widths. In Part IV a very brief description of the model atmosphere program is given, and considerations entering into the choice of models are discussed. The model atmospheres finally chosen as best describing the stars HZ 44, +25°4655, and HD 127493 are presented in table and graph form. In Part V, following a short discussion of the line broadening theories used, is a comparison of the observed hydrogen and helium line profiles with the theoretical emergent profiles computed in the model atmospheres. Abundance determinations of heavier elements in a fine analysis are presented. In the concluding part is a discussion of the probable masses and luminosities of these O-type subdwarfs and their place in the evolutionary scheme.

II. OBSERVATIONAL MATERIAL

Coudé spectrograms of the four O-type subdwarfs being considered were obtained on the Mt. Wilson 100 inch telescope and the Mt. Palomar 200 inch telescope by Drs. Greenstein and Münch during the years 1953 to 1958. An additional four spectrograms of the star +25°4655 were obtained on the 100 inch telescope by the author in 1967. For two of the stars, HD 127493 and +25°4655, there are a few plates at 9 A/mm and 10 A/mm in addition to plates of lower dispersion. For the other two stars, HZ 44 and +75°325, there are plates of 18 A/mm dispersion. The wavelength region covered is in the ultraviolet and blue, that is the region of sensitivity of the IIa-O emulsion. For the star +25°4655 the coverage extends into the red with one J plate to 5300 A, two D plates to 6000 A, and one F plate to 6800 A. With only one plate covering the spectrum beyond 6000 A, it is rather difficult to ascertain the reality of some of the features in that region.

The spectrograms vary in quality, differing in density and in the width of the trailed star spectrum. In addition, of course, the resolution and signal-to-noise characteristics of the best 10 A/mm plates are superior to the best 20 A/mm plates. Only the best plates have been chosen for intensive analysis, since it was found that introducing additional plates of poorer quality into the averages increased the scatter of the data. Table II - 1 summarizes the material used.

Intensity tracings of the spectrograms were made on the C.I.T. microphotometer. For each star spectrogram is a corresponding calibration plate cut from the same emulsion and developed at the same time. The calibration plates were exposed in an auxiliary wedge spectrograph. The conversion from density (actually transmission) to intensity is accomplished in the microphotometer by setting the values of a series of variable resistors in such a way that a tracing of the wedge plate produces a straight line.

Each plate was traced at two magnifications -- X17 and X136 for the 20 A/mm plates, and X9 and X136 for the 10 A/mm plates. Unevenness in the background fog level of as much as 5% of the continuum intensity occurs on some plates and causes a proportional uncertainty in the measured equivalent widths and in the measured line depths (Depth = 1 - Residual Intensity).

In general the resolution at the plate is about 20μ or about 0.2 A at 10 A/mm, 0.4 A at 20 A/mm, and 0.6 A at 30 A/mm. The microphotometer slit for tracing the spectrograms was about 15μ at the plate; slits narrower than that produced no apparent improvement in resolution on the tracings. It can be seen that the profiles of the strong hydrogen and helium lines with full widths at half

TABLE II - 1

Observational Material

Star	Plate #	Emulsion	Wavelength Region (A)	Telescope	Camera	Grating/Order	Dispersion (A/mm)
HZ 44							
	Pd 6555	IIa-O bkd	3575-4750	200"	18"	/3	18
			4750-5050			/2	27
	Pd 1518	IIa-O bkd	3575-4750	200"	18"	/3	18
			4750-5025			/2	27
	Pd 2049	IIa-O bkd	3575-4875	200"	18"	/3	18
+25° 4655							
	Pc 3372	IIa-O bkd	3750-5000	200"	36"	/3	9
	Cec 9998	IIa-O bkd	3650-4850	100"	32"	46B/3	10
	Pd 3575	IIa-O	3750-4725	200"	18"	/3	18
			4725-5050			/2	27
	Pd 3755	IIa-J	4000-4850	200"	18"	/3	18
			4650-5300			/2	27
	Pd 2636	IIa-O bkd	3700-4850	200"	18"	/3	18
			4850-5050			/2	27
	Ced 18910	IIa-D bkd	4375-4725	100"	16"	41B/3	20
			4650-6000			/2	30
	Ced 18911	IIa-O bkd	3575-4700	100"	16"	46B/3	20
	Ced 18912	IIa-D bkd	4375-4725	100"	16"	41B/3	20
			4650-6000			/2	30
	Ced 18913	IIa-O bkd	3575-4700	100"	16"	46B/3	20
	Pd 2213	103a-F3	4800-6800	200"	18"	/2	27

TABLE II - 1 cont.

Star	Plate #	Emulsion	Wavelength Region (A)	Telescope	Camera	Grating/Order	Dispersion (A/mm)
HD 127493							
	Pc 2012	IIa-O bkd	3700-4800	200"	36"	/3	9
	Pd 1950	IIa-O bkd	3700-4800	200"	18"	/3	18
	Pd 1957	IIa-O bkd	3550-3800	200"	18"	/3	18
			4025-4725			/3	18
+75° 325							
	Pd 3177	IIa-O bkd	3750-4850	200"	18"	/3	18
	Pd 3175	IIa-O bkd	4000-4850	200"	18"	/3	18
	Pd 3578	IIa-O	3350-3750	200"	18"	/4	13
			3450-3850			/3	18

maximum of 3 A to 8 A are not degraded appreciably by limited resolution. The situation for the weak, narrow lines of other elements, however, is quite different. The widths expected from Doppler broadening alone are between 0.1 A and 0.2 A. The observed widths of the narrowest lines are 0.35 A on the 10 A/mm plates and about 0.6 A on the 20 A/mm plates. For these lines one can infer very little from the shape beyond placing an upper limit on projected rotational velocity of the star. Only a few of the strongest lines of nitrogen and silicon have observed widths greater than twice the resolution limit.

The position of the continuum was determined first on the small scale tracings and then transferred to the expanded scale tracings in order that the broad wings of the hydrogen and helium lines be more easily taken into account. Only in a few places are the weak lines seriously blended and in general the most difficult decisions came in consideration of the far wings of the strong lines. In regions of isolated narrow lines the continuum was chosen, in principle, so that the noise fluctuations averaged to zero. The difficulty of distinguishing between very weak lines and plate grain introduces some uncertainty. The error, if any, is probably in the direction of over-estimating the number of very weak lines. On the other hand, in spite of the poorer signal-to-noise characteristics of the lower dispersion plates, there seem to be no systematic differences between the equivalent widths of the weakest lines measured on the 10 A/mm plates and on the 20 A/mm plates. This indicates that the continuum level was properly chosen. In most regions of the spectrum the continuum level is unlikely to be wrong by more than 2%. In comparing observed profiles with computed profiles a vertical shift of 1% has been allowed and has been indicated where applied.

Using the small scale tracings as "finding charts", the most prominent lines were identified on the expanded tracings and then the other lines were filled in. The wavelength identifications were tied to the narrow lines of known wavelength and to each other in a self-consistent manner using the known magnification and dispersion which is constant to better than 3 parts in 1000 on the Palomar plates. The process should be capable of predicting the wavelengths of unidentified lines to a few tenths of an Angstrom. This prediction was born out in the case of four fairly prominent (about 50 mA) lines, unidentified in the Moore multiplet tables, which turned out to be NII lines with measured positions only 0.1 A different from the quoted wavelengths. The situation would not be quite so favorable for weaker lines whose measured positions would be more seriously affected by noise fluctuations.

Profiles of selected hydrogen and helium lines were found by measuring the relative intensity before smoothing at every 0.25 A in the line. Each point was averaged over several plates, which were coherent to approximately the spacing of the points. These points were then averaged to every 0.5 A. In addition, for the ionized helium lines, which were expected to be symmetric, the two wings were averaged together. In the case of the asymmetric lines of neutral helium and neutral hydrogen blended with ionized helium where the profiles have been plotted from $\Delta\lambda$ = -20 A to +20 A, weak lines superimposed on the profiles can be seen. The positions of identified lines have been indicated. This still leaves some fluctuations, part of which are due simply to small flaws and plate grain which have not averaged out. Some, however, such as those appearing on the short wavelength wing of HeI λ4472 in all four of the stars investigated, are almost certainly caused by weak unidentified lines. In the case of the HeII profiles an effort has been made to exclude superimposed lines from the average profile.

Equivalent widths measured from different plates were compared for systematic differences. Comparisons were made among the spectrograms for $+25^{\circ}$4655, since these include plates from Mt. Wilson and Mt. Palomar and plates at both 10 A/mm and 20 A/mm. The measured equivalent widths of isolated lines were compared for Pc 3372 and Cec 9998 to investigate possible systematic differences between Mt. Palomar and Mt. Wilson plates. Table II - 2 summarizes the results for each range of equivalent width and each range of wavelength investigated. It was concluded that there were no important systematic differences as a function of equivalent width or as a function of wavelength. Next the average of two 20 A/mm plates was compared with the average of the two 10 A/mm plates mentioned above. Here there is some evidence of systematic differences as a function of measured equivalent width and for wavelengths less than 4100 A. Table II - 3 summarizes these results. No systematic corrections were applied to the data, although the higher dispersion plates were weighted more heavily whenever they were available.

Noise fluctuations due to plate grain differ from plate to plate and at different wavelengths depending on the width of the spectrum and on the density. The accuracy to which a weak line can be measured depends on the size of these fluctuations. Lines weaker than about twice the noise level become very difficult to identify and measure. The appropriate cutoff in equivalent width corresponding to this criterion occurred approximately at 20 mA for 10 A/mm plates, 30 mA for 20 A/mm, and 40 mA for 30 A/mm. Differences in quality from plate to plate were approximately taken into account by weighting the averages.

TABLE II - 2

Differences in Measured Equivalent Widths between Wilson (Cec) and Palomar (Pc) Plates

W(mA)	20-40	40-60	60-80	80-100	100-120	120-200
No. of lines	56	24	19	9	9	6
$\langle W(Cec)-W(Pc)\rangle$	+3	-2	-1	0	-1	+12
$\langle [W(Cec)-W(Pc)]^2\rangle^{\frac{1}{2}}$	10	10	20	10	18	20

λ(A)	3900-4100	4100-4300	4300-4500	4500-4700
No. of lines	23	31	20	28
$\langle (Cec)-W(Pc)\rangle$	0	+3	-1	0
$\langle [(Cec)-W(Pc)]^2\rangle^{\frac{1}{2}}$	12	13	18	13

TABLE II - 3

Differences in Measured Equivalent Widths between 20 A/mm and 10 A/mm Plates

W(mA)	20-40	40-60	60-80	80-100	100-120	120-200
No. of lines	29	23	18	9	8	6
$\langle W(20)-W(10)\rangle$	0	+2	+4	+6	+8	+23
$\langle [W(20)-W(10)]^2\rangle^{\frac{1}{2}}$	13	10	17	16	21	27

λ(A)	3900-4100	4100-4300	4300-4500	4500-4700
No. of lines	20	20	18	22
$\langle W(20)-W(10)\rangle$	+11	-3	+2	+3
$\langle [W(20)-W(10)]^2\rangle^{\frac{1}{2}}$	17	11	11	14

III. LINE IDENTIFICATIONS AND EQUIVALENT WIDTHS

Line identifications and equivalent width measurements have been made from microphotometer tracings as described in Part II. The Moore Multiplet Table has been used extensively for identifying lines. Since the Multiplet Table is a reprinting of the 1945 edition, it does not include spectrum analyses made since that year. Where they are available, more recent analyses have also been consulted. In Table III-1 are listed in abbreviated form the sources used in identifying lines. The complete references can be found at the end of the paper.

A composite line list comprised of lines in the wavelength region 3700 - 4900 A certainly present in any of the four stars is given in Table III-2. The list should be reasonably complete for lines stronger than about 40 mA (30 mA for +25°4655) in the region from 3850 - 4750 A. The equivalent widths of these lines are estimated to be accurate to about 20% unless followed by a colon (:), indicating less accuracy due generally to blending with other lines or, in some cases, greater than normal dispersion among measurements from different plates.

Equivalent widths have been given down to about 30 mA in HZ 44, HD 127493, and +75°325, and to about 20 mA in +25°4655. Equivalent widths less than 40 mA should be

TABLE III - 1 Sources for Line Identifications

General	Moore (1959)
CII	Glad (1954)
CIII	Bockasten (1955)
CIV	Bockasten (1956)
NII	Eriksson (1958)
NIV	Hallin (1966a)
NV	Hallin (1966b)
NeII	Persson and Minnhagen (1968)
MgII	Risberg (1955)
AlIII	Isberg (1968)
SiIII	Toresson (1960-61) Moore (1965) Same analysis
SiIV	Toresson (1960) Moore (1965) Same analysis
AII	Minnhagen (1963-64)
CaIII	Borgström (1968)
FeIII	Glad (1956)

considered less accurate than for the stronger lines. Again, a colon following the equivalent width denotes even less certainty. In some cases where the equivalent width is not given, the presence of a weak or very shallow line is indicated by a subjective classification of A or B based on the appearance of the line on several plates, with A implying almost certainly present and B probably present.

Column 1 gives the element identification, state of ionization, and the multiplet number if the line is listed in Moore. Column 2 gives the laboratory wavelength as given in Moore or in the more recent analyses listed in Table III-1. In columns 3, 4, 5, and 6 are the measured equivalent widths in mA of the line in HZ 44, +25°4655, HD 127493, and +75°325 respectively if the line is identified in the star. A number in column 7 indicates a comment following the table. Important unresolved blends are indicated by brackets in the equivalent width columns; less important contributions are mentioned in the comments. Lines which are partially blended usually have separately listed equivalent widths followed by colons to indicate the uncertainty in the values.

Tables III-3 and III-4 list lines occurring in the wavelength regions 4900 - 5050 A and 3700 - 3350 A respectively. The arrangement of the tables is the same as for Table III-2. The ultraviolet list in particular is not complete due to low plate densities. The equivalent widths are given primarily as an intensity indication and in general decrease in accuracy with decreasing wavelength.

The most prominent unidentified lines are listed in Table III-5 with their equivalent widths. A broad unidentified feature which appears on the blue wing of HeI λ4472 in all four of the stars studied has been listed as three separate lines in the table, however the individual wavelengths and equivalent widths are probably not very accurate due to blending and the presence of the helium line. It may be noted that besides the hydrogen and helium lines, all the lines identified in +75° 325 are due to NIII, NIV, and SiIV, plus the MgII line at λ4481. All four stars have in common NIII and SiIV and the MgII line. The unidentified lines common to the four stars may be very high excitation lines of NIII, while the lines peculiar to +75° 325 may be very high excitation lines of NIV.

TABLE III - 2 Identifications and Equivalent Widths

of Lines in the Wavelength Region 3700 - 4900 A

Ion	λ_o	HZ 44	+25°4655	HD 127493	+75°325	Notes
HeI(25) HeI(25)	3705.003 3705.140	[1870	[3170	[1020		
SIII(1) NeII(1)	3709.371 3709.621	[49	[32:	A		
NeII(1) AlIII(4)	3713.077 3713.123	[81	[83	[45		
SIII(6)	3717.775	39	40:			
NeII(5)	3727.102	83	100	25		1
HeI(24) HeI(24)	3732.861 3732.992	[110	[240:	[68:		
NeII(1)	3734.935	95:	50:			
NIII(4)	3745.83	53	49	42	50::	
NIV(8)	3747.54				90:	
OII(3)	3749.49		37			
NeII(1)	3751.246		37			
NIII(4)	3754.62	52	56	54	70::	

TABLE III - 2 Cont.

Ion	λ_o	HZ 44	+25° 4655	HD 127493	+75° 325	Notes
OIII(2)	3759.87	25	37			
SiIV(3)	3762.435	75	83	58		
NeII(1)	3766.260	38	60	B		
H 11	3770.632	B				2
NIII(4)	3771.08	68	56	56	45:	
SiIV(3)	3773.151	40	55	32		
NeII(1)	3777.16	28	44			
SiIII(5)	3791.41	30	56			
NIII(11)	3792.87	47				
SiIII(5)	3796.114	65:	80			
H 10	3797.900	A		A		2
HeII	3799.965		36:			
SiIII(5)	3806.544	54	108			
HeI(22) HeI(22)	3819.606 3819.761	[2270	[2980	[1520	[97	

TABLE III - 2 Cont.

Ion	λ_o	HZ 44	+25° 4655	HD 127493	+75° 325	Notes
NeII(39) NII(30)	3829.753 3829.793	[50	[49	[35:		
H 9	3835.386	A		A		3
NII(30)	3838.374	54	62	B		4
NII(30)	3842.183	28:	40			
NII(30)	3847.409		35:			
NII(30)	3855.100		28:			
NII(30)	3856.057	29:	34:			
HeI(20) HeI(20)	3867.477 3867.631	[265	[500	[180		
HeII(4) H 8	3887.44 3889.051	[1800		[770:	[A	
HeI(2)	3888.646	260	785	285	88:	
NII(17)	3918.999	47	59	25		
HeII(4)	3923.48				A	
SiIII(8.14)	3924.468	53	62			

TABLE III - 2 Cont.

Ion	λ_o	HZ 44	+25° 4655	HD 127493	+75° 325	Notes
HeI(58)	3926.530	A	A	A		5
SIII(8)	3928.615	36	28			
CaII(1)	3933.664	87:	38:	29:		6
NIII(8)	3934.41	47:	56:	42:	30:	7
NIII(8)	3938.52	67	66	57	24:	
NII	3939.57	47	63	31:		
NII	3940.66	[46	48	[31:		
NII	3941.23		49			
NIII(8)	3942.78	62:	23	30		
FeIII(120)	3954.326	40	30:	A		
NII(6)	3955.851	28	53			
HeI(5)	3964.727	285	774	260:		
HeII(3)	3968.43	[2850		[1530	[940:	
H_ϵ	3970.074					

TABLE III - 2 Cont.

Ion	λ_o	HZ 44	+25°4655	HD 127493	+75°325	Notes
CaII(1) FeIII(120)	3968.47 3968.718	[50:	[45	[B		8
OII(6)	3973.263		30			
SIII(8)	3983.77	27:	21:			
NII(12)	3994.998	124	111	55		
NIII(16)	3998.69	108	82	70	75	
NIII(16)	4003.64	102	79	80	81	
HeI(55)	4009.27	A	A	A		
HeII(3) HeI(18) HeI(18)	4025.60 4026.189 4026.362	[3330	[3910	[2400	[960	
NII(39)	4035.080	60	63	31		
NII(39)	4041.311	98	99	36		
NII(39)	4043.529	65	87	B		
NII(39)	4044.777	53	31:	B		
NII(39)	4056.90	45:	35			

TABLE III - 2 Cont.

Ion	λ_o	HZ 44	+25°4655	HD 127493	+75°325	Notes
NIV(3)	4057.759				110	
OII(10) OII(10)	4069.636 4069.897	[39:	[38			
OII(10)	4072.164		32			
NII(38)	4073.042	39:	49	A		
OII(10)	4075.868		30			
NII(38)	4082.270	49:	63	28		
NII(37)	4087.303		32			
SiIV(1)	4088.854	150	188	97	28	
NIII(1)	4097.31	140:	180:	155:	102:	9
HeII(3) Hδ	4100.04 4101.737	[3560	[530:	[2320	[2000:	
NIII(1)	4103.37	118:	155:	101:	55:	9
SiIV(1)	4116.097	138	129	92	29	
HeI(16) HeI(16)	4120.812 4120.993	[413	[650	[267		

TABLE III - 2 Cont.

Ion	λ_o	HZ 44	+25° 4655	HD 127493	+75° 325	Notes
NII(65)	4124.078	42:	B			
NII	4131.782	24	32			
NII(65)	4133.669	29	34			
HeI(53)	4143.759	1590	1790	800		
NII(65)	4145.776	31:	25:			10
AlIII(5) AlIII(5)	4149.915 4150.173		[27			
NII	4154.77		22			
NII(51) NII(50)	4156.39 4157.01	[B	[44			
NII(51) NII(50)	4160.50 4161.14	[B	[21:			
FeIII(118)	4164.731	82	37			
HeI(52)	4168.971	34:	50:			11
NII(43)	4171.607	44	66			
NII(50)	4173.572		32			

TABLE III - 2 Cont.

Ion	λ_o	HZ 44	+25°4655	HD 127493	+75°325	Notes
NII(42)	4176.161	59	84	B		
NII(50)	4179.674	50:	59			
NII(49)	4181.10		34			
NIII(6)	4195.70	81	102	48	39:	12
HeII(3)	4199.83	A		A	2220:	
NIII(6)	4200.02	101	109	49	34::	13
NII HeII(53) NII	4206.11 4206.498 4206.51	[45:	[75			
NII	4207.50	55:	63			
SiIV(5)	4212.407	79	84	33	41	
NIII(6)	4215.69	35	37	B	B	
NeII(52)	4217.178		25			
NeII(52)	4219.747	32:	51			
NII(33)	4227.743	70	67	B		

TABLE III - 2 Cont.

Ion	λ_o	HZ 44	+25° 4655	HD 127493	+75° 325	Notes
NeII(52)	4231.546	B	35			
NeII(52)	4231.637					
NII(48)	4236.91	96	120	A		
NII(48)	4237.05					
NII(47,48)	4241.784	122	125	37:		
SIII(4)	4253.59	31	54			
NIII	4284.51	39:	60	25		
SIII(4)	4284.991					
NIII	4288.72	48:	40	29:		
NeII(57)	4290.376	120:	90:	79:	40:	
NIII	4290.55					
NeII(57)	4290.601					
NIII	4290.80					
FeIII(121)	4296.854	32	B			
SiIV(4)	4314.104	A	24			
SiIV(4)	4328.175	A	41			
SIII(4)	4332.71	B	A	40:		
HeII(3)	4338.67	4180	1570	2900	3000:	
Hγ	4340.468					

TABLE III - 2 Cont.

Ion	λ_o	HZ 44	+25° 4655	HD 127493	+75° 325	Notes
OII(2)	4345.562		24	34:		14
OII(2)	4349.426		26			
FeIII(122)	4372.31					
FeIII(122)	4372.53	[40	[35			
FeIII(122)	4372.81					
NIII(17)	4379.09	[135	[131	[117	91	
NeII(56)	4379.549					
HeI(51)	4387.928	1400	2650	1050		
NeII(57)	4391.990		28	B		15
NeII(56)	4397.990		28	B		
NeII(57)	4409.302	28	44			
NeII(55)	4412.596					
NeII(57)	4413.116	[40	[43			
NeII(57)	4413.215					
OII(5)	4414.909		33			
OII(5)	4416.975	[29	[49			
NII	4417.07					

TABLE III - 2 Cont.

Ion	λ_o	HZ 44	+25° 4655	HD 127493	+75°325	Notes
NII(56)	4427.236	[	55:			
NII(55)	4427.964	85:	44:			
NeII(57) NeII(57)	4428.515 4428.632	]	[48:			
NeII(56)	4430.925		39			
NII(55)	4431.816	24:	29			
NII(55)	4432.735	[91:	74			
NII(55)	4433.475	]	37			
HeI(50)	4437.549	126	208	59		16
NII(55)	4442.018	31:	60			
NII(15)	4447.033	85	74	33		
HeI(15) HeI(14) HeI(14)	4469.92 4471.477 4471.688	[3200	[4370	[2490	[338	17
AlIII(8) AlIII(8)	4479.892 4479.968	[A	[35			18
MgII(4) MgII(4)	4481.129 4481.327	[103	[95	[47	[38	

TABLE III - 2 Cont.

Ion	λ_o	HZ 44	+25° 4655	HD 127493	+75° 325	Notes
NII(21)	4507.557		31			
NIII(3)	4510.92	107	95	94	45:	
AlIII(3)	4512.564	25:	27	B		
NIII(3)	4514.89	92	92	97	44	
NIII(3)	4518.18	70	72	53	38	
NIII(3)	4523.60	86	53	50	35	
NIII(13)	4527.86	40:	33	B		
AlIII(3) AlIII(3)	4528.942 4529.194	[35:	[56	[B		
NII(59) NIII(3)	4530.410 4530.84	[73	[99			
NIII(3) NIII(13)	4534.57 4535.11	[64:	[70	[59		19
HeII(2)	4541.59	A	A	2630	2160	
NIII(12)	4544.80	47:	27:			
NIII(13)	4546.36	B	28:	B		
NII(58) SiIII(2)	4552.527 4552.616	[53	[100			

TABLE III - 2 Cont.

Ion	λ_o	HZ 44	+25° 4655	HD 127493	+75° 325	Notes
SiIII(2)	4567.823	59:	87			
SiIII(2)	4574.759	32:	46			
OII(15)	4590.971		27			
NII(5)	4601.480	80	78			
NII	4602.53		24			
NIV	4606.33				66	
NII(5)	4607.157	40	74			
NII(5)	4613.866	47	63			
NII(5)	4621.394	61	83	A		
NII(5)	4630.543	100:	128:	74:		
SiIV(6)	4631.241	117:	98:	72:	48	
NIII(2)	4634.16	129	127	94	67	
OII(1)	4638.854		25:			
NIII(2)	4640.64	157	147	122:	85	
NIII(2)	4641.90	86	80	83	48	

TABLE III - 2 Cont.

Ion	λ_o	HZ 44	+25°4655	HD 127493	+75°325	Notes
NII(5)	4643.085	91	73			
CIII(1)	4647.42	38	48			
OII(1)	4649.139	23	42		28:	
CIII(1)	4650.25	58:	37			
SiIV(7)	4654.323	172	181	121	42	
NII(11)	4667.206		29	B		
NII(62)	4678.14	48:	51	B		
HeII(1)	4685.682	1720	1950	2700	2530	
NII(62)	4694.637	B	48:			
OII(25)	4705.355		26			
NIV	4707.31				60	
HeI(12) HeI(12)	4713.143 4713.373	366	660	353	65	
SiIV(8.09)	4716.651		39:			
NII(20)	4779.241	42:	54			

TABLE III - 2 Cont.

Ion	λ_o	HZ 44	+25° 4655	HD 127493	+75° 325	Notes
NII(20)	4781.190	B	25:			
NII(20)	4788.131		48			
NII(20)	4793.650		31			
NII(20)	4803.289	67:	57:	48:		
NII(20)	4810.306	B	35	B		
SiIII(9)	4813.330	31:	46			
SiIII(9)	4819.718	68:	69			
SiIII(9)	4828.968	66	60	B		
HeII(2) Hβ	4859.323 4861.332	[4300:	[1890	[4260	[2700	
NIII(9)	4867.18		46	40		
NIII(9)	4873.58		B	30:		
NIII(9)	4884.14		39	B		

Notes for Table III - 2

1 blend OII

2 very shallow

3 shallow; blend HeI; blend HeII in HD 127493

4 blend SIII

5 blend HeII in HD 127493

6 interstellar K; blend NIII

7 blend interstellar K

8 interstellar H

9 blend Hδ

10 blend HeI

11 blend NII, OII

12 blend NII

13 blend HeII in +75° 325

14 blend Hγ

15 blend HeI

16 asymmetric

17 forbidden component

18 blend HeI

19 blend HeII

TABLE III - 3 Identifications and Equivalent Widths of lines in the wavelength region 4900-5050 A

Ion	λ_o	HZ 44	+25°4655	HD 127493	Notes
AlIII	4904.10		49	54:	
HeI(49) HeI(48)	4920.35 4921.929	[1900:	[2350:	[1720:	1
NII(24)	4987.367		46:		
NII(64)	4994.363	90:	93	60:	
NII(19) NII(19)	5001.136 5001.477	[117:	[173:	[78:	
NII(19, 64)	5005.149	105:	113	127:	
NII(24)	5007.325		72:		
NII(4) NII(64) NII(64)	5010.620 5011.30 5012.029	[120:	[186:	[104:	
HeI(4)	5015.675	485	873	288:	2
NII(64)	5023.048		67:		
NII(19)	5025.662		46:	A	
NII(19)	5040.72	A	A		
NII(4)	5045.100	A	A		
HeI(47)	5047.736	163:	420		

Notes for Table III - 3

1 forbidden component

2 blend NII

TABLE III-4

Identifications and Equivalent Widths
of Lines in the
Wavelength Region 3700-3350A

Ion	λ_o	HZ 44	+25°4655	HD 127493
NeII(1)	3694.22	54	98	44
NeII(1)	3664.09	40	55	40
NeII(5)	3643.929		B	
HeI(28)	3634.373	[A	[A	[A
HeI(28)	3634.235			
SIII(1)	3632.022		B	
HeI(6)	3613.641			200
AlIII(1)	3612.352	[254	[320	
NeII(26)	3612.326			
NII(26)	3609.097		B	
NII(26)	3593.597		B	
HeI(31)	3587.396	[A	[A	[A
HeI(31)	3587.252			

Ion	λ_o	+75°325
NIV(1)	3484.96	74
NIV(1)	3482.99	200
NIV(1)	3478.71	190
NIV(7)	3463.37	A
NIV(7)	3461.36	A
NIII(5)	3374.06	B
NIII(5)	3367.36	B
NIII(5)	3361.90	B
NIII(5)	3358.72	B
NIII(5)	3353.78	B

TABLE III - 5 Unidentified Lines

λ	HZ 44	+25° 4655	HD 127493	+75° 325	Notes
3936.9	43	35			
4077.0				37	1
4080.7				31	2
4185.6		27			
4302.7	40				
4381.5	47				
4455.1	31:				3
4456.1	44:	27	30:	43:	3
4457.7	34:		34	31	3
4474.5				50	4
4504.2	46:	33			
4592.1	50	64	61	B	5
4610.4	66	51	38	52	5

Notes for Table III - 5

1 NIV?

2 NIV?; OIII 4081.10?

3 blended; NIII?; NeII?

4 NIV?; OIII 4474.95?

5 NIII?

IV. MODEL ATMOSPHERE CALCULATIONS

A series of model atmospheres has been computed on an IBM 7094 computer using a program, the fundamental design of which has been described by Strom and Avrett (1964, 1965). The program (ATLAS) used here includes refinements in the basic data and computational techniques developed by R. Kurucz of the Harvard-Smithsonian group. The basic assumptions are that the stellar atmosphere can be described by a plane-parallel, semi-infinite model in radiative and hydrostatic equilibrium. Local thermodynamic equilibrium is assumed throughout in the models constructed for this investigation. The opacity sources include bound-free and free-free absorption by neutral hydrogen, neutral helium, and ionized helium, and electron scattering. Radiation pressure is taken into account, in the sense that it is considered as a perturbation on the gas pressure. The Avrett-Krook temperature correction is used in an iterative scheme to attain a constant flux model.

The optical depth scale is defined at a standard wavelength chosen to correspond with the frequencies at which the atmosphere is most transparent. At the temperatures prevailing in these model atmospheres, most of the flux emerges in the far ultraviolet; the standard wavelength has been chosen at 912^{+}A in order that the models converge in a reasonable number of iterations. In fact, convergence of the high helium models is not entirely satisfactory. The HeI absorption, which constitutes an important source of opacity in these models, goes through a fairly sharp maximum as a function of depth as the neutral helium fraction first increases with increasing pressure and then decreases with the increasing temperature. In Figure IV-1 the absorption coefficient per gram at 912^{+}A is plotted as a function of optical depth for the model (43 000, 6.7, 0.9)*. The situation at very short wavelengths, in particular shortward of the HeI discontinuity at 504^{-}A is worse. Here, since neutral helium is the dominant source of opacity at nearly all depths, the total absorption coefficient goes through a maximum. Figure IV-2 shows the absorption coefficient at 504 A. Large increases in temperature are accompanied by only small increases in the monochromatic depth, causing a discontinuity in J_ν at the depth where κ_ν goes through a maximum. This in turn causes a large flux derivative which is given by

$$\frac{dH(\tau)}{d\tau} = \int_0^\infty d\nu \ \kappa_\nu(\tau) \ [J_\nu(\tau) - S_\nu(\tau)] \quad .$$

*(T_e [°K], log g [cgs], Y [helium fraction by number])

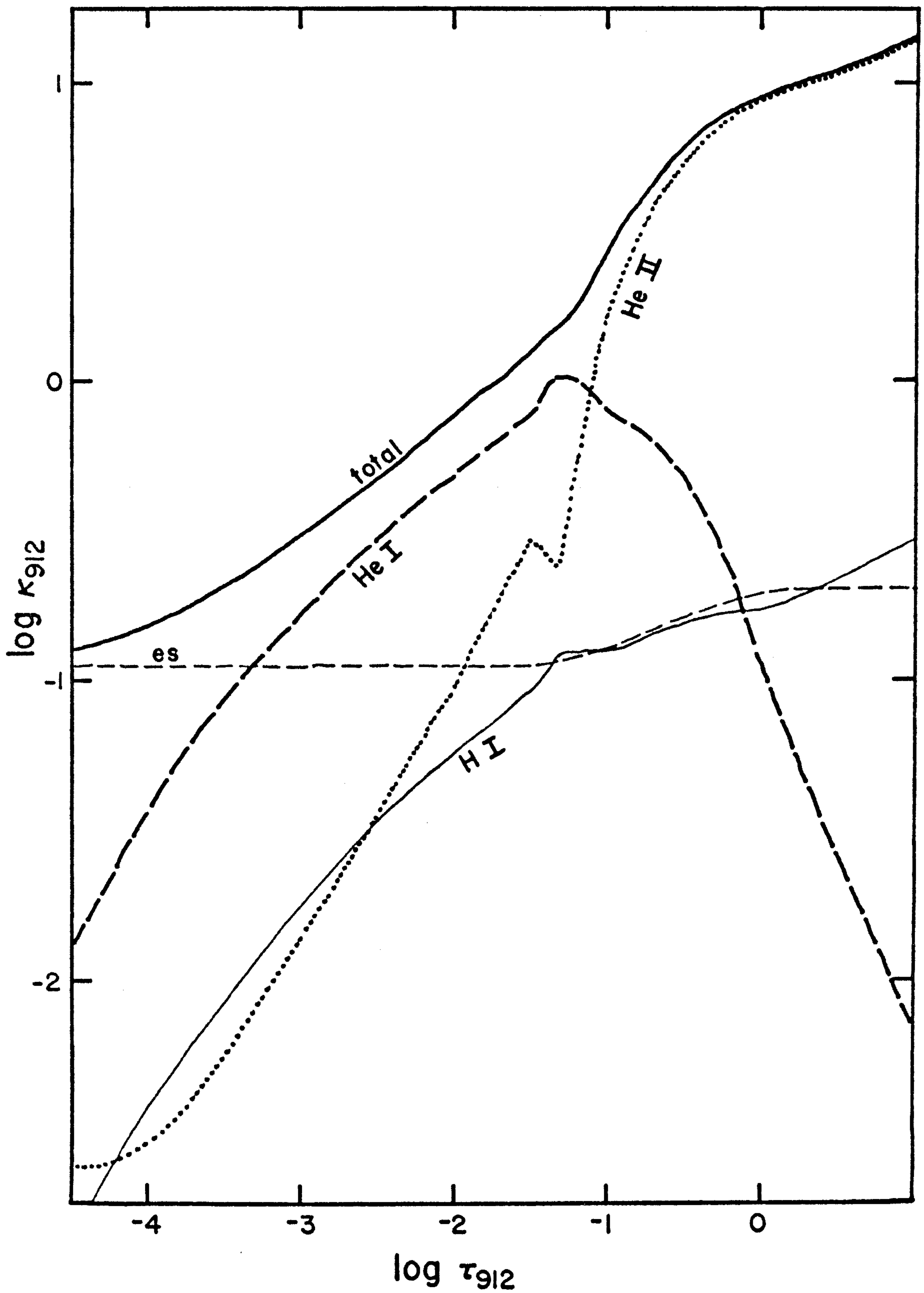

FIG. IV-1 The absorption coefficient per gram at 912+ A for model (43 000, 6.7, 0.9)

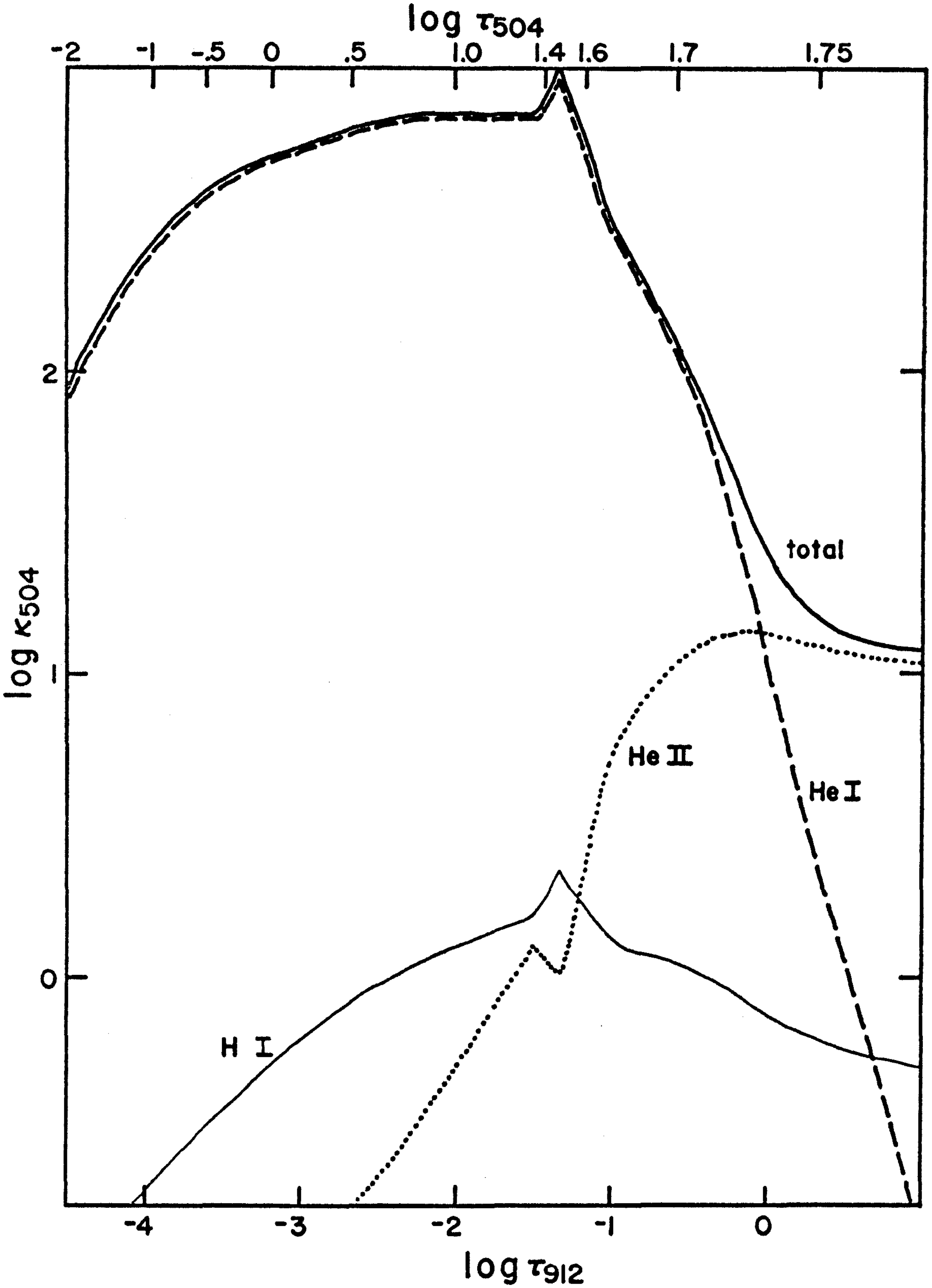

FIG. IV-2 The absorption coefficient per gram at 504 A for model (43 000, 6.7, 0.9)

Since the difference between J_ν and S_ν is weighted by κ_ν the wavelengths shortward of 504 A are quite important in the flux derivative.

The problem is largely an artificial one, since other sources of opacity begin to be important at the temperatures and wavelengths under consideration. The importance of bound-free absorptions by carbon, nitrogen, oxygen, and neon from the ground and low excited levels of the first four ionization states has been investigated by D. M. Peterson (1969). A program to compute these opacities has kindly been supplied by him. The inclusion of C, N, O, and Ne opacities into the model atmosphere program appears to eliminate the discontinuity in the temperature distribution. The model (43 000, 6.7, 0.9), for which the added opacity was expected to be most important, has been calculated with and without the opacity from C, N, O, and Ne. The effect of the increased ultraviolet opacity is twofold. At the very deepest layers of the atmosphere, the temperatures are lower than in the model without the metal opacities; this has little effect on lines in the visible part of the spectrum, since at those wavelengths the optical depth is very large for the layers in question. Continued iterations on the model reduce the flux derivative at all levels and in the process the surface temperature of the model drops.

The model atmospheres have as parameters the effective temperature, the surface gravity, and the chemical composition, in particular the helium abundance. The final choice of models was made by considering several criteria. The primary consideration was comparison of the computed profiles for Hγ + HeII, HeI λ4472, and HeII λ4686 with the observed profiles. The profile of the HeII Pickering line at λ4542 was also considered. (A discussion of the broadening theories used is included in the following chapter.) The helium abundance computed from the narrow neutral helium lines was compared with the helium abundance assumed for the atmosphere. As a check on the temperature and gravity the abundances derived for an element from lines in different stages of ionization were expected to agree.

The determination of atmospheric parameters for these stars is rather difficult since in general it is not possible to consider the effects of temperature, gravity, and helium abundance separately. The ionization equilibria of nitrogen and silicon are essentially independent of the helium abundance, although a large change in the helium abundance may change the structure of the atmosphere and thus the depth at which the lines are formed. The hydrogen lines are most sensitive to the effective gravity, but they also depend on the temperature in a complicated way which includes the decreasing strength of the hydrogen lines and the increasing strength of the HeII blend. While for low helium models the hydrogen lines are not very sensitive to the helium abundance, this is no longer necessarily the case for the models considered here. In fact, in the case of +25°4655 where the Balmer lines are very weak compared to the helium lines, the helium abundance, or more properly the hydrogen abundance, was determined principally by the Hγ profile; the strong neutral helium line at λ4472 was quite insensitive to the helium abundance assumed in the model.

In general, however, the profile of λ4472 is sensitive to all three of the atmospheric parameters varied. Since helium is almost entirely singly ionized at all levels of interest for line formation, the number of neutral atoms depends strongly on the temperature and pressure. (However, in an atmosphere where neutral helium is the dominant source of opacity, as for +25°4655, increases in the line absorption will be accompanied by increases in the continuous absorption, and the relative line strength becomes nearly independent of the abundance.)

In contrast the ionized helium line at λ4686 was found to be much less sensitive to any of the parameters for a broad range of values. The strength of λ4686 goes through a broad maximum for models with effective temperatures between 42 000 and 45 000 °K. Below 40 000 °K the line becomes narrower and decreases in strength quite rapidly. Figure IV-3 shows this behavior. The sensitivity of λ4686 to temperature for atmospheres of effective temperature less than 40 000 °K can be understood in terms of the high excitation potential of the n = 3 level (48.16 ev) from which λ4686 arises and the decreasing excitation of the model atmospheres.

In the Introduction it was noted that one of the characteristics of the class of hot subdwarfs being considered is the presence of λ4686 at nearly constant strength in stars with a wide range of excitation conditions implied by the rest of the spectrum. Thus it is possible to put a lower limit of 40 000 °K to the effective temperatures of models describing this class of subdwarfs.

Sargent and Searle (1968) suggest that the Pickering lines of ionized helium may be a good gravity indicator among O-type stars. As can be seen in Figure IV-4, the Pickering lines, arising from the n = 4 level, present a very different appearance from λ4686 for these high gravity model atmospheres. Figures IV-5 and IV-6 compare the emergent profiles from two model atmospheres with different surface gravity for λ4686 and λ4542. Unfortunately the lack of an adequate line broadening theory

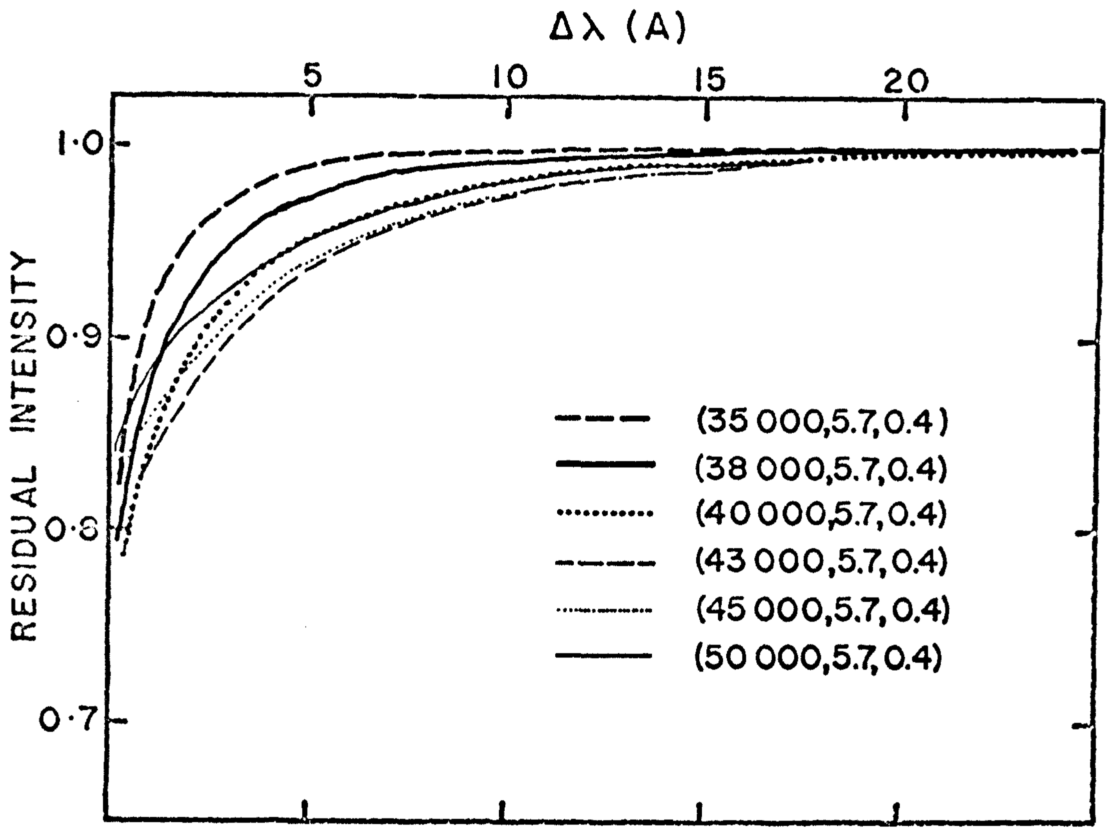

FIG. IV-3 The temperature dependence of HeII λ4686

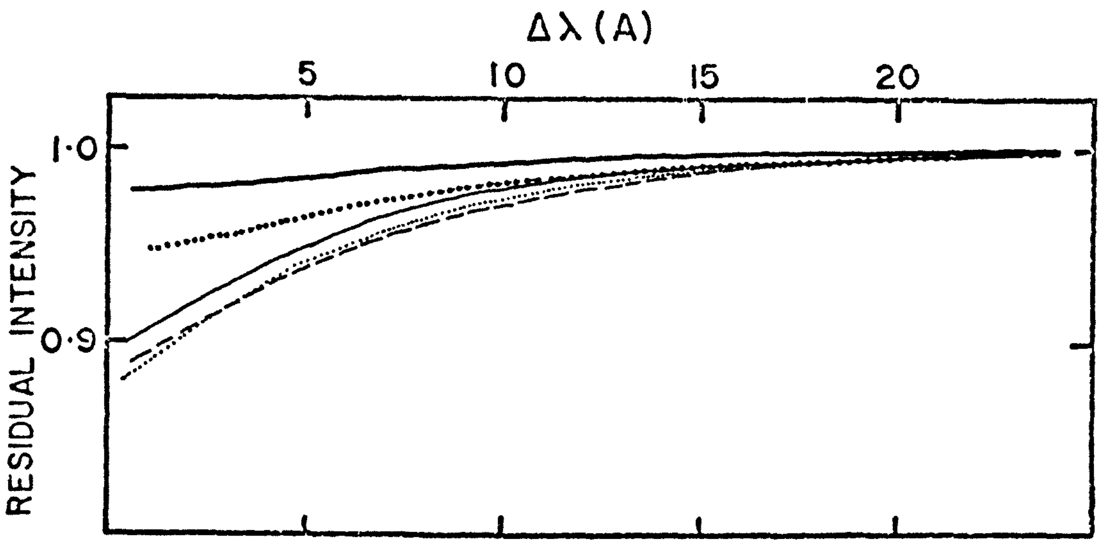

FIG. IV-4 The temperature dependence of HeII λ4542 using quasi-static broadening for ions and electrons

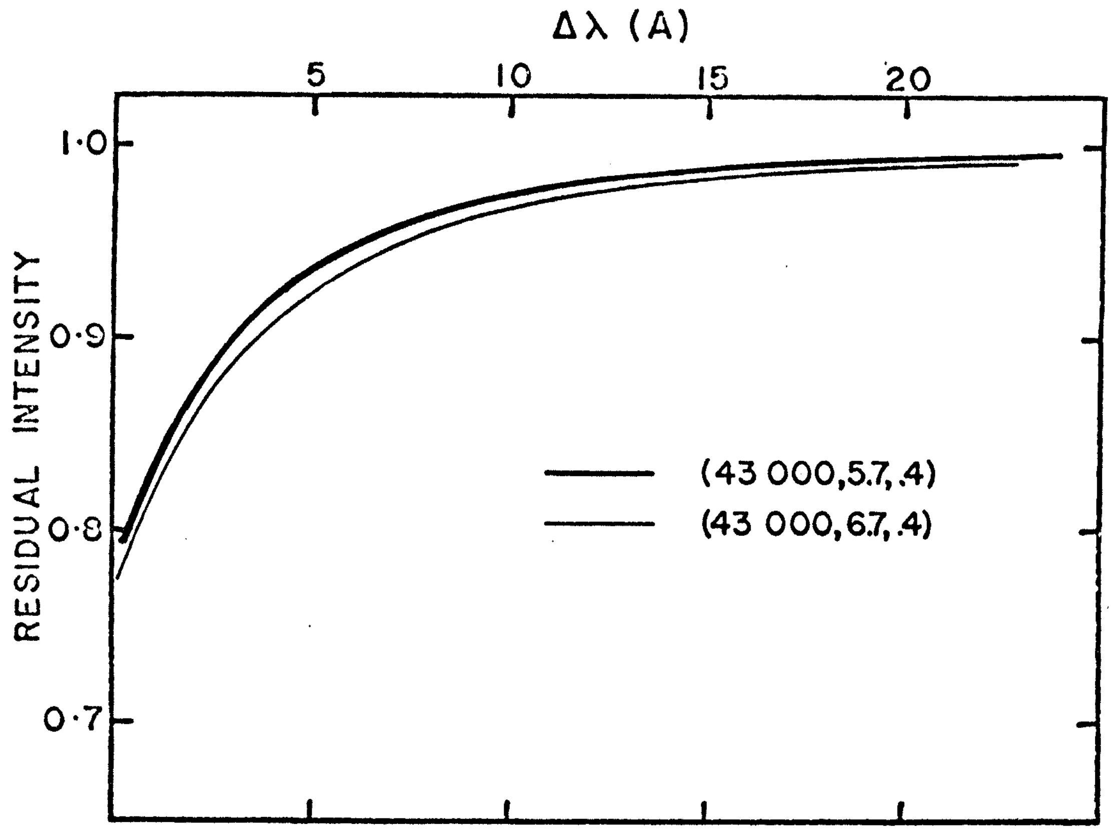

FIG. IV-5 The gravity dependence of HeII λ4686

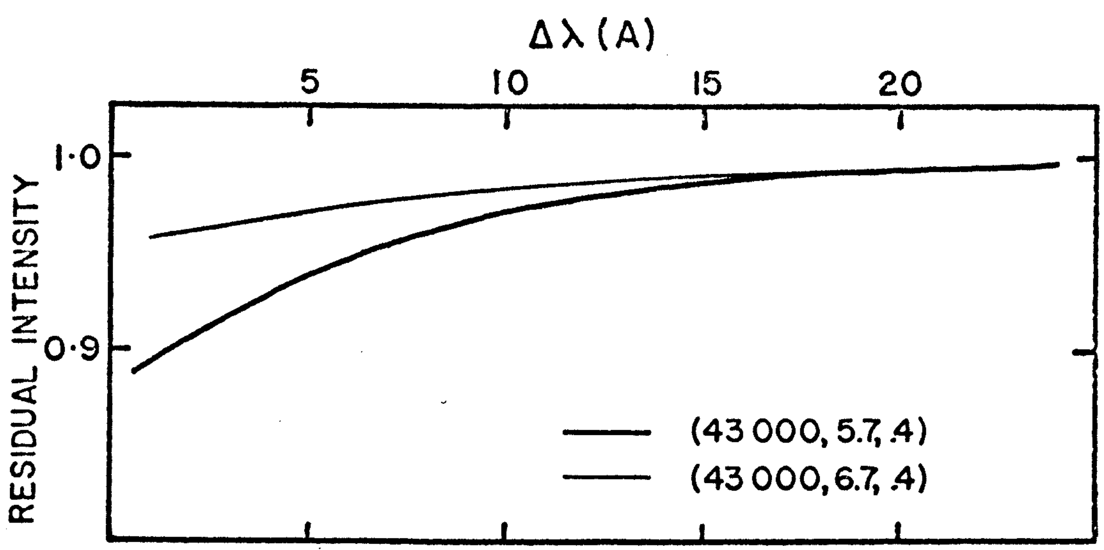

FIG. IV-6 The gravity dependence of HeII λ4542 using quasi-static broadening for ions and electrons for the Pickering lines makes it difficult to use them quantitatively. The $\lambda4542$ profiles computed here assume quasi-static broadening by ions and electrons. (The problem of which approximate line broadening theory to use is discussed in more detail in Part V.) In this approximation the electron contribution is small, and since Sargent and Searle based their suggestion on a calculation assuming broadening by quasi-static ions, it is not surprising that the results here show the gravity sensitivity predicted by them. Note, however, the similarity of the profiles from the atmosphere (40 000, 5.7, 0.4) and (43 000, 6.7, 0.4).

A general problem with the line profiles is that the computed cores of the strong lines are not as deep as the observed cores. This is most probably due to the temperature structure of the outer layers of the model atmospheres. The effect is most prominent in the core of the HeI line at $\lambda4472$, in general the deepest line observed in these hot subdwarf spectra. For such a strong line the central depth is given by the expression

$$D_o = 1 - \frac{F(\text{line center})}{F(\text{cont})} = 1 - \frac{B_\lambda(T_o)}{F_\lambda} , \qquad \text{(IV-1)}$$

where T_o is the boundary temperature and F_λ is the flux in the continuum. Table IV-1 compares the observed central depth with the depths computed from the model atmospheres. Also given is the value of T_o required in Equation IV-1 to give the observed central depth. The problem of explaining the deep cores of strong lines in hot stars is not new and has been discussed, though not solved, elsewhere; see e.g. Underhill (1968; 10 Lac) and Hardorp and Scholz (1969; τ Sco and λ Lep). The procedure here has been to ignore the cores and to fit the wings instead. In the far wings, however, the observed line depth is influenced by the placement of the continuum. Therefore, the strongest weight for fitting line profiles has been placed on the middle wing region. The compromise appears to work quite satisfactorily in general except for λ4472 in the star +25°4655. Here a problem, which may systematically affect the choice of models, becomes acute. That is, the computed HeI lines are generally a little weak compared with the observed profiles. A lower temperature model helps the HeI line, but then Hγ becomes stronger and the nitrogen and silicon ionization equilibria for +25°4655, which already imply a slightly higher temperature, become less well satisfied.

Several considerations provide approximate parameters for constructing a series of models. The study of the hydrogen and helium lines in HZ 44 by Münch (1958) gives an important starting point. It should be noted that

TABLE IV - 1 Observed and Computed Central Depths for HeI λ4472

Star	D_o Observed	T_o Model	D_o Model	T_o (IV-1)
HZ 44	0.34	29100	0.26	27200
+25° 4655	0.38	28500	0.30	26400
HD 127493	0.34	32100	0.23	29100

his approximate model with parameters (34000, 5.7, 0.23) is based on a consideration of the temperature structure as a function of optical depth in the visible region of the spectrum. Depending on the meaning of $\bar{\kappa}$ in that model, the effective temperature of a model atmosphere with a similar temperature structure computed with ATLAS would be nearer 38 000 or 40 000 °K.

Approximate curve-of-growth treatment of the ionization equilibria of nitrogen and silicon also yields information on the range of models to be considered. The particular curve of growth used is not critical for this purpose since all that is required is the relative numbers of atoms in the two ionization states. The more serious assumption is that one temperature and pressure can describe the conditions under which lines with a wide spread of excitation potentials and in two different ionization states arise. Another problem is that one does not know exactly how this temperature and pressure are related to the effective temperature and gravity of a model atmosphere.

Wrubel's (1949) exact curves of growth for pure scattering in the Milne-Eddington atmosphere were used. Figure IV-7 shows the silicon curve of growth for HZ 44 plotted with $\theta = 0.14$. The solid lines are the theoretical curves for $B^{(0)}/B^{(1)} = 10/3$ with the damping parameter log a = -1 for the upper curve and log a = -3 for the lower one. The smaller symbols have lower weight because of poorer equivalent widths or f-values. The quantity Δ is the horizontal shift required to fit the plot of log $W/\Delta\lambda_D$ against the quantity (log $gf\lambda - \theta\chi$ - log $\kappa_\lambda/\kappa_{4000}$) to the theoretical curve of growth. Figure IV-8 shows a similar plot of the nitrogen curve of growth for HZ 44. The silicon and nitrogen curves of growth of +25°4655 are plotted in Figures IV-9 and IV-10 respectively. Figures IV-11 and IV-12 give the nitrogen curves of growth for HD 127493 and +75°325 respectively.

From the Saha equation and the definition of the abscissa of the theoretical curve of growth

$$\Delta_r - \Delta_{r+1} = \log P_e + \theta I_r - 2.5 \log T \quad ,$$

where r refers to the lower state of ionization. Allowed pairs of θ and log P_e have been determined for each star, and their loci in the log P_e - θ plane are plotted in Figure IV-13. The results from nitrogen and silicon are very similar and have been averaged together for HZ 44 and +25°4655. The values plotted refer to the depth at which the lines are formed. Note the very much higher excitation implied by the nitrogen equilibrium in +75°325.

The direct application of the Inglis-Teller relation

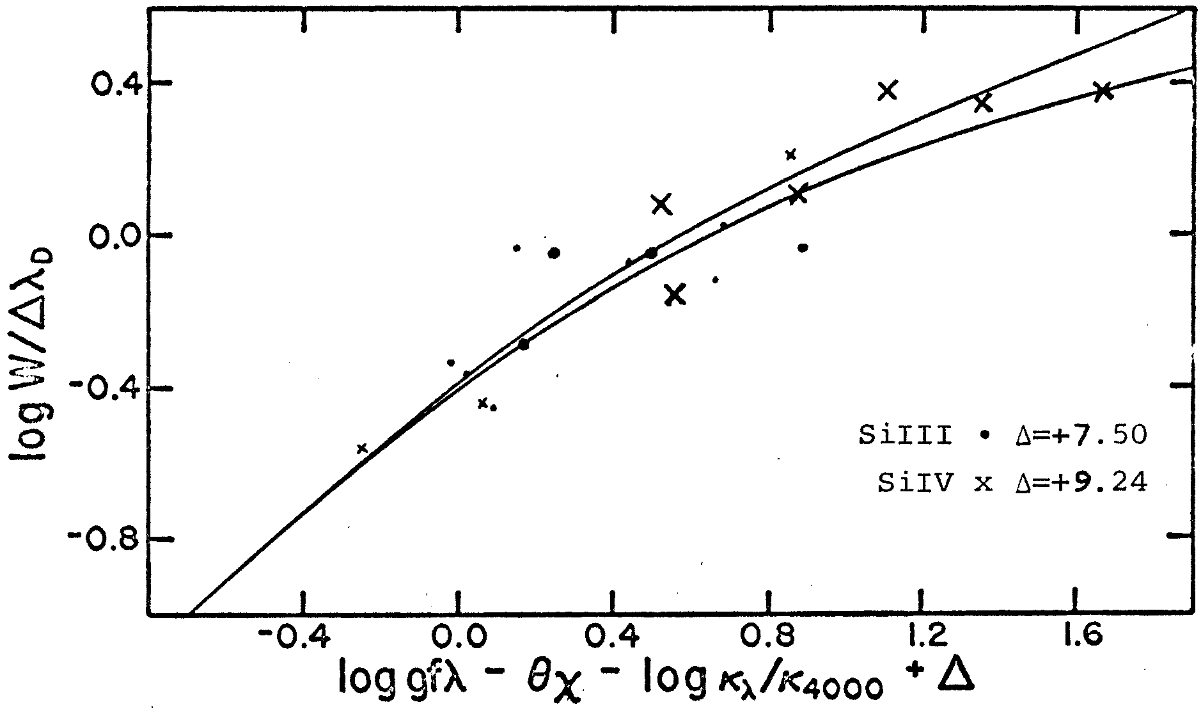

FIG. IV-7 Silicon curve of growth for HZ 44; θ = 0.14

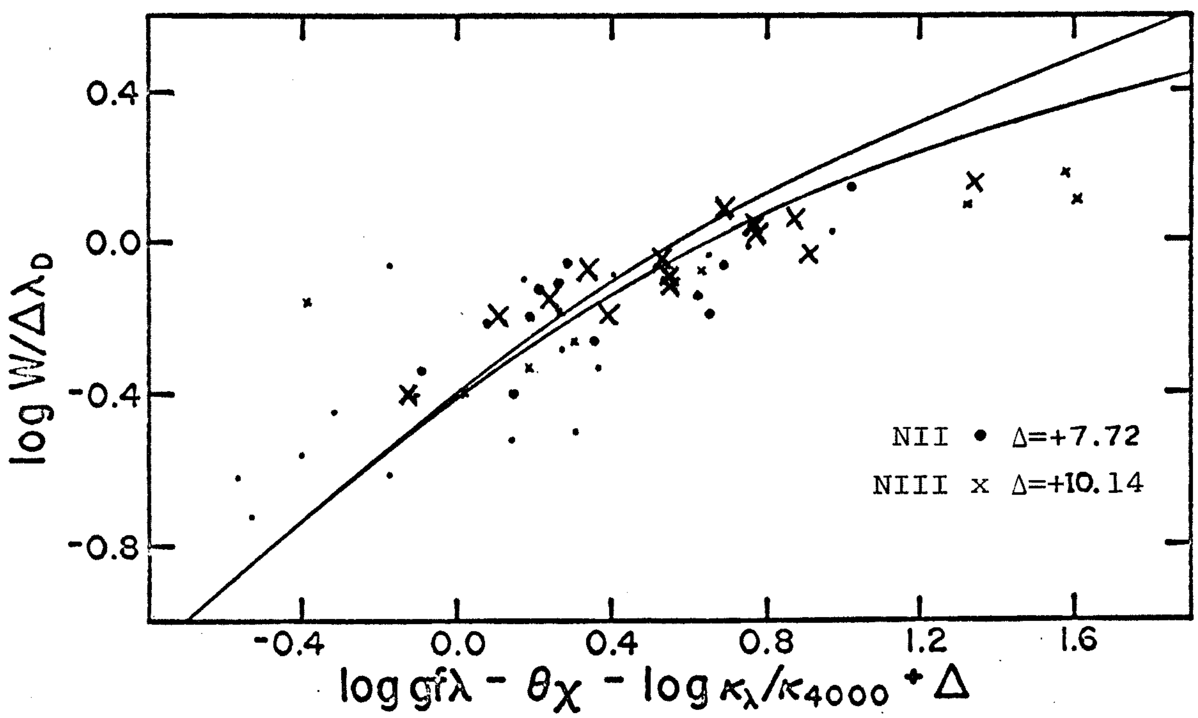

FIG. IV-8 Nitrogen cuve of growth for HZ 44; θ = 0.14

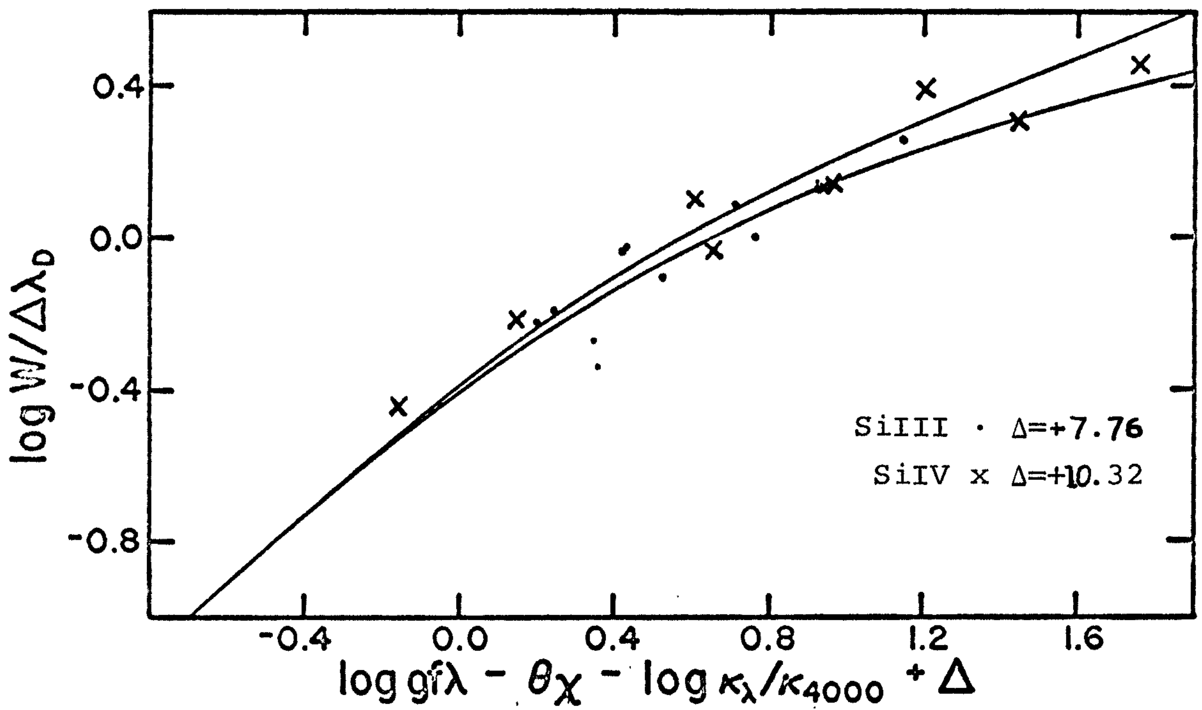

FIG. IV-9 Silicon curve of growth for +25°4655; θ = 0.14

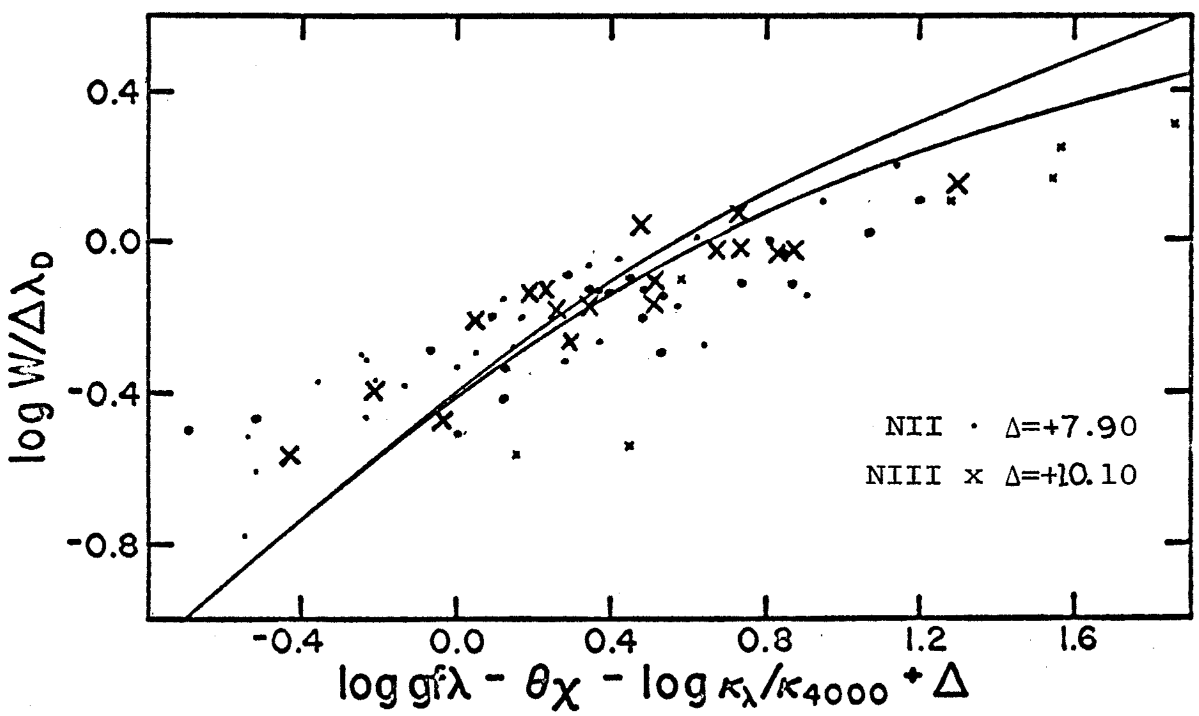

FIG. IV-10 Nitrogen curve of growth for +25°4655; θ = 0.14

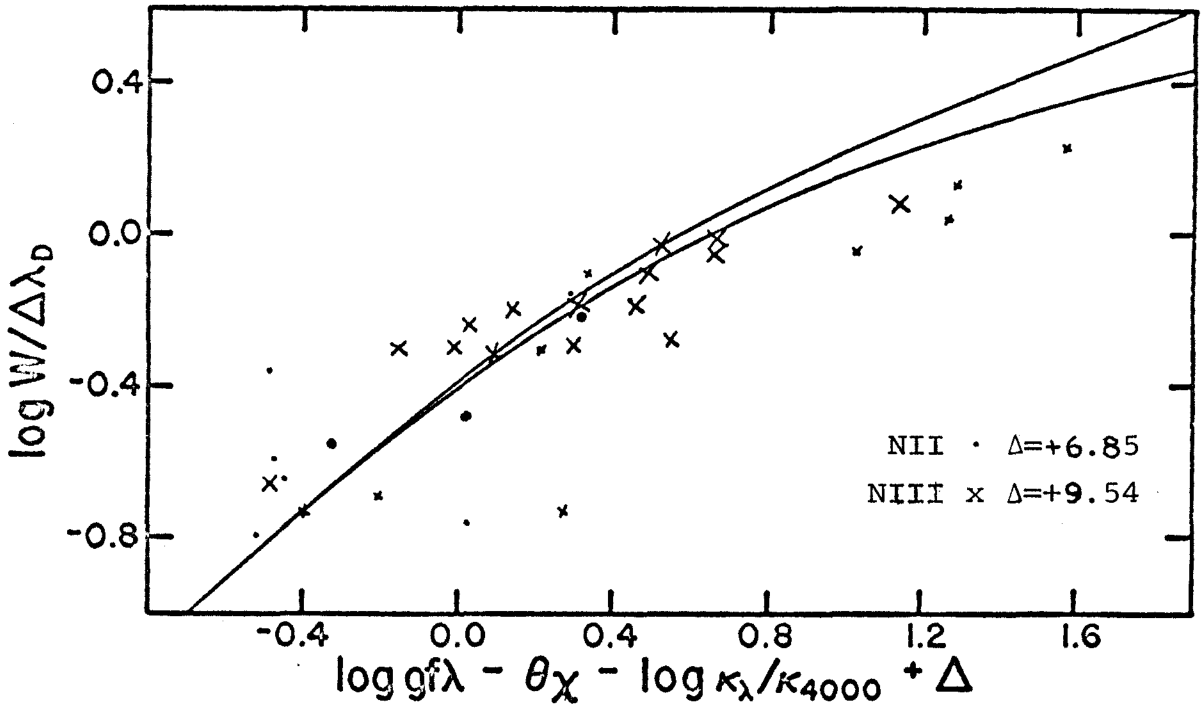

FIG. IV-11 Nitrogen curve of growth for HD 127493; θ = 0.13

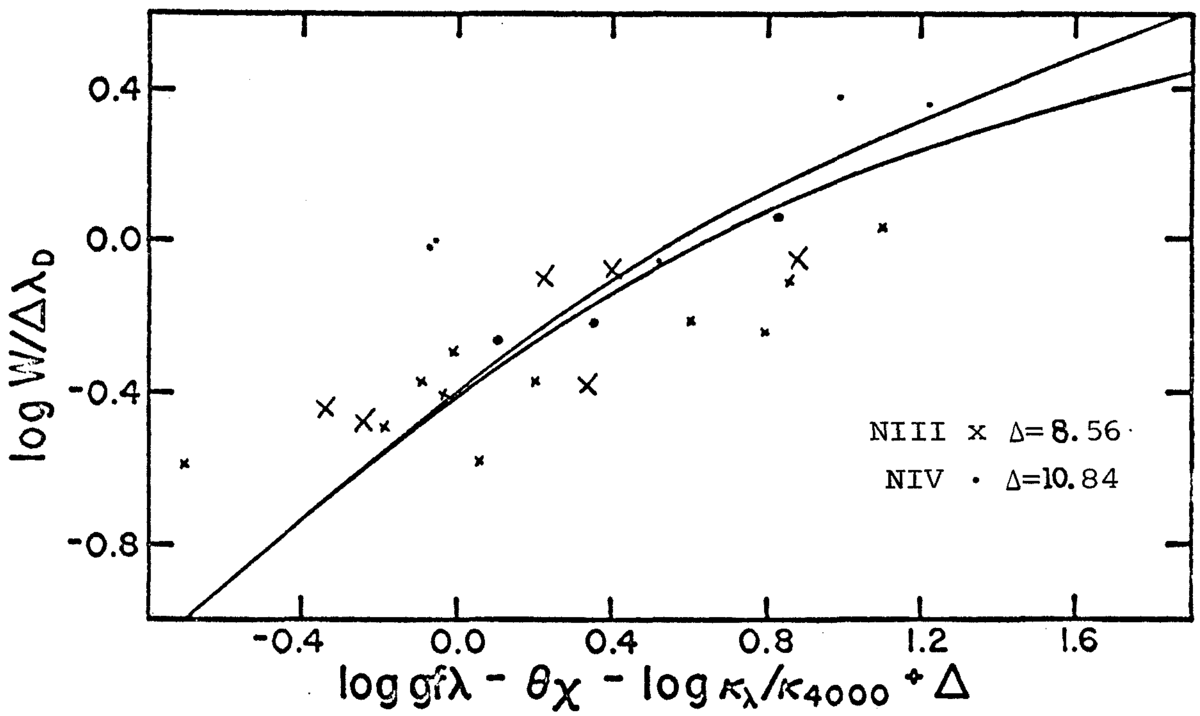

FIG. IV-12 Nitrogen curve of growth for +75°325; θ = 0.112

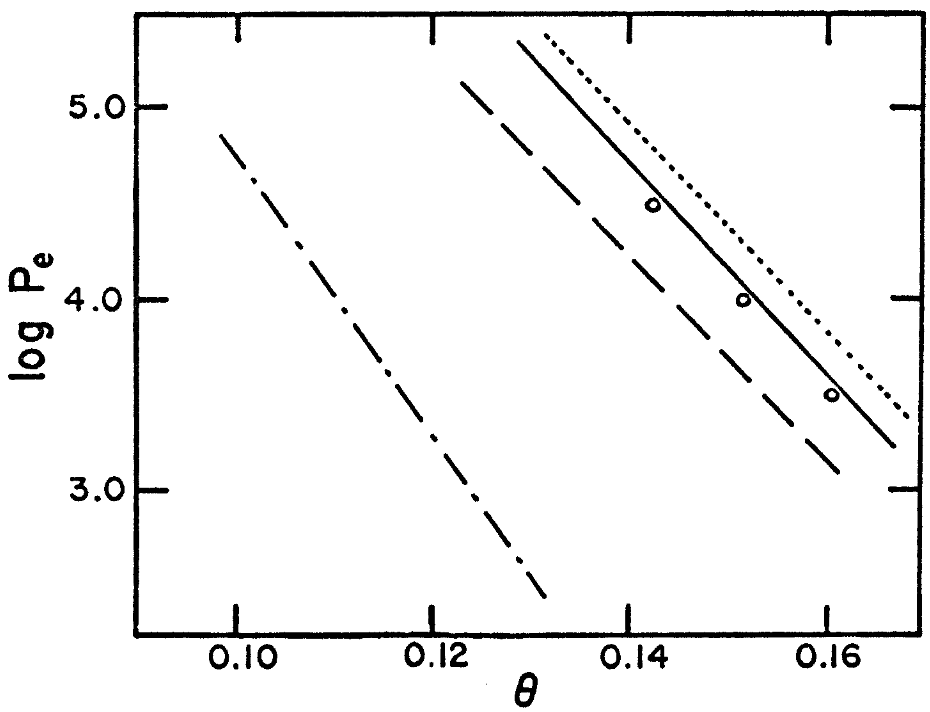

FIG. IV-13 Loci of allowed pairs of log P_e and θ for the depth at which the lines are formed; ——— HZ 44; ...... +25°4655; — — — HD 127493; —.—.—. +75°325; the open circles represent values determined by Münch (1958) for HZ 44 to these stars with high helium abundance may not be warranted. In the case of +25°4655 it is certainly not the overlapping of the wings that causes $H\delta$ to be the last Balmer line visible. On the other hand, if the atmosphere is primarily composed of helium, it may be possible to apply the relation to the ionized helium lines or even to the neutral helium lines which become hydrogenic for high quantum numbers. It is interesting in any case to use the formula for approximate information about the electron pressure, remembering that it is likely to overestimate the pressure if the abundance is important in determining the line strength. With the dependence on ionic charge z included, the Inglis-Teller criterion is given by

$$\log N_e = 23.26 - 7.5 \log n_m + 4.5 \log z$$

or

$$\log (P_e\theta) = 11.10 - 7.5 \log n_m + 4.5 \log z$$

where n_m is the upper quantum number of the last visible line.

The quantum number of the last visible line was determined for the Balmer lines of hydrogen, the $2^3P - n^3D$ lines of neutral helium, and the Pickering lines of ionized helium. The central depth of each line was measured on a low dispersion tracing. The line depth approaches zero for high quantum numbers in approximately a straight line when plotted as a function of the logarithm of the upper quantum number. Table IV-2 gives the value of the last quantum number and also the value of log $(P_e \theta)$ implied by it.

Unfortunately, the depths to which the ionization equilibria and the Inglis-Teller results refer are unknown. Even when reasonable estimates can be made for the optical depths of line formation, there is still the problem of relating the physical variables at different depths and then the depth scales at different wavelengths. This is a non-trivial problem and essentially requires a detailed model atmosphere calculation for each case, since with the helium abundance an important variable, the sources of opacity change, thus changing the structure of the atmosphere. What can be done is to compare the temperatures and pressures from the finished models, which are chosen primarily on the basis of line profiles, with the results implied by the approximate treatment.

It was possible to find models which reasonably satisfied the criteria described earlier to represent three of the four stars studied. The models used to compute line profiles and abundances for HZ 44, +25°4655, and

TABLE IV-2

Application of Inglis-Teller Criterion

	H		HeI		HeII	
Star	N_m	$\log(P_e\theta)$	N_m	$\log(P_e\theta)$	N_m	$\log(P_e\theta)$
HZ 44	11	3.30	10-11	3.45		
+25°4655	6-7	(5.00)	10-11	3.45	11:	4.65:
HD 127493	9-10	3.76	10	3.60	14:	3.85:
+75°325					15-16	3.53

HD 127493 are given in tabular form in the Appendix, along with graphs showing the flux errors and flux derivatives as a function of optical depth. In Table IV-3 are given the model designation and model atmosphere parameters for each star. Figure IV-14 shows the temperature-pressure relation for each model. The small temperature inversion at very small optical depths is not physical and gradually diminishes with further iterations. The irregularity in the temperature distribution at log $\tau_{912} \approx -1.3$ (log $\tau_{4000} \approx 0.$) occurs when neutral helium is the dominant source of opacity. The irregularity is most strongly present in model (43 000, 6.7, 0.9) and not present in model (43 000, 5.7, 0.6) where the HeI opacity no longer dominates. Note that the introduction of additional sources of opacity shortward of 504 A in model (43 000, 6.7, 0.9, M) greatly reduces the temperature discontinuity.

In Figure IV-15 the pressure-temperature relations implied by the nitrogen and silicon equilibrium and the pressure-temperature relations implied by the Inglis-Teller criterion are plotted in the log P_e - θ for HZ 44. Also plotted are the pressure and temperature at $\tau_{4000} = .1$ and $\tau_{4000} = 2/3$ from the model atmosphere for HZ 44. As can be seen from the figure the results are quite consistent.

TABLE IV-3 Model Atmosphere Parameters

Star	HZ 44	+25°4655	+25°4655	HD 127493
Model Designation	(40 000,5.7,0.4)	(43 000,6.7,0.9)	(43 000,6.7,0.9,M)	(43 000,5.7,0.6)
Effective Temperature (°K)	40 000	43 000	Same as for (43 000,6.7,0.9) opacity due to C,N,O,Ne included	43 000
Gravity (cgs)	5×10^5	5×10^6		5×10^5
Helium Abundance (by number)	0.4	0.9		0.6

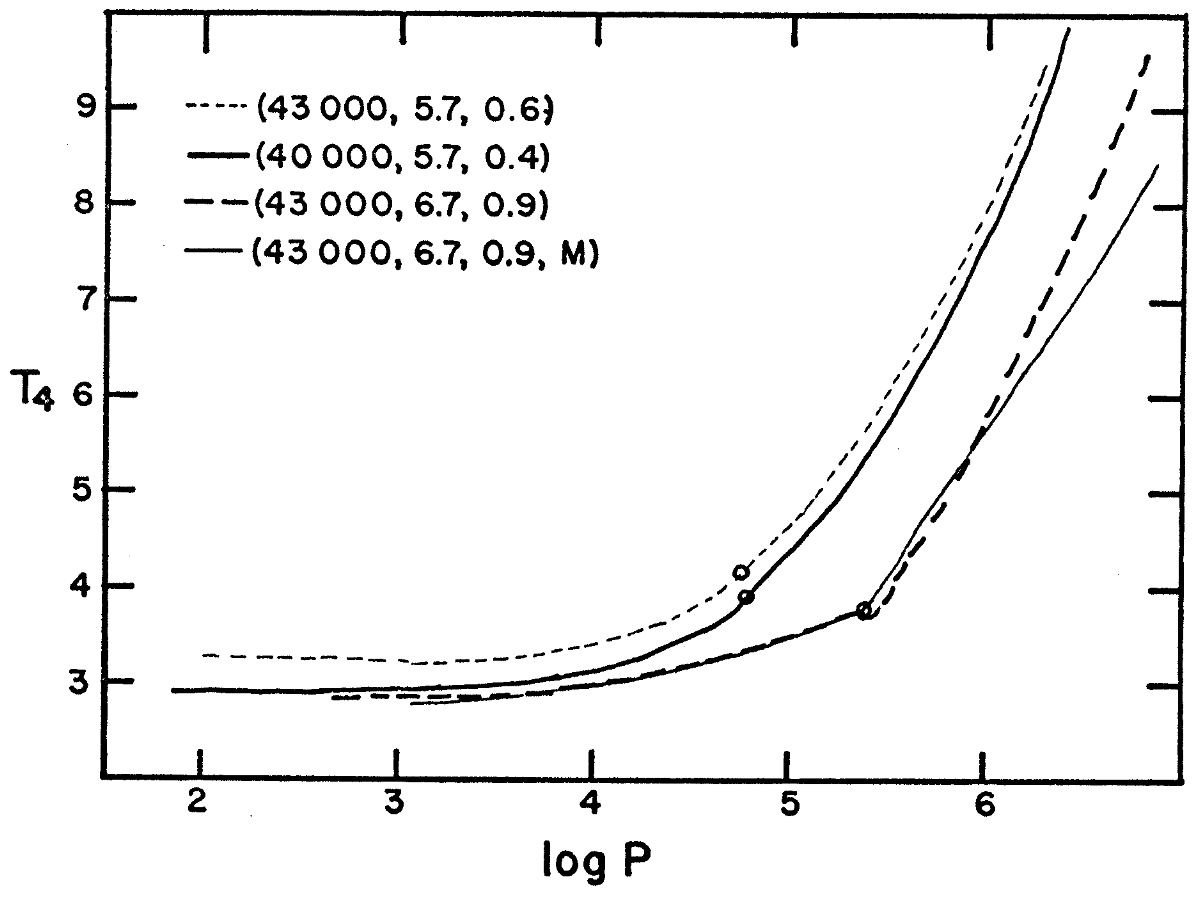

FIG. IV-14 The temperature as a function of the total gas pressure for each model; ——— (40 000,5.7,0.4); — — — (43 000,6.7,0.9); - - - - (43 000,5.7,0.6); ——— (43 000,6.7,0.9,M); the open circles show the point at which τ_{4000}=1.0

Figure IV-16 is a similar diagram for +25°4655. As was suspected, the use of the Inglis-Teller criterion on this star is of very doubtful value. The neutral helium series implies an electron pressure much lower than that given by the model, and the ionized helium lines imply an electron pressure much higher. In the case of HD 127493 in Figure IV-17, the Inglis-Teller relation applied both to the hydrogen lines and to the ionized helium lines implies somewhat higher pressures than given by the model for that star. The principal inference to be made here is that one must exercise care in the use of the Inglis-Teller formula for stars not primarily composed of hydrogen.

In order to test the implicit assumption made in the curve of growth treatment - that all the nitrogen lines are formed at one depth $\tau_{4000} \approx 0.1$ - contribution functions for <u>weak</u> lines of NII and NIII have been calculated for the model atmosphere (40 000, 5.7, 0.4). The method using weighting functions is described by Aller (1960). The calculation indicates that unsaturated lines of nitrogen are formed at depths $\tau_{4000} > .1$ and that the NIII lines are formed deeper than the NII lines. In examples given by Aller for carbon and silicon in hot stars, the lines from higher ionization states are formed in deeper layers, and the corresponding theoretical curves of growth are flatter. A flatter theoretical curve of growth would fit the NIII

FIG. IV-15 FIG. IV-16

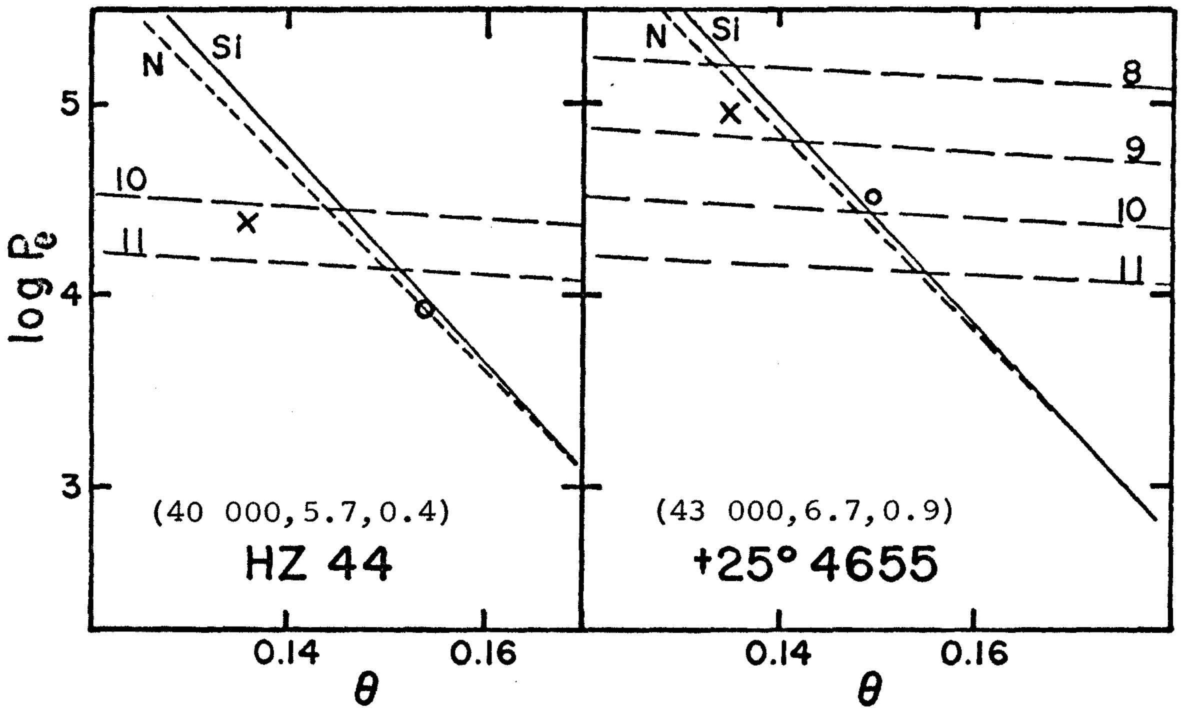

Nitrogen and silicon equilibria and Inglis-Teller relation for hydrogen; point marked o gives log P_e and θ for τ_{4000}=.1; x marks values at τ_{4000} =2/3

FIG. IV-17 FIG. IV-18

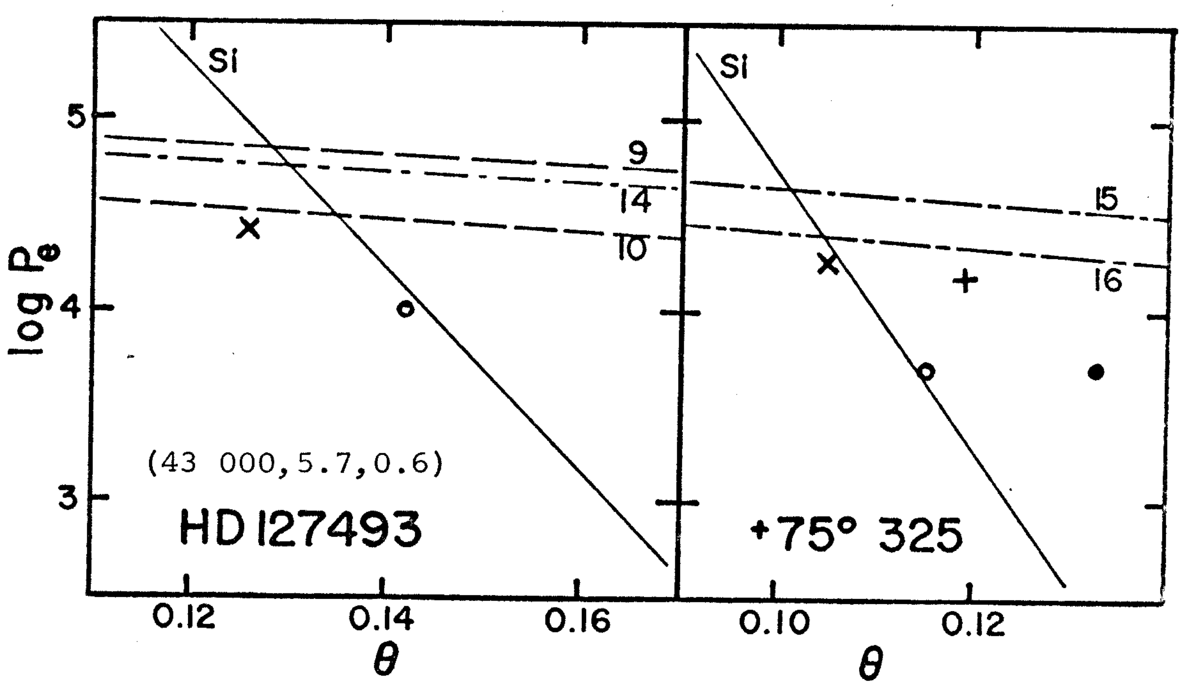

Nitrogen equilibrium and Inglis-Teller relation for hydrogen — — — and for HeII —.—.—. ; points marked o and • give log P_e and θ for τ_{4000}=.1; x and + mark values at τ_{4000} =2/3; in Fig. IV-18 o and x are from the model (55 000,5.3,0.6), and • and + are from the model (45 000,5.3,0.6) lines better. In addition, the ionization equilibrium relation (Figure IV-15) would be shifted to higher temperatures. The point plotted for $\tau = 0.1$ in Figure IV-15 from the model atmosphere would then be plotted instead for a deeper and therefore hotter layer. Thus the total effect on the comparison between the results from the curve of growth and the model atmosphere would be reduced. It must be realized that the calculation for weak lines is an extreme case. As can be seen from Figure IV-8 very few of the lines are actually unsaturated. The inclusion of a saturation function in the calculation shifts the maximum of the contribution function back to smaller optical depths.

It was not possible to find a model atmosphere which satisfactorily fits the observed characteristics of +75°325. The ionization equilibrium between NIII and NIV implies a much higher temperature than the helium line profiles. While the nitrogen equilibrium is satisfied by a model with parameters (55 000, 5.3, 0.6), the helium lines are better described by a model with parameters (45 000, 5.3, 0.6). Even ignoring the implications of the nitrogen equilibrium it is difficult to find a model to simultaneously describe HeI λ4472, HeII λ4686, and Hγ + HeII. The computed profiles for λ4472 tend to be too strong while the profiles predicted for the HeII lines are too weak. The line profile theories assume ion broadening by protons; in these very hot atmospheres most of the helium is doubly ionized; the microfield distribution will be different if there are large numbers of doubly ionized particles. In addition, the hydrogen and neutral helium profiles are not tabulated for the very high temperatures reached in the hottest models, and asymptotic forms are used in the calculation of the theoretical profiles. The only sources of opacity still contributing in models with $T_e \sim 50\ 000^\circ$ are electron scattering and singly ionized helium, and the latter is already dropping off due to increasing double ionization. Additional sources of opacity, not included here, could change the structure of the models. It should be mentioned however, that including opacity from C, N, O, and Ne in the far ultraviolet does not make a significant difference for a model with parameters (50 000, 5.7, 0.4). Figure IV-18 shows the nitrogen ionization relation and also points at $\tau_{4000} \approx .1$ and $\tau_{4000} \approx 2/3$ for models (55 000, 5.3, 0.6) and (45 000, 5.3, 0.6).

The emergent flux from the model atmospheres can be compared with photoelectric scans made by Oke (1969). Scans for HZ 44 and +25°4655 are compared with the flux from models (40 000, 5.7, 0.4) and (43 000, 6.7, 0.9) respectively in Figures IV-19 and IV-20. Both the model fluxes and photoelectric observations have arbitrary zero points. Some of the scatter, especially in the blue, is due to the presence of strong helium lines. The scatter at low frequencies is probably noise due to low flux levels.

The theoretical UBV colors and the bolometric correction may be derived by folding the filter responses of the UBV system with the emergent flux distribution of the model atmospheres. A program to accomplish this has been developed by D. M. Peterson. Table IV-4 gives the B.C. and shows a comparison between the observed and computed colors.

As can be seen from both the scans and the colors, either the models are too hot, or there is a fairly large amount of reddening, or the calibrations are in error. It may be noted that HZ 44 has a galactic latitude of about 80° and an interstellar K line with equivalent width $W \approx 90$ mA, and +25° 4655 has a galactic latitude of about -20° with an interstellar K line of equivalent width $W \approx 35$ mA. The points from the photoelectric scans are based on Oke's 1964 calibration of α Lyr. Preliminary results from a more recent calibration (Oke 1969) indicate a steeper Paschen continuum, by about

.1 magnitudes between 4000 and 8000A. This reduces the discrepancy between the model and the photoelectric scans considerably. The difference between the observed and computed colors must also be considered with caution. A possibility mentioned by D. M. Peterson is that since the original UBV system has been very difficult to duplicate exactly, the sensitivity curves for the filters may not be exactly the same as those used to define the system. The computed colors are normalized to agree with the UBV system for A0 stars and a discrepancy for very hot stars is possible. The effect of blanketing by the strong helium lines has not been included in the computed colors.

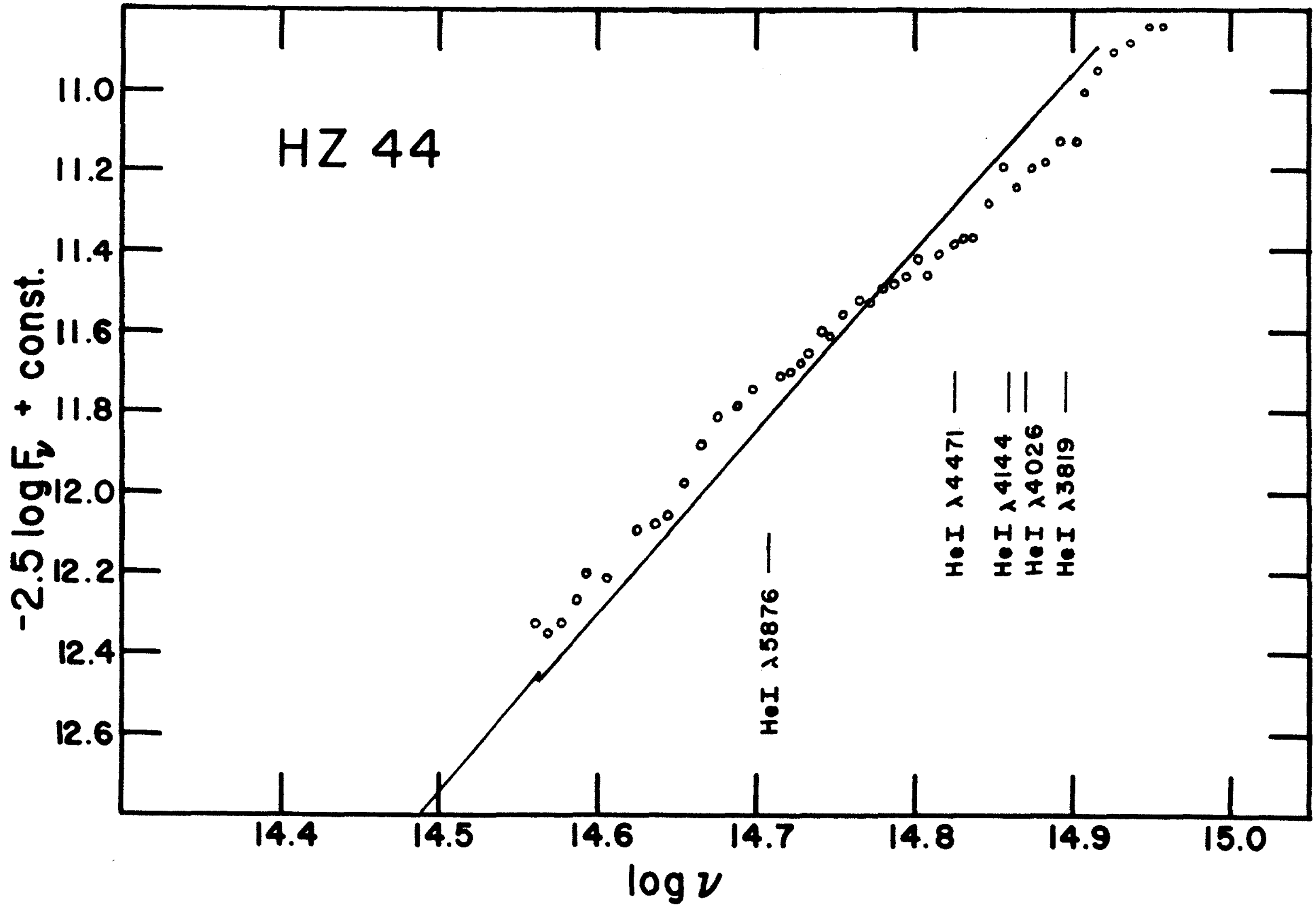

FIG. IV-19 The solid line represents the emergent flux from model (40 000,5.7,0.4) in magnitudes per unit frequency interval; the plotted points are from photoelectric scans of HZ 44

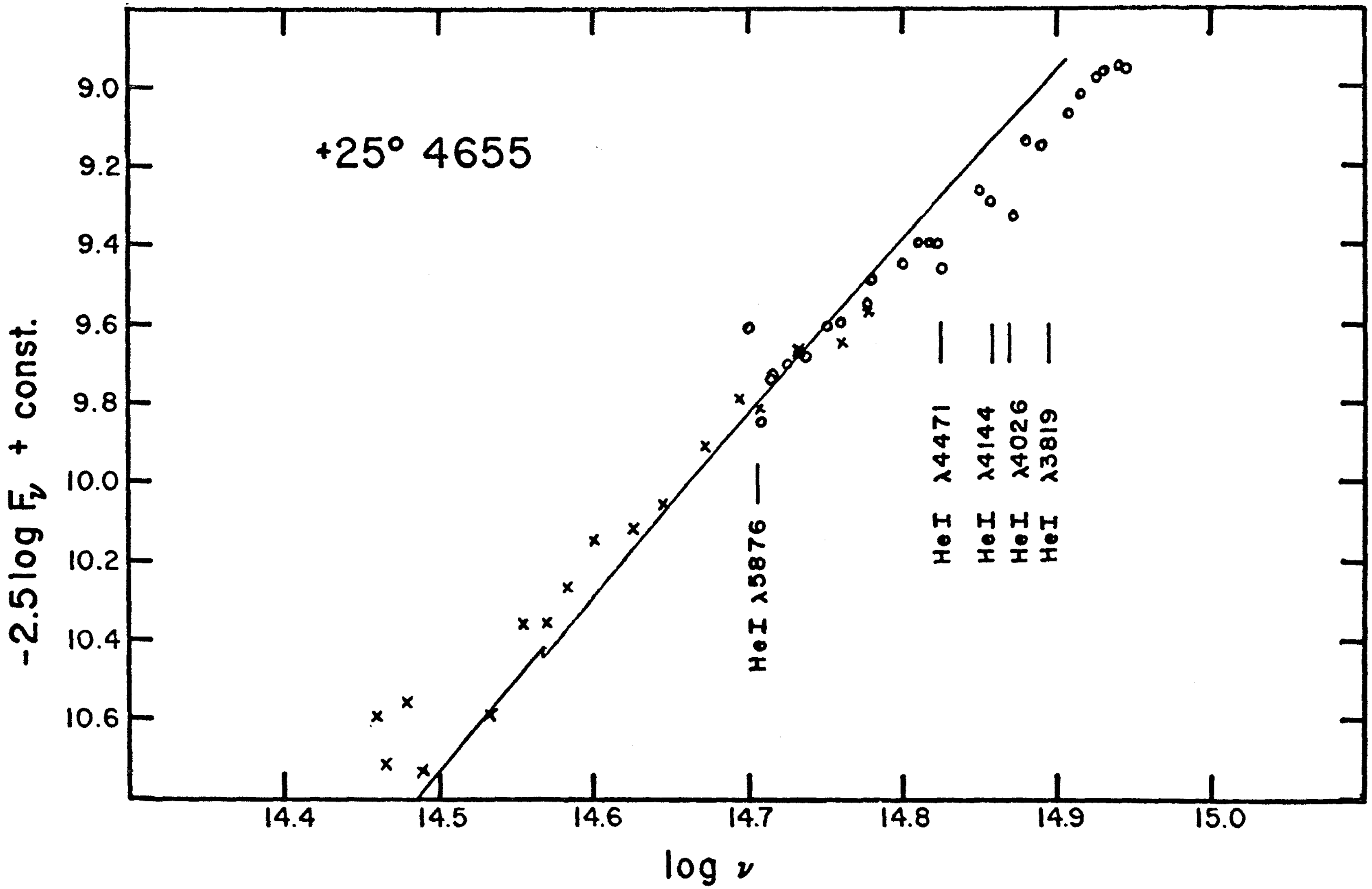

FIG. IV-20 The solid line represents the emergent flux from model (43 000,6.7,0.9) in magnitudes per unit requency interval; the plotted points are from photoelectric scans of +25°4655

TABLE IV-4

Colors and Bolometric Corrections

Star		B-V	U-B	B.C.
HZ 44	Observed	-0.29	-1.19	
	Model	-0.38	-1.34	-3.85
+25°4655	Observed	-0.27	-1.20	
	Model	-0.36	-1.37	-4.14
HD 127493	Observed	-0.28		
	Model	-0.38	-1.34	-4.05

V. LINE PROFILES AND ABUNDANCES

Analyses of the spectra have been carried out with the aid of computer programs which calculate theoretical profiles and equivalent widths for given model atmospheres and abundances. The original ALGOL program is described by Baschek et al. (1966). A translation of the program into FORTRAN is described by Peytremann et al. (1967). The version used in this investigation has been modified and extended by Scholz (1968) who has kindly made it available. The basic assumptions made in the original program are a homogeneous, plane-parallel atmosphere, LTE, true absorption, no rotation or macroturbulence, Voigt profile for the line absorption coefficient, and modified asymptotic wing formula from Griem (1962) for hydrogen. The modified version of the program also allows computation of hydrogen and helium line profiles according to several different theories.

For this investigation there were available several detailed line profile theories. These include the Kepple, Griem (1968; hereafter referred to as KG) and the Edmonds, Schlüter, Wells (1967, hereafter referred to as ESW) theories for the Balmer lines of hydrogen, the Griem (1968) theory for HeI λ4472, and the Griem (1964; tabulated central profiles, asymptotic wings) theory for HeII λ4686. An entirely quasi-static treatment for hydrogenic lines is possible using Pfennig's (1966) theory for hydrogen, and for HeI λ4472 using the theory by Pfennig and Trefftz (1966; hereafter referred to as PT; see also Messerschmidt et al. 1967). The application of Pfennig's quasi-static theory for hydrogen to lines of ionized helium has been suggested by Hardorp and Scholz (1969). In addition hydrogenic line profiles may be calculated using a slightly modified version of the asymptotic formulae given by Griem (1962; see Baschek et al. 1966 for modification).

For computing Balmer line profiles, there is a choice between the KG and ESW theories. In general, the ESW theory gives somewhat narrower profiles than does the KG theory. This in turn requires a higher gravity model in order to fit the same observed profile. The KG theory has been developed in the framework of fairly high densities ($N_e \sim 10^{14}$ to 10^{18} cm^{-3}) and agrees quite well with laboratory measurements under these conditions. (See KG 1968 for a detailed description of the theory.) The ESW semi-empirical theory, on the other hand, has been developed in order to provide a more adequate description of hydrogen lines under low density conditions (ESW 1967 for details). Since the atmospheres of the hot subdwarfs being investigated appear to have densities in the range considered by the KG theory, it has been used to describe the hydrogen lines of these stars.

The Griem (1968) and Pfennig-Trefftz (1966) theories for HeI λ4472 give fairly similar profiles in the cases where both theories have been used with a given model atmosphere. There is no particular basis in this study for distinguishing between the two theories. The profiles finally used are calculated from the Griem theory.

Griem's (1964) theory has been applied for HeII λ4686. Comparison with computed profiles using Griem's theory with profiles using Pfennig's quasi-static (QS) hydrogen theory applied to ionized helium, show that the two theories give almost identical emergent profiles for λ4686. The Griem asymptotic theory as approximated by Baschek et al. (GA-BHT) gives a narrower profile.

An adequate theoretical description of the Pickering lines of ionized helium is not yet available. Such a theory would be useful in the analysis of very hot stars. Since the Pickering lines with their high upper quantum numbers ($n = 4 \longrightarrow n' > n$) are more sensitive to Stark broadening than is λ4686 ($n = 3 \longrightarrow n' = 4$), a comparison of the profiles of λ4686 and λ4542, for example, may provide a luminosity criterion for very hot stars (Sargent and Searle 1968). In addition the Balmer lines of hydrogen will be affected by blends with the even-numbered Pickering lines. For this study there were available a completely quasi-static description (QS) and the asymptotic formulation due to Griem (GA-BHT). It will be shown that the GA-BHT formulation cannot be expected to provide a valid description of the Pickering lines for the model atmospheres under consideration, and that there is some evidence that the QS theory provides a qualitatively valid description.

While ion broadening is well-described by the quasi-static approximation for nearly all cases of astrophysical interest, electron broadening presents a more complicated problem. Under certain circumstances the electron contribution to Stark broadening may be described by the quasi-static approximation, in others by the opposite extreme of the impact approximation; in intermediate conditions neither approximation is strictly valid for all the electrons.

Since the $H\gamma$ profile may be computed not only with the KG theory, but also with the QS or GA-BHT theories, the behavior of the two approximate theories may be compared with the detailed theory, in conjunction with consideration of the validity criteria for the two approximate theories. In the KG theory a Maxwellian distribution of electron velocities is assumed, and the velocity dependence of the limits of integration over impact parameter is considered before averaging over velocity. In the Griem asymptotic theory for hydrogenic lines average values of the electron velocity are used in defining the boundaries of applicability for the asymptotic forms.

The frequency shift due to a singly charged perturber at distance r is given by

$$\Delta\omega \approx \frac{h\, b^2}{2\pi m r^2 z} \qquad \text{(V-1)}$$

(see eg. Griem 1964) where b is the upper quantum number, h is Planck's constant, m is the mass of the electron, and z is the ionic charge. The quasi-static approximation is valid provided that the perturber does not move significantly during the time characteristic of the frequency, i.e. that

$$v(\Delta\omega)^{-1} << r \qquad \text{(V-2)}$$

where v is the velocity of the perturber. Following Griem and Shen (1961), if r in Eq. (V-1) is chosen such that

$$\Delta\omega = \Delta\omega_s = 5\left(\frac{b^2 h}{2\pi m z}\right) N^{2/3} \qquad \text{(V-3)}$$

corresponding to the (half) half-width of the Holtsmark profile, then condition (V-2) for the validity of the quasi-static approximation can be translated into a condition on the density by substituting (V-3) into (V-2). Thus for

$$N >> \left(\frac{2\pi mvz}{5h\ b^2}\right)^3 = N_s \qquad \text{(V-4)}$$

the quasi-static approximation is an appropriate description of the line broadening. Alternatively one may consider at what value of $\Delta\lambda$ ($\Delta\lambda = \Delta\omega\ \lambda^2/2\pi c$) condition (V-2) will be satisfied. With r now given by Eq. (V-1) the quasi-static approximation should be valid for

$$\Delta\lambda >> \frac{\lambda^2\ v^2\ mz}{ch\ b^2} = \Delta\lambda_w \qquad \text{(V-5)}$$

The impact approximation at the opposite extreme is applicable when

$$(\Delta\omega)^{-1} >> r/v \quad , \qquad \text{(V-6)}$$

that is, when the time characteristic of the frequency shift is long compared with the characteristic time of the interaction. With r equal to the Debye radius

$$\rho_D = \left(\frac{kT}{4\pi Ne^2}\right)^{1/2} \quad , \qquad \text{(V-7)}$$

condition (V-6) is equivalent to

$$\Delta\lambda << \frac{\lambda^2}{c} v \left(\frac{Ne^2}{\pi kT}\right)^{1/2} = \Delta\lambda_p \quad . \qquad \text{(V-8)}$$

For $\Delta\lambda > \Delta\lambda_p$ the total electron contribution to the broadening cannot be described simply by the impact approximation. In the Griem asymptotic theory (1962) an intermediate formula smoothly connects the region of impact approximation with the region of quasistatic approximation.

In developing the asymptotic theory Griem makes another assumption which becomes important at high densities. The nearest neighbor approximation is used for the distribution of perturber distances,

$$W(r) \sim 4\pi r^2 \qquad \text{(V-9)}$$

which is valid for $r << N^{-1/3}$. This in turn requires, when considered with (V-1) that

$$\Delta\lambda >> \frac{\lambda^2 hb^2}{4\pi^2 cmz} N^{2/3} = \Delta\lambda_m \qquad \text{(V-10)}$$

for the asymptotic formulae to be valid. On the basis of comparison with earlier computed profiles, Griem estimates that errors from the use of the asymptotic formulae will be less than 20 percent for $\Delta\lambda \approx 20\Delta\lambda_m$.

Table V-1 gives the temperature and electron pressure at $\tau_{4440} \approx .6$ for two model atmospheres. Table V-2 gives values for some of the parameters in the Griem asymptotic theory. Here the velocity v is chosen so that $v^2 = kT/M$, where M is the mass of the perturbing particle, in agreement with Griem's choice for a representative velocity.

As expected, the ion contribution can be quite adequately described by the quasi-static approximation. The values of N_s and $\Delta\lambda w$ for electrons imply that the quasi-static approximation for electrons is not really appropriate for these models. If the asymptotic theory is expected to be valid for $\Delta\lambda \gtrsim 20\,\Delta\lambda m$, then it too must be discarded. On the basis of comparison with Hγ profiles computed by the detailed Kepple-Griem theory, however, the quasi-static approximation appears to give a better representation of the line than the Griem asymptotic theory. Figures V-1 and V-2 compare emergent Hγ profiles computed using the GA-BHT formulation and the QS approximation for both ions and electrons with the Hγ profile calculated from the KG theory. For model (40 000, 5.7, 0.4) it can be seen in Figure V-1 that the two approximate theories differ from the KG theory by about the same amount although in opposite directions, and there is no clear preference. In Figure

TABLE V-1

Temperature and Electron Pressure at $\tau_{4440} \approx .6$ for Models (40 000,5.7,0.4) and (43 000,6.7,0.9)

Model	(40 000,517,0.4)	(43 000,6.7,0.9)
τ_{4440}	0.6	0.6
$T(\tau_{4440})$	35700	36310
$N_e(\tau_{4440})$	4.0×10^{15}	1.5×10^{16}

TABLE V-2

Parameters for the Griem Asymptotic Theory

Model	(40 000,5.7,0.4)		(43 000,6.7,0.9)	
	H γ	λ4542	Hγ	λ4542
protons				
N_s	1.7×10^{12}	4.0×10^{11}	1.7×10^{12}	4.1×10^{11}
$\Delta\lambda\omega$ (A)	0.10	0.07	0.10	0.07
electrons				
N_s	1.3×10^{17}	3.1×10^{16}	1.3×10^{17}	3.2×10^{16}
$\Delta\lambda\omega$ (A)	190	130	190	130
$\Delta\lambda m$(A)	0.7	1.3	1.7	3.1
$\Delta\lambda p$(A)	3.5	3.9	6.9	7.5

V-2 for model (43 000, 6.7, 0.9), however, while there is good agreement in the far wings ($\Delta\lambda \gtrsim$ 8A) among all three theories, the GA-BHT profile differs from the KG profile for smaller separations from the center, by much more than the QS approximation does.

Since the QS approximation improves with increasing upper quantum number, it should provide a better description of the Pickering lines of ionized helium than of $H\gamma$. Figures V-3 and V-4 compare emergent profiles of λ4542, the n = 4 to n = 9 transition of HeII, using the two approximate theories, for models (40 000, 5.7, 0.4) and (43 000, 6.7, 0.9) respectively. Note in Figures V-2, V-3, and V-4 that the GA-BHT profiles diverge from the KG and QS profiles for $\Delta\lambda \lesssim 5\,\Delta\lambda m$, that is, in a region for which the asymptotic theory is not expected to give good results. Griem (1967), in a more recently developed asymptotic theory, finds that the quasi-static approximation for electrons should provide an upper limit for the electron contribution. Finally, at least qualitatively, the observed profiles are better described by profiles computed with the QS approximation.

In Figures V-5 through V-17 the computed profiles of selected hydrogen and helium lines are compared with the average observed profiles in HZ 44, +25°4655, and HD 127493. Figure V-5 shows the average observed profile

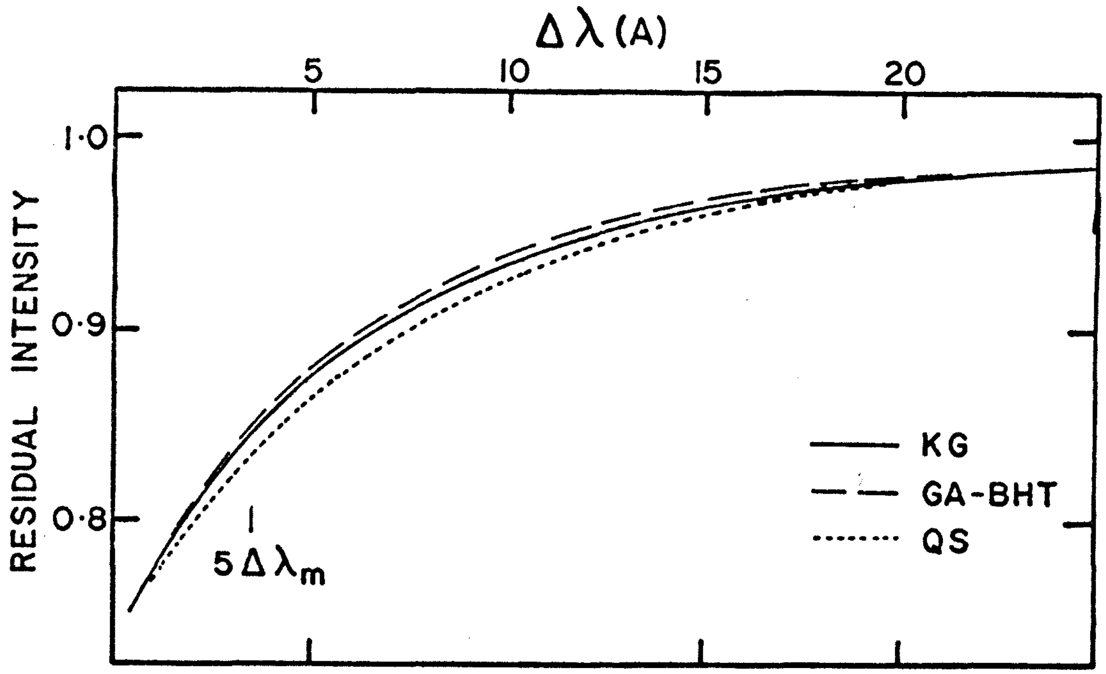

FIG. V-1 Computed emergent Hγ profiles for model (40 000, 5.7, 0.4)

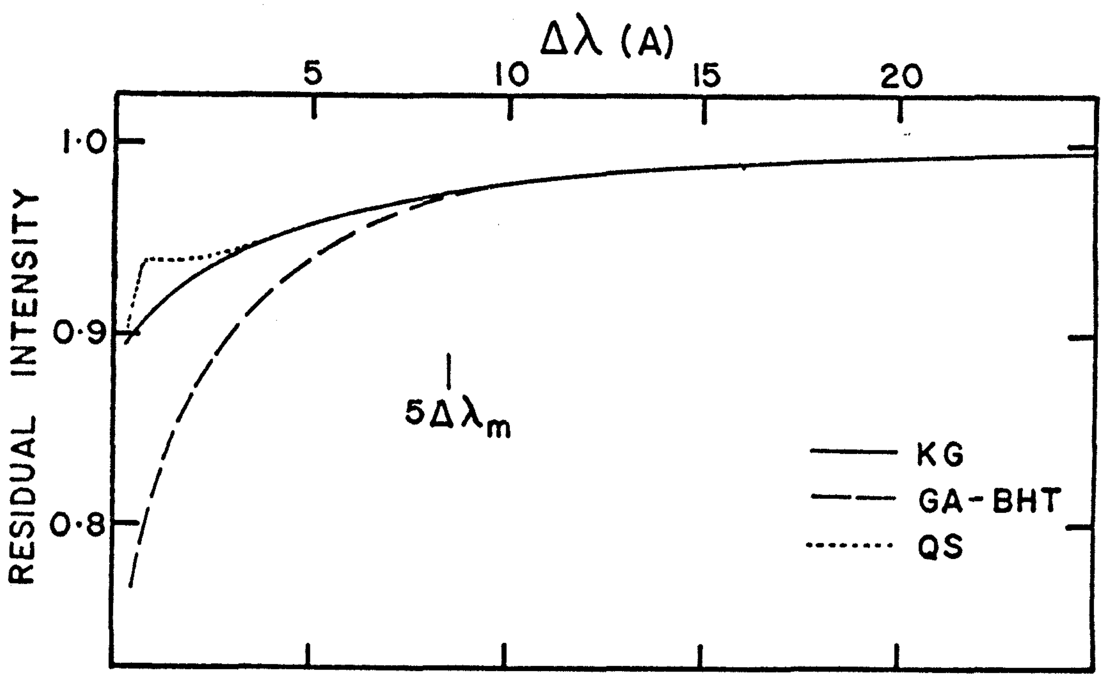

FIG. V-2 Computed emergent Hγ profiles for model (43 000, 6.7, 0.9)

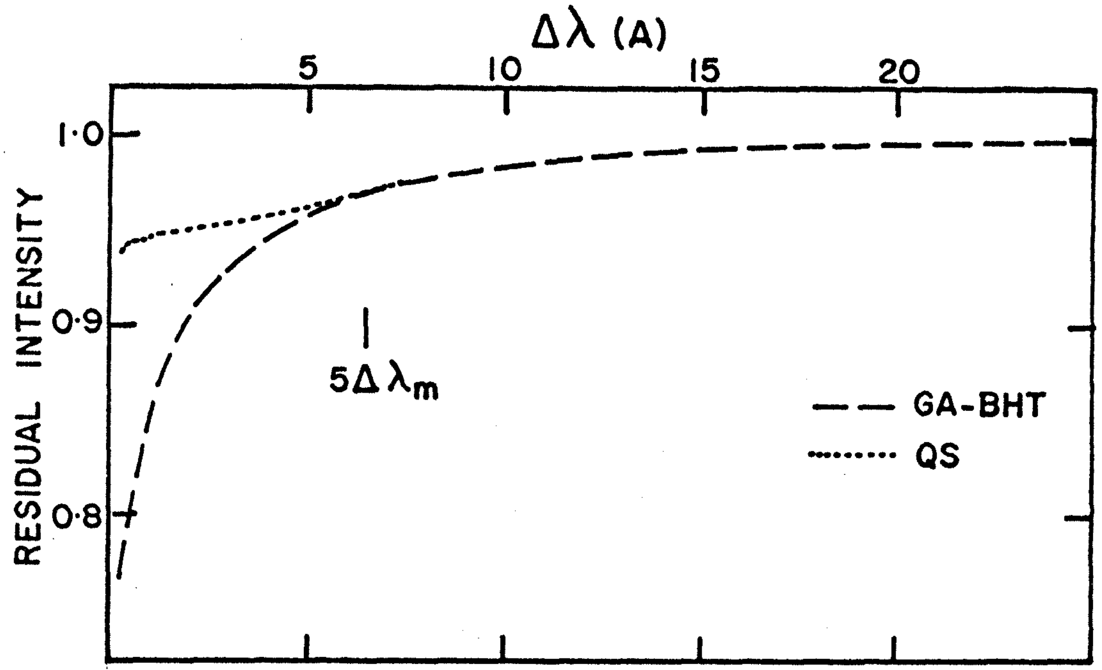

FIG. V-3 Computed emergent HeII λ4542 profiles for model (40 000, 5.7, 0.4)

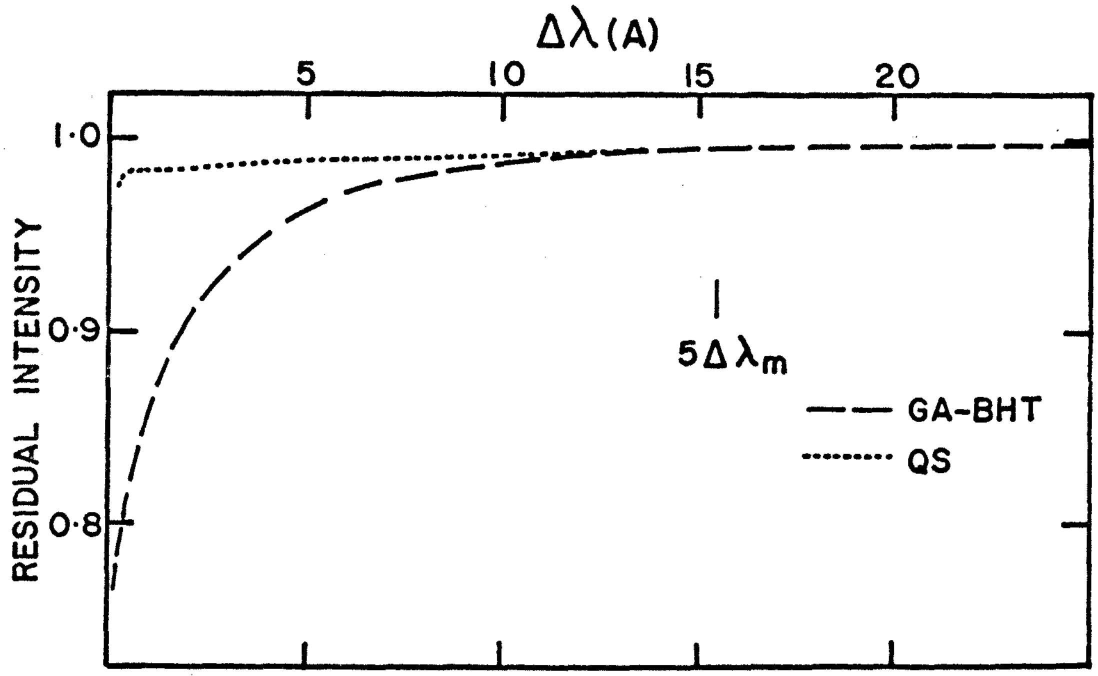

FIG. V-4 Computed emergent HeII λ4542 profiles for model (43 000, 6.7, 0.9) at Hγ for HZ 44. Superimposed lines of SIII and SiIV are indicated. The solid line is the computed emergent profile of the blend Hγ (KG theory) plus HeII (QS theory) for the model atmosphere (40 000,5.7,0.4). Figure V-6 gives the observed profile of HeI λ4472 and the computed profile for model (40 000,5.7,0.4) using Griem's theory. The position of the continuum in the average observed profile has been lowered by 1 percent. The plot is centered on the forbidden component, which is included in the profile calculation. The position of the MgII line at 4481.2 A is indicated. A blend of unidentified lines can be seen on the blue wing between 10 and 15 A from the center. Figures V-7 and V-8 show the HeII lines of HZ 44 at λ4686 and λ4542 respectively. The two wings are averaged together; small dots indicate points with a contribution from one wing only. The line at λ4542 has many superimposed lines of nitrogen which are difficult to subtract out and thus cause a lot of scatter in the profile points. The solid lines are theoretical emergent profiles for the model (40 000, 5.7, 0.4) using Griem's theory for λ4686 and the QS theory for λ4542.

Figures V-9 through V-12 compare the average observed profiles in +25°4655 with the profiles computed with the model (43 000, 6.7, 0.9) for the lines Hγ, λ4472, λ4686, and λ4542 respectively. Figure V-13 shows

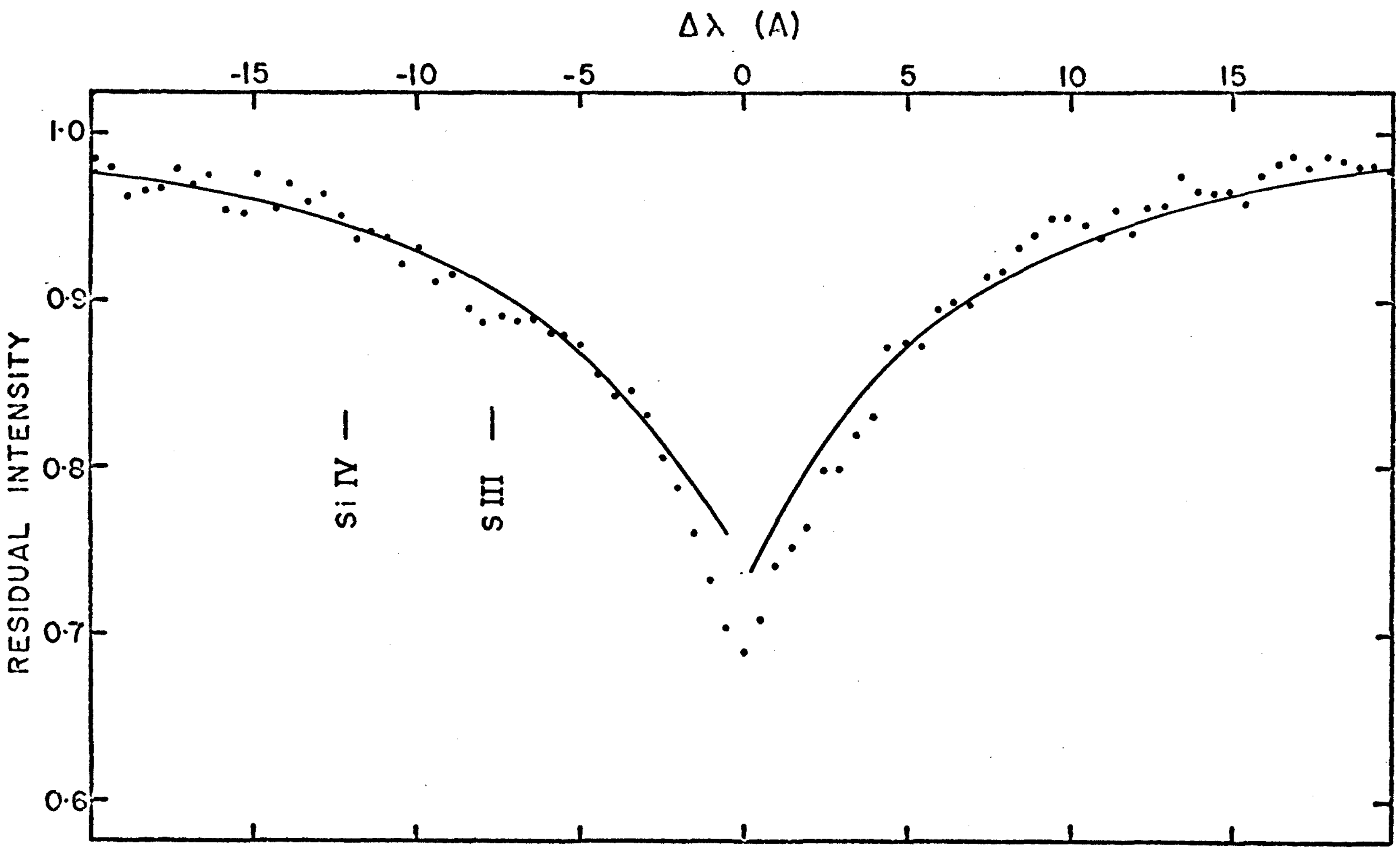

FIG. V-5 Hγ + HeII profile for HZ 44; average from 3 plates; computed profile for model (40 000, 5.7, 0.4); Δλ=0 at 4340.5 A

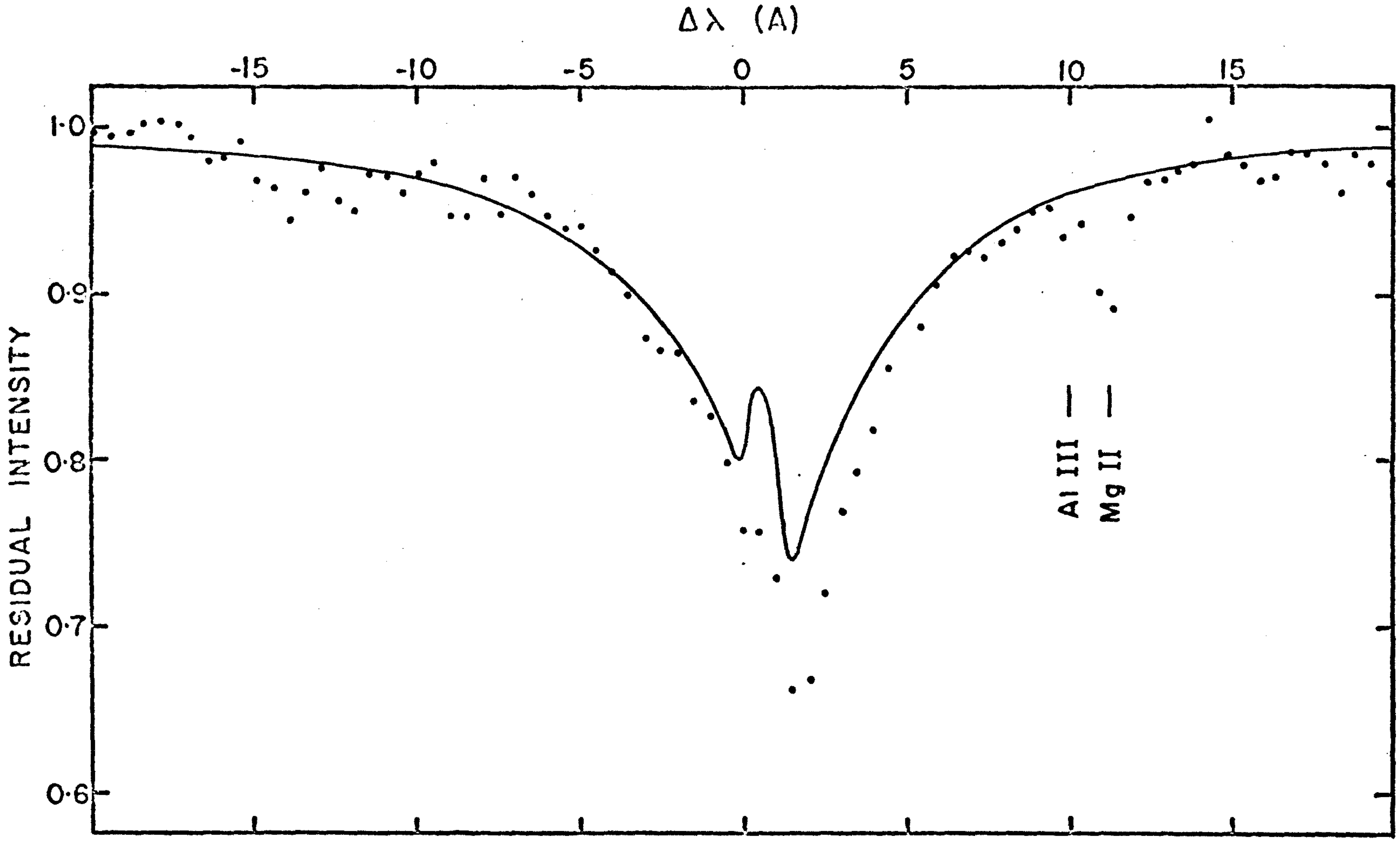

FIG. V-6 HeI λ4472 profile for HZ 44; average from 3 plates (continuum lowered 1%); computed profile for (40 000, 5.7, 0.4); Δλ=0 at 4469.9 A

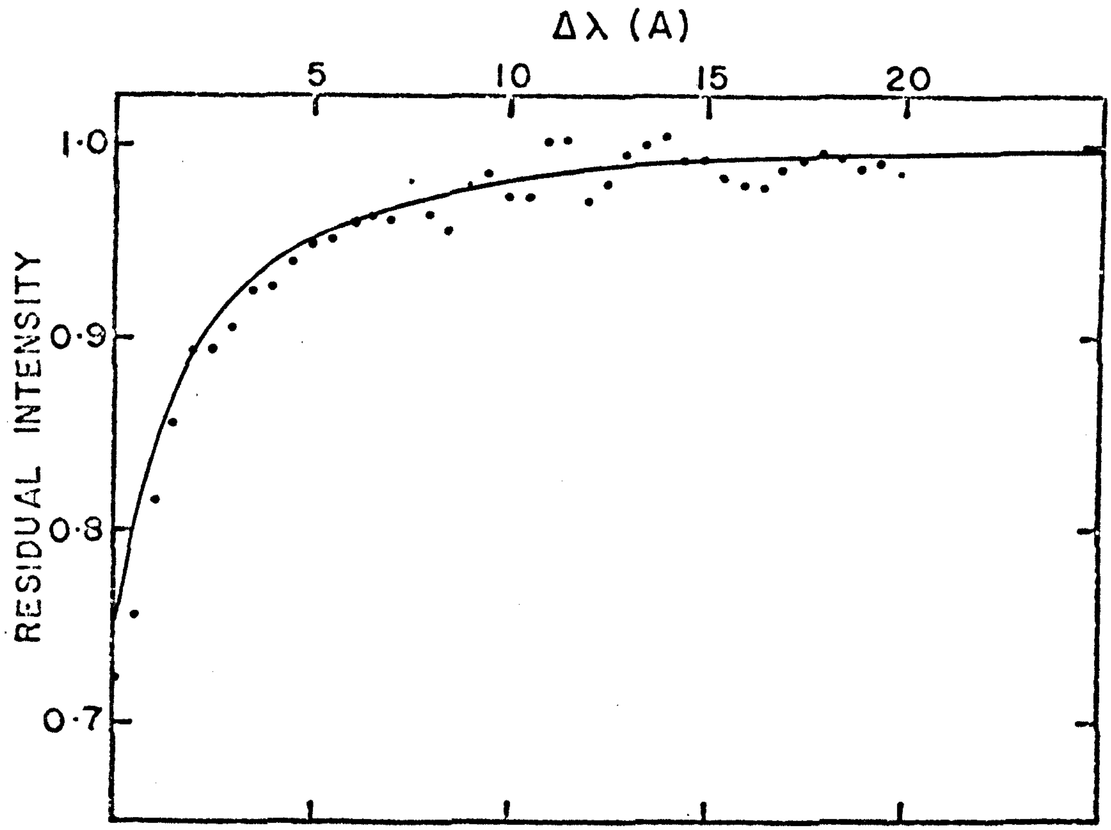

FIG. V-7 HeII λ4686 profile for HZ 44; average from 3 plates (continuum lowered 1%); computed profile for model (40 000, 5.7, 0.4)

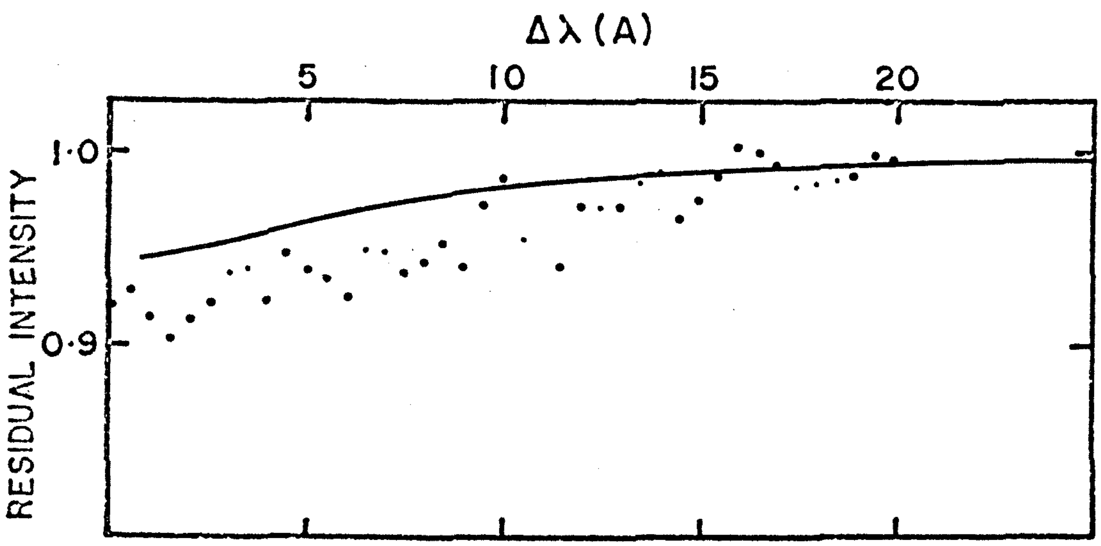

FIG. V-8 HeII λ4542 profile for HZ 44; average from 3 plates (continuum lowered 1%); computed profile for model (40 000, 5.7, 0.4)

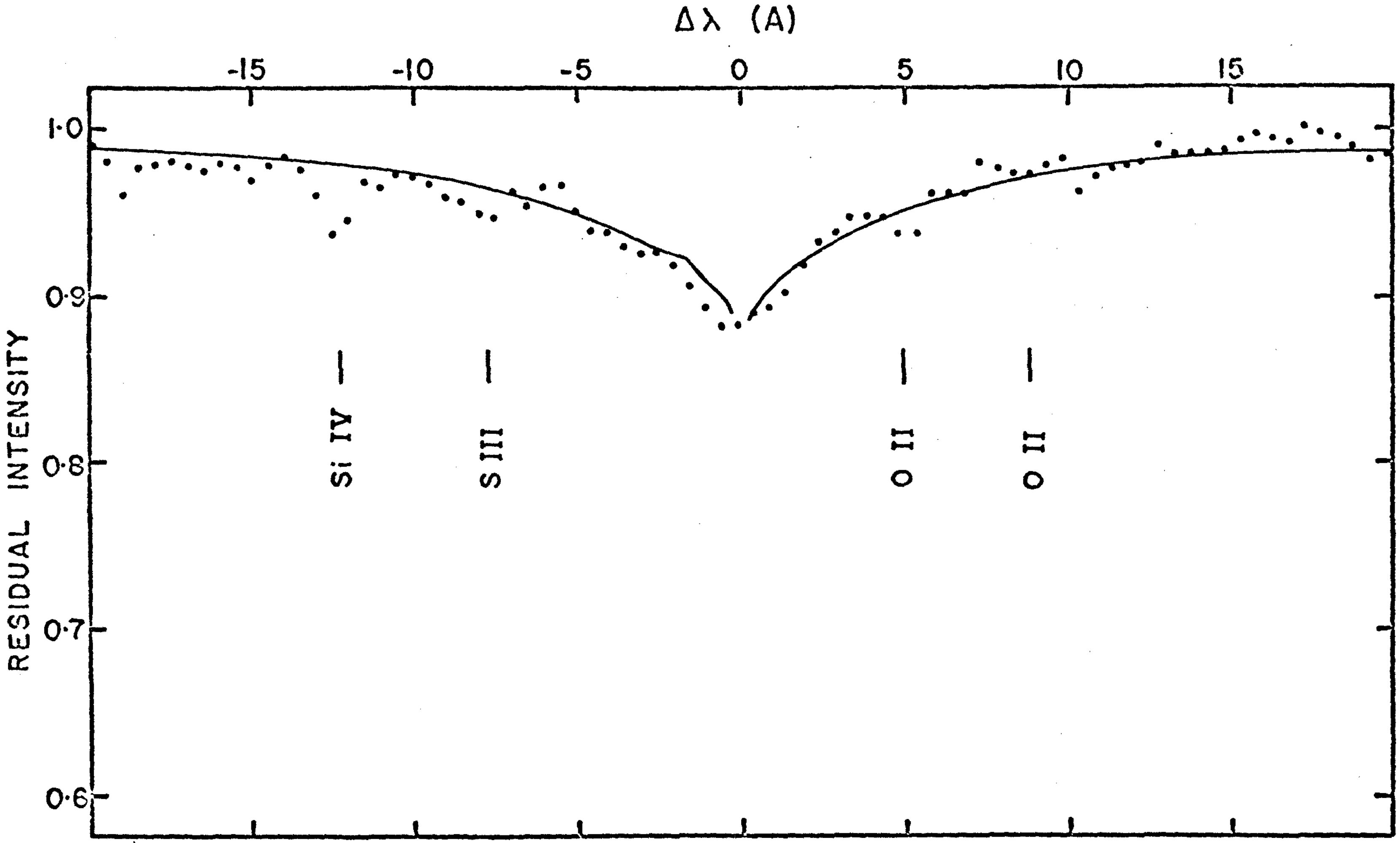

FIG. V-9 Hγ + HeII profile for +25°4655; average from 5 plates (continuum lowered 1%); computed profile for (43 000, 6.7, 0.9)

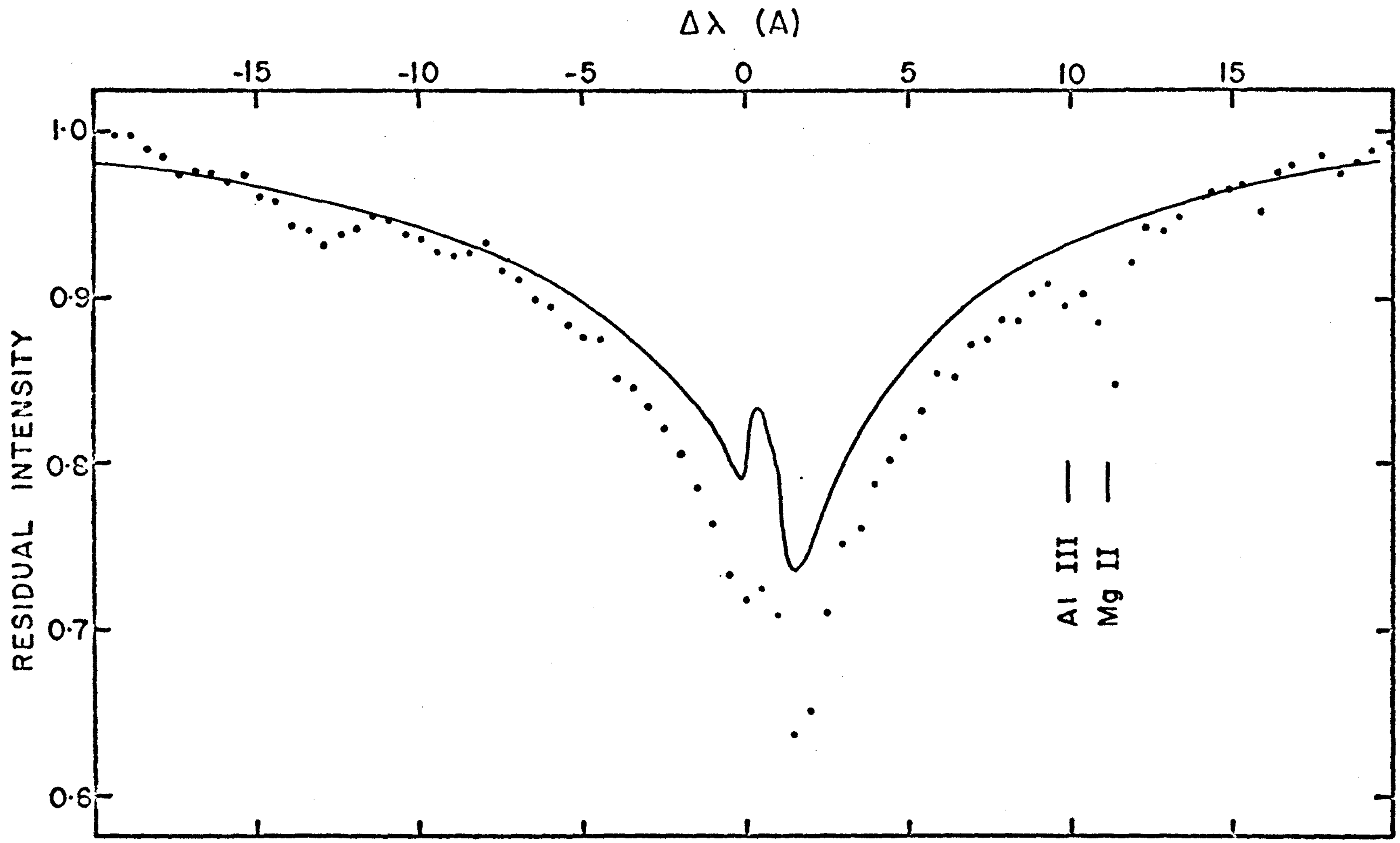

FIG. V-10 HeI λ4472 profile for +25°4655; average from 5 plates (continuum lowered 1%); computed profile for model (43 000, 6.7, 0.9)

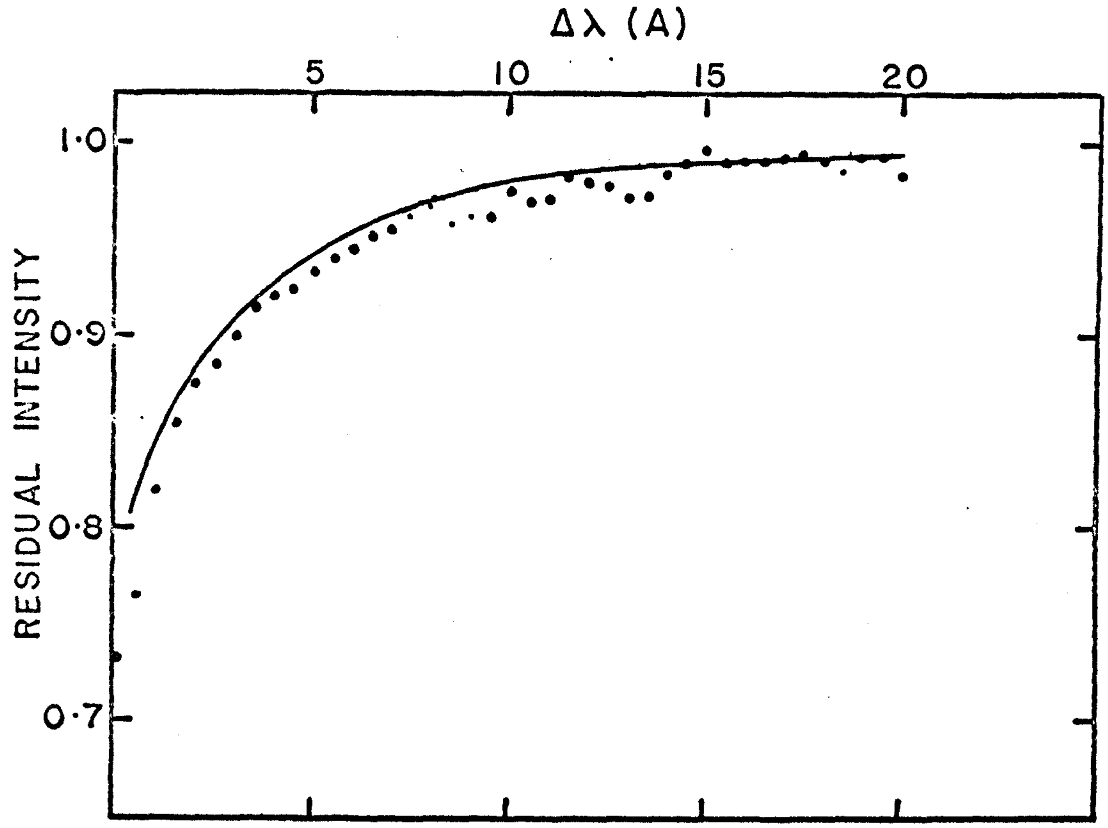

FIG. V-11 HeII λ4686 profile for +25°4655; average 5 plates (continuum lowered 1%); computed profile for (43 000, 6.7, 0.9)

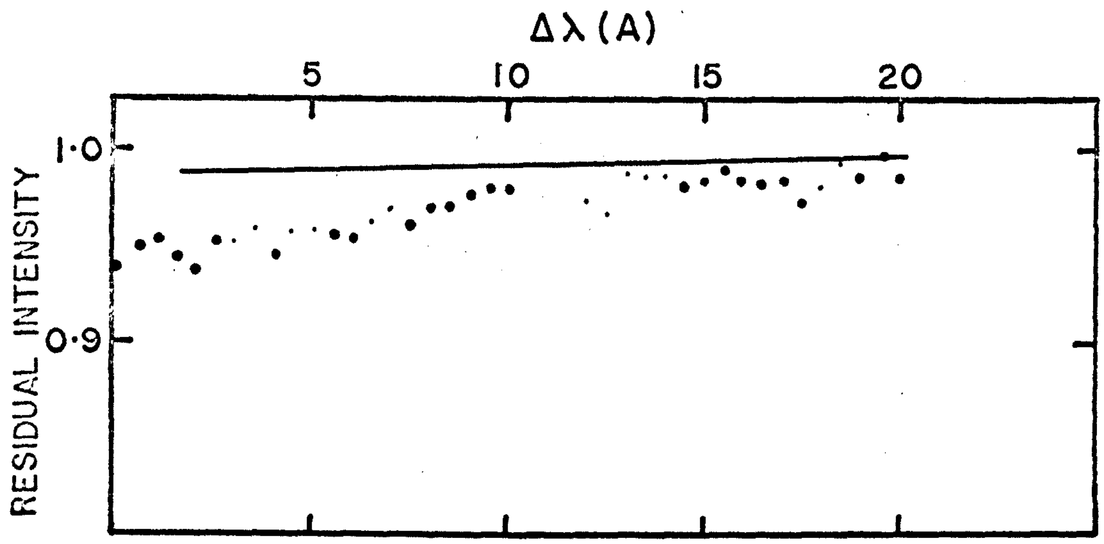

FIG. V-12 HeII λ4542 profile for +25°4655; average from 5 plates (continuum lowered 1%); computed profile for model (43 000, 6.7, 0.9)

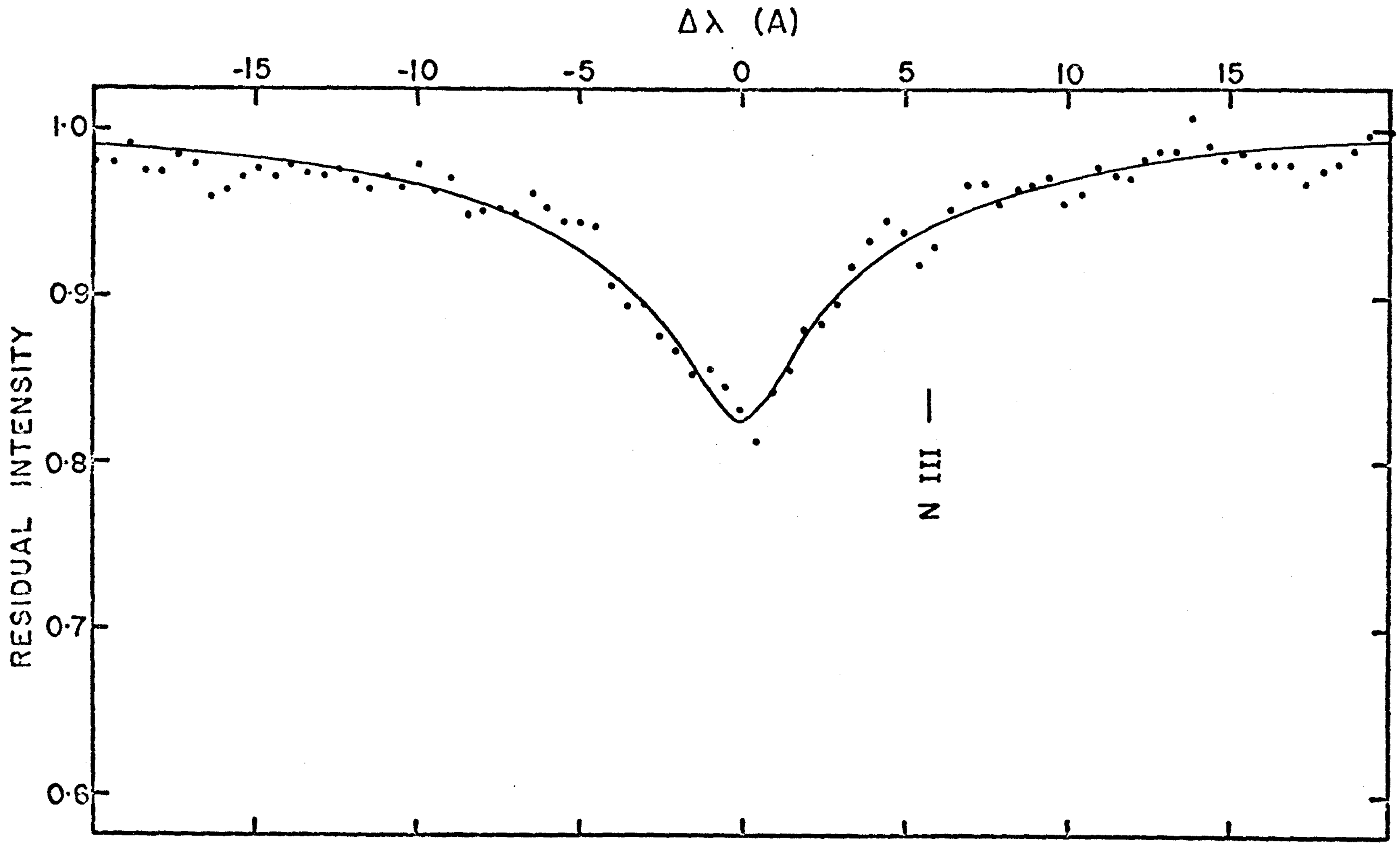

FIG. V-13 Hβ + HeII profile for +25°4655; average from 5 plates (continuum lowered 1%); computed profile for model (43 000, 6.7, 0.9); Δλ=0 at 4861.3 A

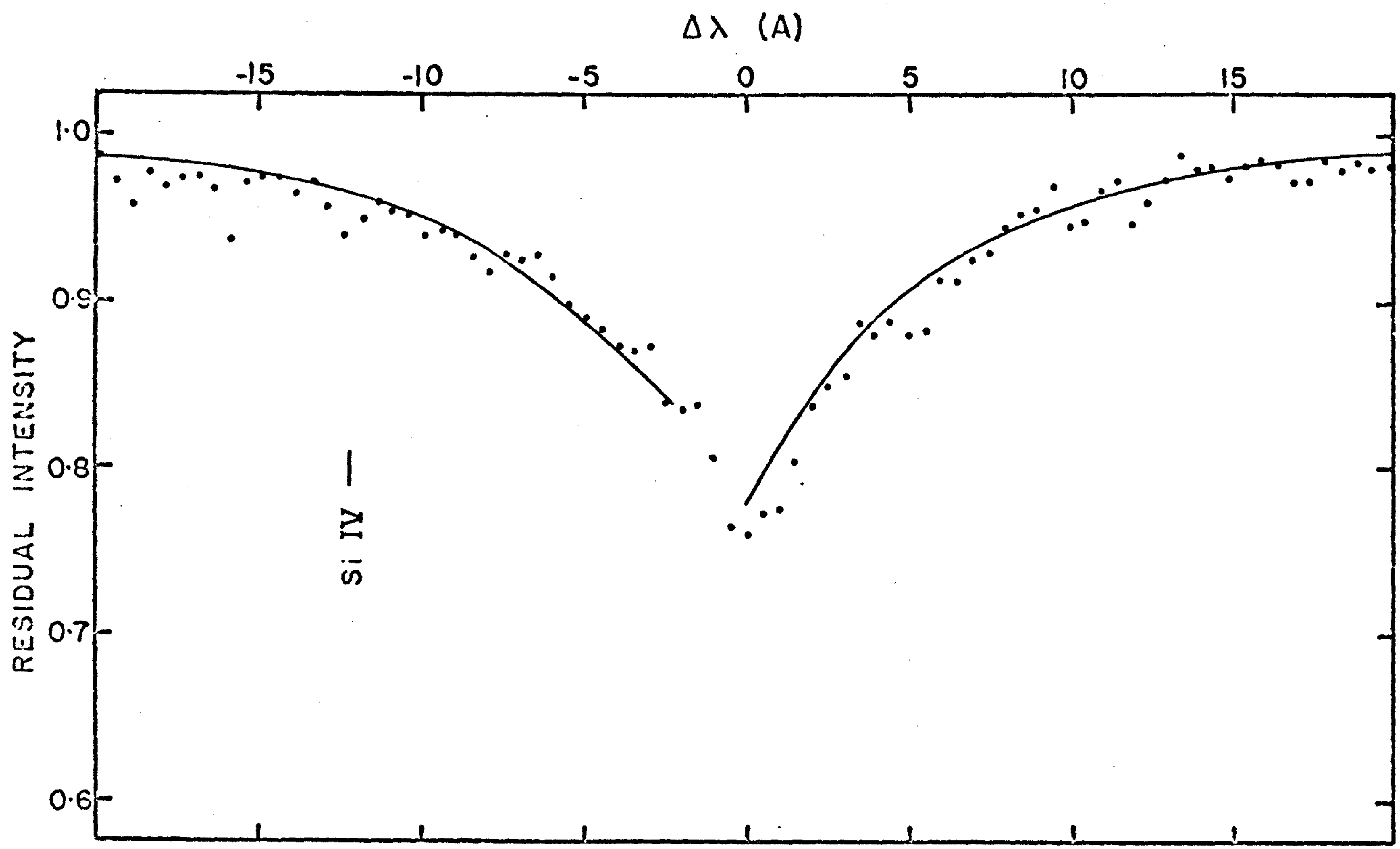

FIG. V-14 Hγ + HeII profile for HD 127493; average from 2 plates; computed profile for model (43 000, 5.7, 0.6)

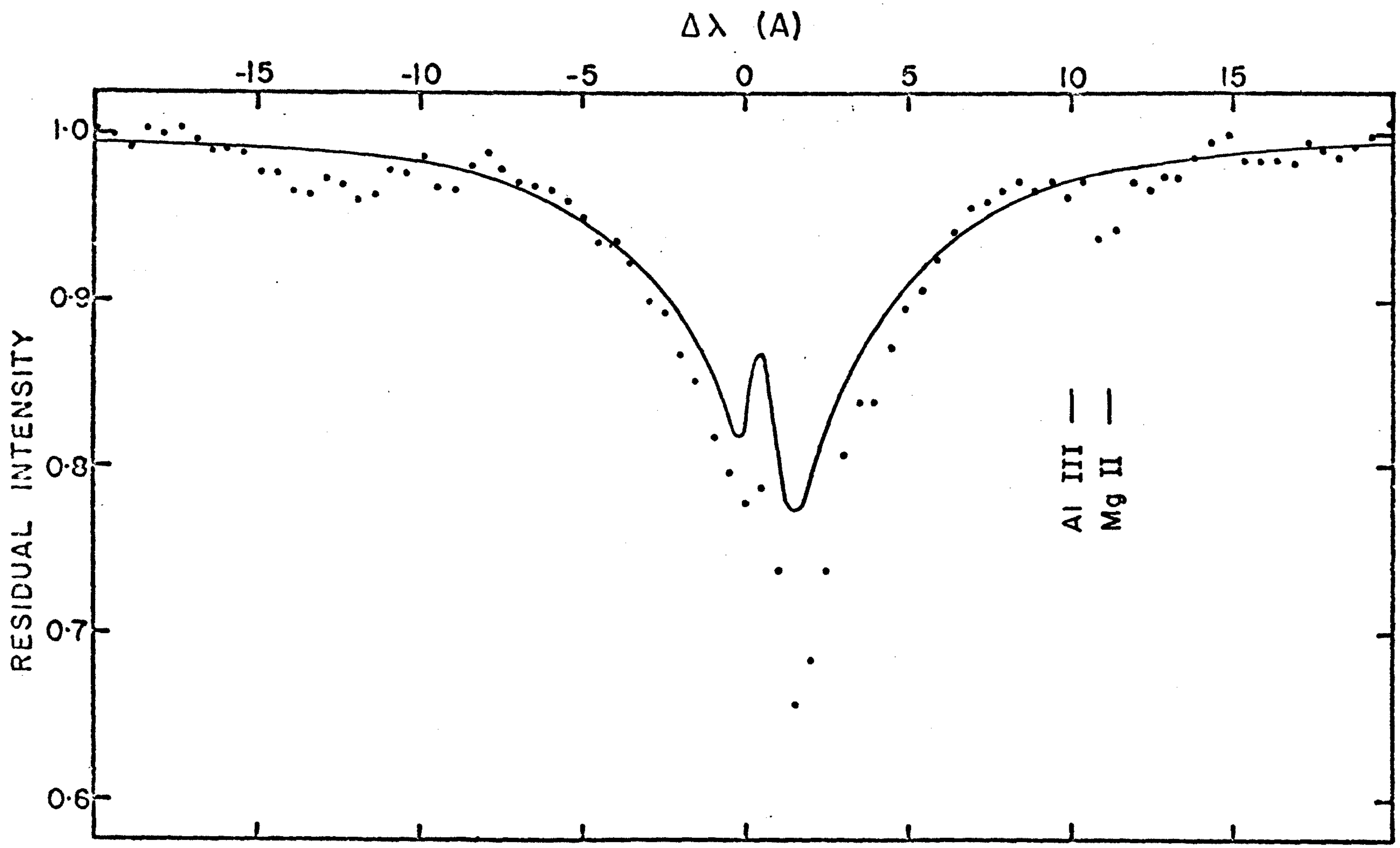

FIG. V-15 HeI λ4472 profile for HD 127493; average from 3 plates (continuum lowered 1%); computed profile for model (43 000, 5.7, 0.6)

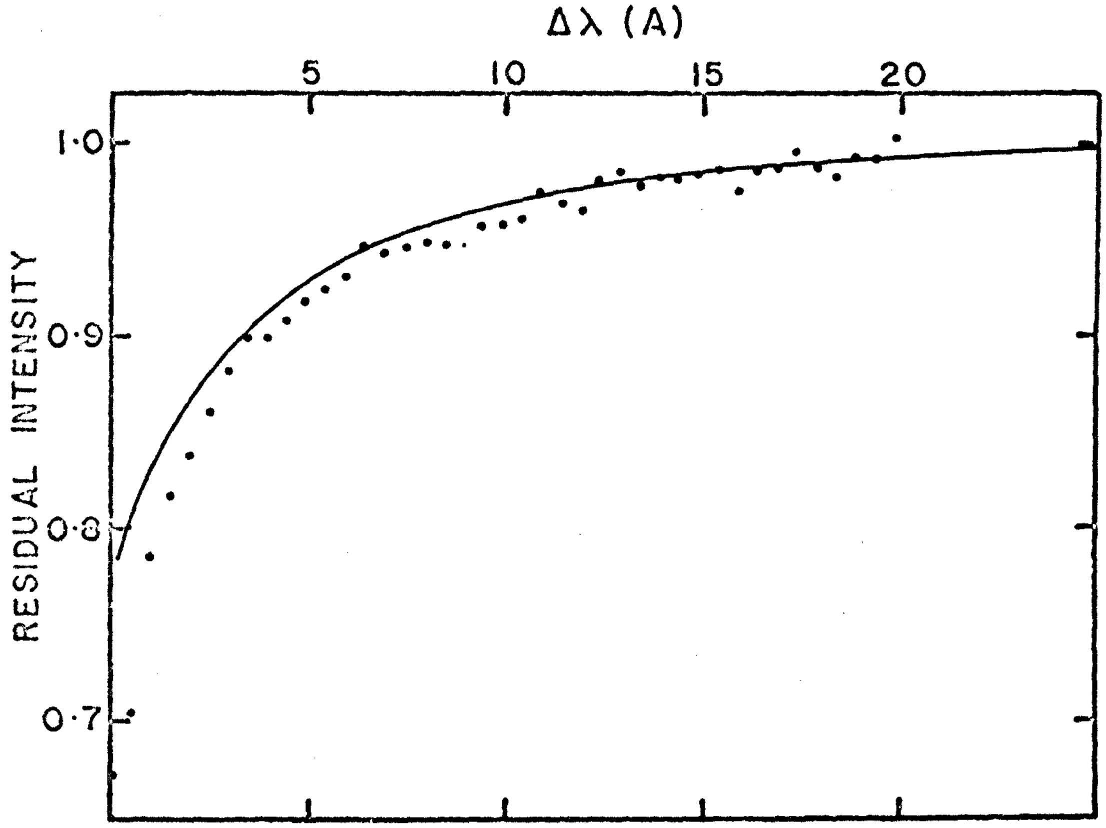

FIG. V-16 HeII λ4686 profile for HD 127493; average from 3 plates (continuum lowered 1%); computed profile for model (43 000, 5.7, 0.6)

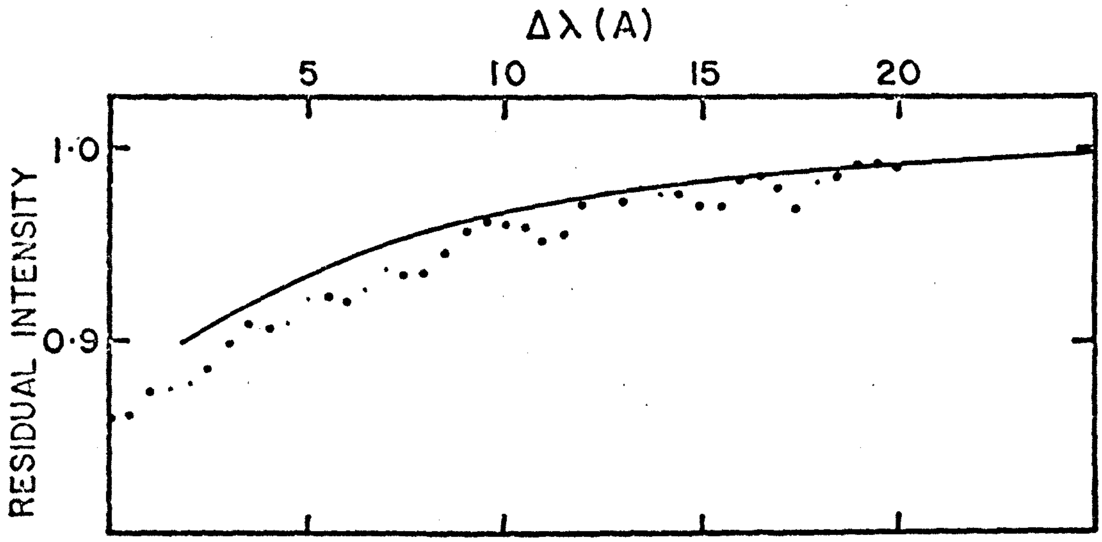

FIG. V-17 HeII λ4542 profile for HD 127493; average from 3 plates (continuum lowered 1%); computed profile for model (43 000, 5.7, 0.6)

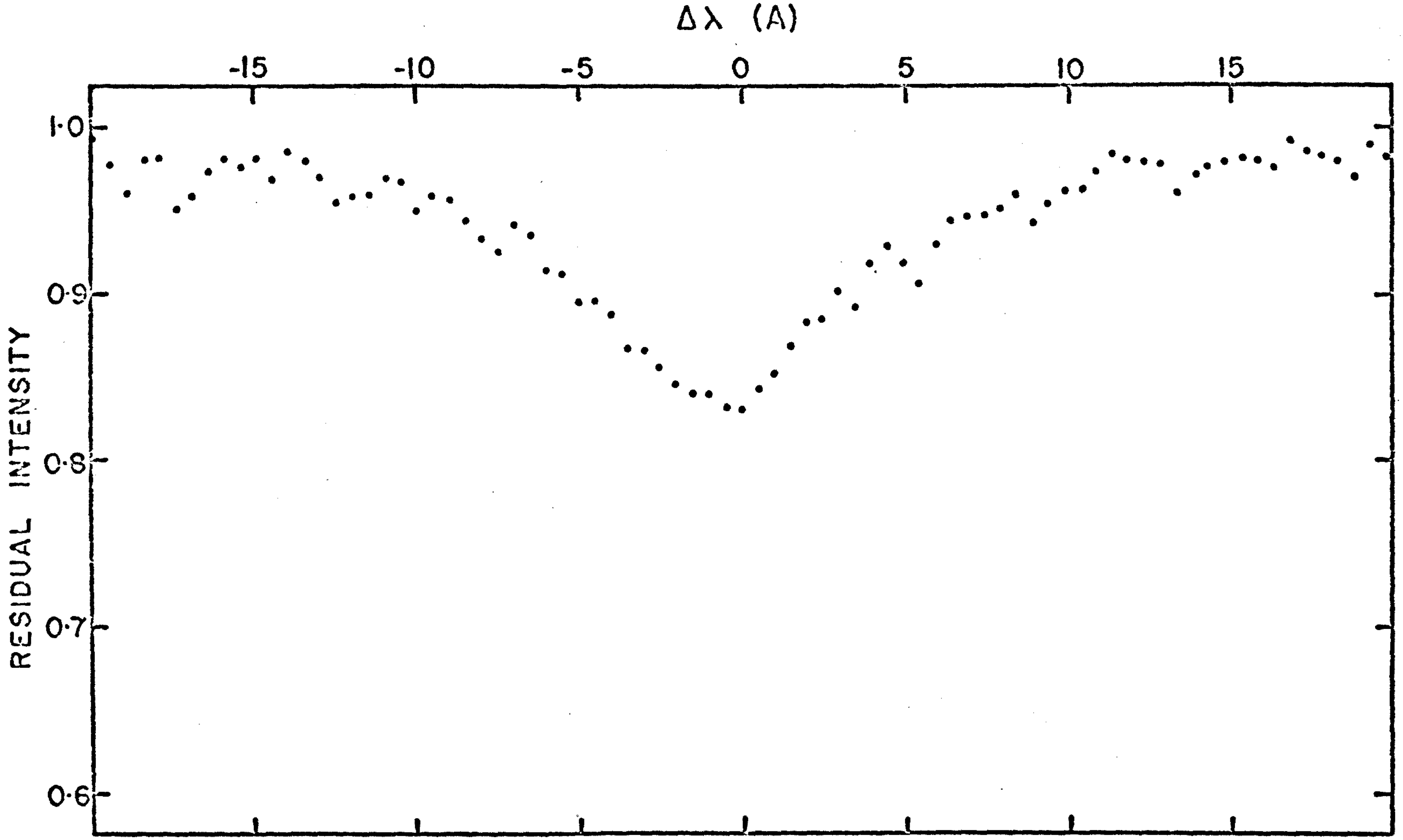

FIG. V-18 Hγ + HeII profile for +75°325; average from 2 plates

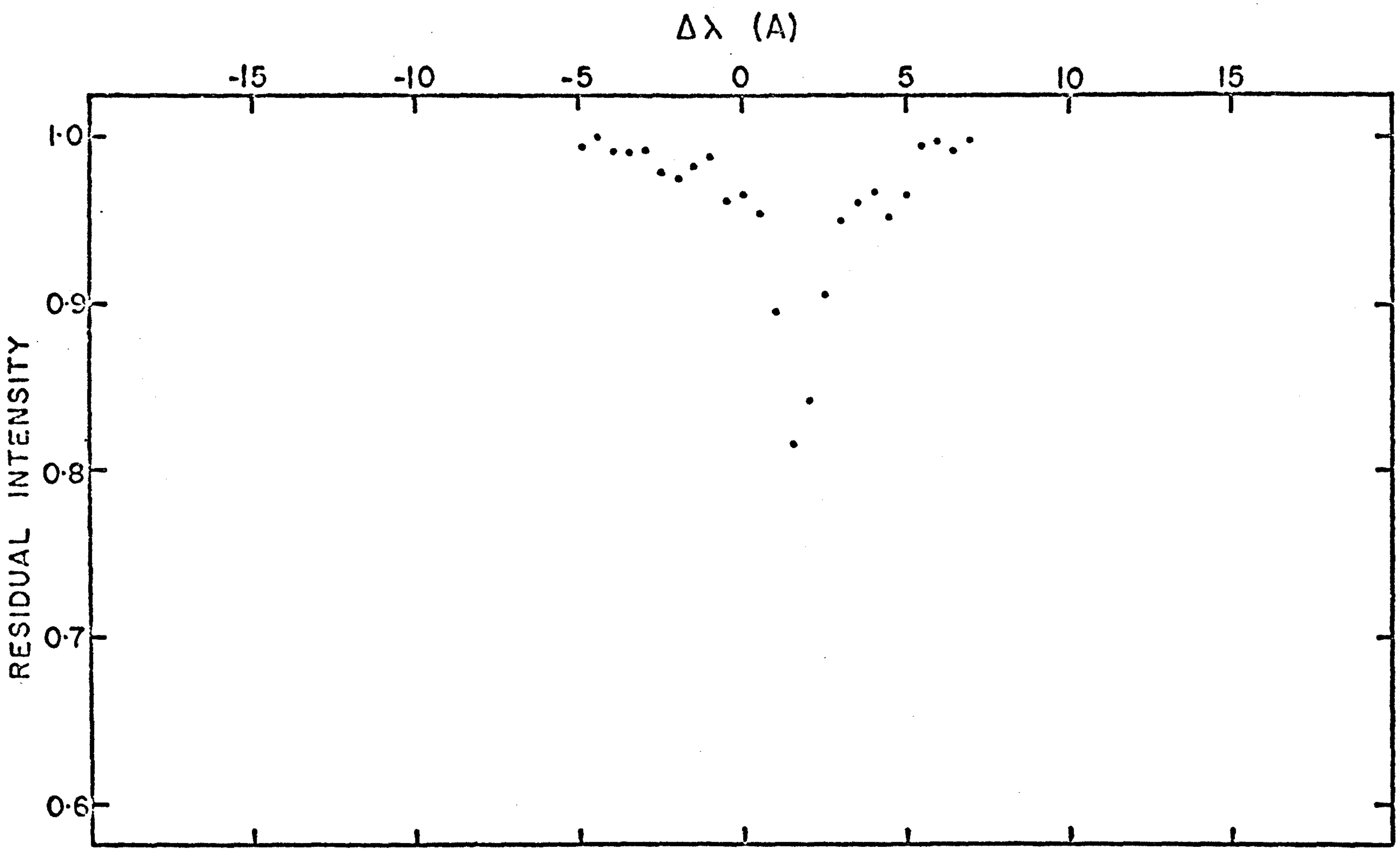

FIG. V-19 HeI λ4472 profile for +75°325; average from 2 plates

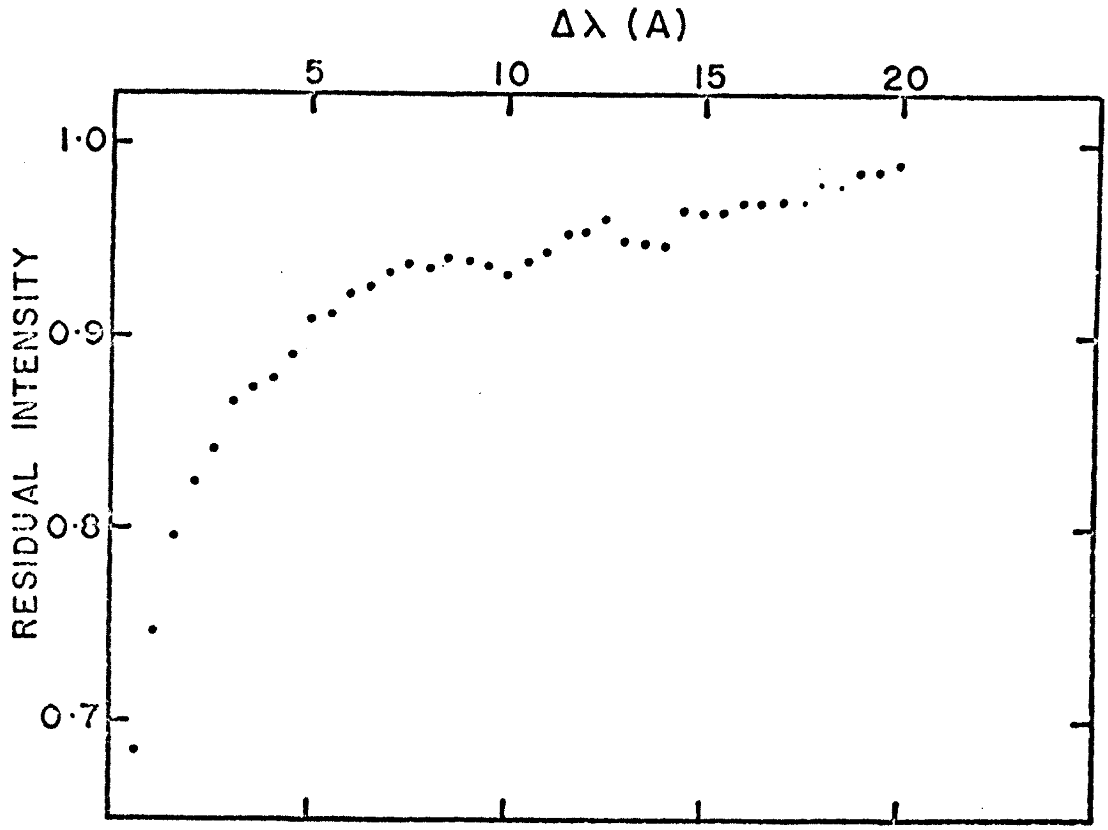

FIG. V-20 HeII λ4686 profile for +75°325; average from 2 plates

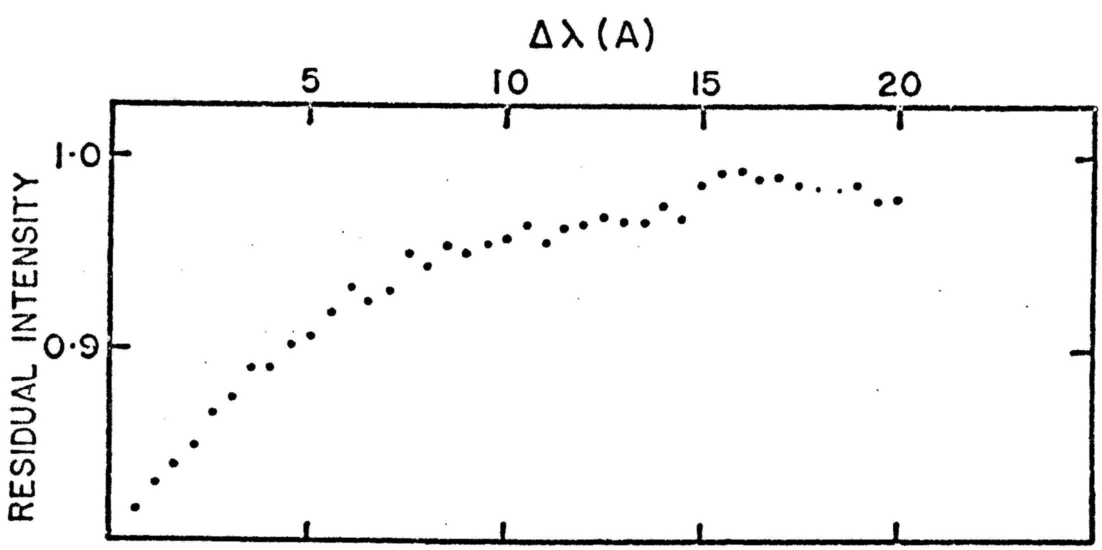

FIG. V-21 HeII λ4542 profile for +75°325; average from 2 plates

Hβ for +25°4655. Figures V-14 through V-17 give the profiles for HD 127493 and model (43 000, 5.7, 0.6), Figures V-18 through V-21 show the observed profiles for +75°325.

Abundances for several elements have been determined with the aid of the spectrum analysis program described at the beginning of the chapter. The equivalent width of a spectral line can be calculated for a given model atmosphere when the oscillator strength, quadratic Stark effect constant C_4, and the radiation damping parameter are known. Oscillator strengths have been taken from the tables by Wiese, Smith, and Glennon (1966) for hydrogen through neon when possible. Other values are taken from the tables by Griem (1964). For other sources, see Hardorp and Scholz (1969).

The Stark effect constants C_4, and the radiation damping parameters have been calculated using computer programs by Scholz. The constants C_4 are calculated from the Stark broadening parameters for neutral and singly ionized lines given by Griem (1964). In general the quadratic Stark effect constants for lines from higher ionization states are not available, in which case equivalent widths have been computed without broadening from the Stark effect. The radiation damping parameters have been computed quantum-mechanically in most cases; otherwise they have been set equal to ten times the classical value.

An abundance is derived from each line by an iterative procedure which compares the computed equivalent width with the measured equivalent width. Large micro-turbulent velocities have been inferred from the dependence of the derived abundance on the measured line strength. Underhill (1968) finds it necessary to introduce a micro-turbulent velocity on the order of 10 to 15 km/sec to explain the observed lines in the spectrum of 10 Lac. On the other hand, it has been pointed out by Hardorp and Scholz (1969) that "microturbulence" should probably be considered a fitting parameter, since its presence in O and B type stars is not really understood. They also suggest that if the outer layers of the models are too hot, the computed lines may have cores that are too shallow; saturation effects will become important sooner, and in order for the computed equivalent widths to match the measured equivalent widths, greater abundances must be assumed for the stronger lines. In the high gravity model atmospheres used for the hot subdwarfs, it is expected that broadening by the Stark effect will be important. If so, then it will be more important for the stronger lines and the dependence of the derived abundance on line strength for doubly and triply ionized atoms may occur because Stark broadening has not been included in the calculation of the equivalent widths.

The helium abundance has been iteratively derived from several of the "narrow" helium lines as a check on the model atmospheres. Unfortunately most of the lines are quite strong and use of the Voigt profile is not strictly justified. In an analysis of τ Sco, Scholz (1967) finds that the helium abundances derived from lines stronger than about 200 mA are systematically greater than the abundances derived from the weakest lines. Table V-3 lists the helium lines, the measured equivalent widths, and the derived abundances for each star.

The helium line at λ4438 is probably the best single line to use in a determination of the He abundance in that it is a comparatively weak line yet is well measured. However, its appearance in the stars HZ 44 and +25°4655 is somewhat asymmetrical and apparently shifted toward longer wavelengths by about 0.2 or 0.3 A. No identified lines are likely to make a significant contribution to the helium line. The shift is in the same direction as is predicted from the Stark effect. The line of λ4168 should also have provided a good determination of the helium abundance. However, it is

TABLE V-3 Helium Lines

Transition n	λ	HZ 44 W(mA)	HZ 44 $\log N_{He}/N_H$	+25°4655 W(mA)	+25°4655 $\log N_{He}/N_H$	HD 127493 W(mA)	HD 127493 $\log N_{He}/N_H$
2^1S-n^1P							
3	5015.673	485	-0.05	873	1.08	288:	(0.08)
4	3964.727	285	-0.68	774	0.80	260:	(-0.17)
5	3613.641	250	-0.38	275		170:	(-0.05)
2^1P-n^1s							
4	5047.736	163:	(-0.25)	420	1.20		
5	4437.549	126	-0.25	208	1.01	59	-0.04
6	4168.971	34:	(-0.54)	50:	(0.62)		
2^3P-n^3S							
4	4713.2	366	-0.20	660	1.00	353	0.25
5	4120.9	413	-0.10	650	0.95	267	0.16
6	3867.5	265	-0.25	500	0.99	180	0.14
7	3732.9	110	(-0.20)	240:	(0.50)	68:	(-0.19)
2^3S-3^3P							
	3888.646	260	-0.85	785	0.75	285	-0.27
Average			-0.20		+1.04		+0.13
Model Abundance			-0.18		+0.95		+0.18
Abundance			-0.25		+1.01		-0.04

blended with lines of NII and OII and the equivalent width is very uncertain. It is possible that the importance of the blends has been overestimated because of an intrinsic asymmetry of the helium line. The helium lines at λ3965 and λ3888 are strongly blended with hydrogen Balmer lines and thus should not be used at all for an abundance determination. Note that in +25°4655 where the Balmer lines are very weak, the abundances derived from these two lines is not as discrepant as in the other stars. The logarithmic average abundance for each star, excluding λ3965, λ3888, and lines with uncertain equivalent widths, is given at the end of Table V-3. Also given is the abundance derived from λ4438 alone.

The abundances derived from the "narrow" helium lines are reasonably consistent with the assumed model abundances. On the basis of the profile calculations and the abundance determinations above, final estimates for the helium fraction by number Y are

HZ 44	$Y = 0.38 \pm 0.05$
+25°4655	$Y = 0.91 \pm 0.05$
HD 127493	$Y = 0.50 \pm 0.10$

The nitrogen spectrum is well represented in these hot subdwarfs. An abundance has been derived from each line for which atomic data are available. The NIII lines have been analyzed without including damping due to the Stark effect; the NII lines have been analyzed with quadratic Stark parameters calculated from tables by Griem.

In Figures V-22, V-23, and V-24 the abundance derived from each nitrogen line has been plotted as a function of the measured equivalent width for HZ 44, +25°4655, and HD 127493 respectively. Small symbols are used for lines with uncertain equivalent widths or f-values. The systematic dependence of the derived abundance on the measured line strength is strongest for the NIII lines, although the NII lines in HZ 44 also show a systematic effect. The introduction of a microturbulent velocity of 10 to 15 km/sec removes most of the effect. (The Doppler velocities are on the order of 6 km/sec.) This procedure is a rather artificial one and, as can be seen from the figures, the final abundance determination is quite sensitive to whether or not a microturbulent velocity has been introduced into the line calculations. The difference between the abundance determined with v_r = 10 km/sec and v_r = 15 km/sec is not very great, however. Whether the curve of growth effect is due to microturbulence, or to underestimated damping parameters, or to theoretical profiles that are too shallow, the effect will be smallest on the weakest lines. In principle then, the weakest lines give the best abundance determination,

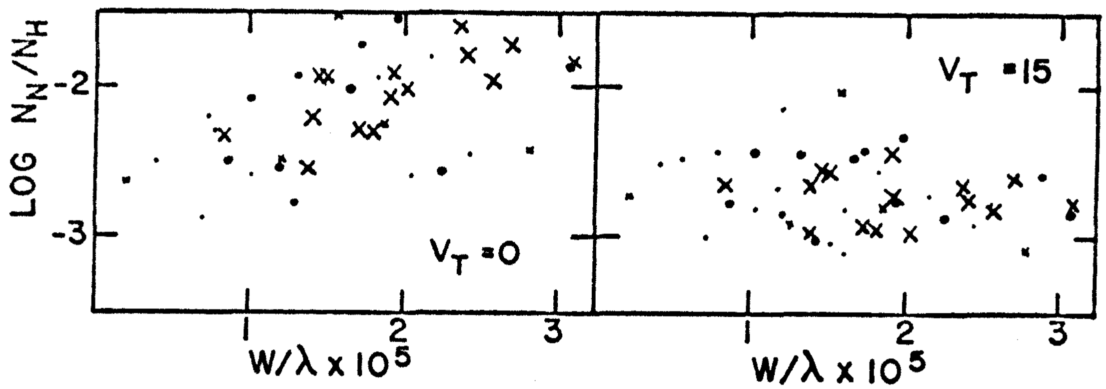

FIG. V-22 Derived abundance as a function of measured equivalent width for HZ 44; · NII; x NIII

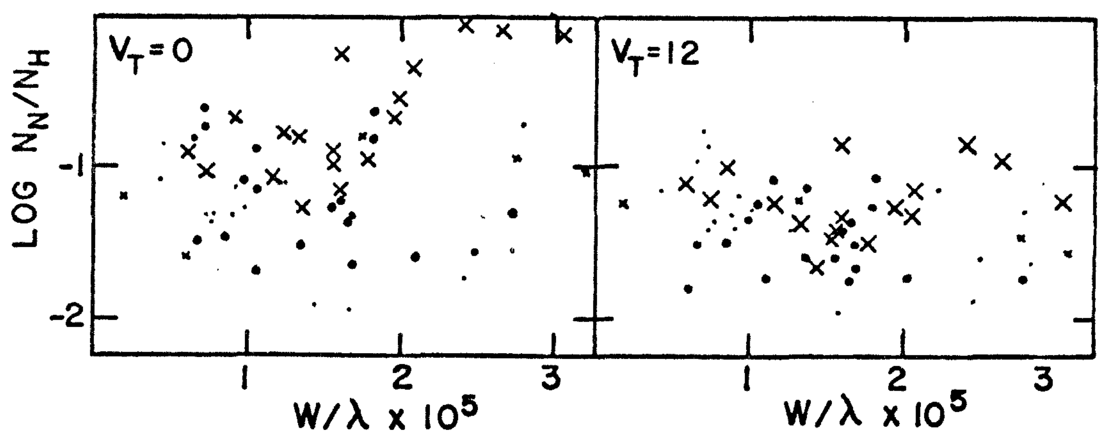

FIG. V-23 Derived abundance as a function of measured equivalent width for +25°4655; · NII; x NIII

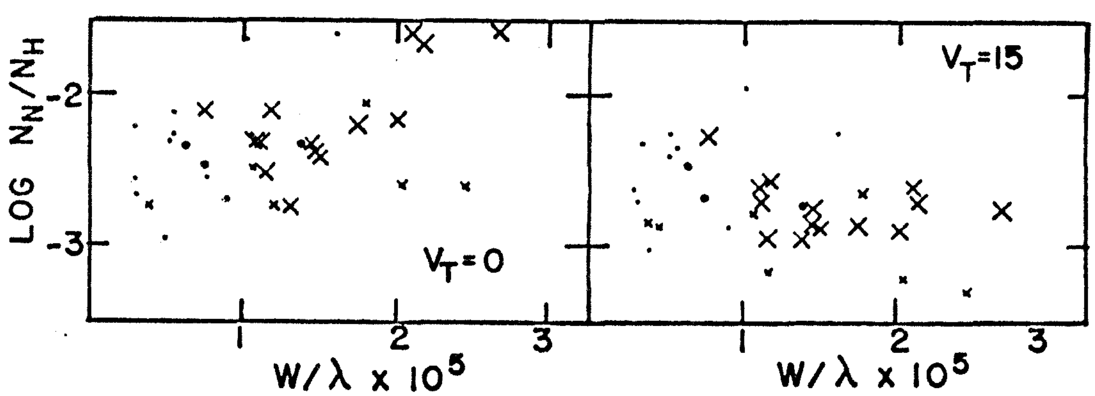

FIG. V-24 Derived abundance as a function of measured equivalent width for HD 127493; · NII; x NIII but in practice the scatter in the measured line strengths is too great, and instead a "microturbulent" velocity is used as a parameter to cause the strong lines to give the same abundance as the weak lines. The final abundance determinations for nitrogen are

HZ 44	$\log(N_N/\Sigma N_i)$	$= -2.9 \pm .2$
$+25^\circ 4655$	$\log(N_N/\Sigma N_i)$	$= -2.35 \pm .2$
HD 127493	$\log(N_N/\Sigma N_i)$	$= -3.1 \pm .2$

where the quoted errors refer to the scatter among individual measurements and do not include systematic effects.

The lines of SiIII and SiIV have been analyzed in the same manner as the nitrogen lines. The abundance determined from each silicon line is plotted as a function of the measured equivalent width for HZ 44 and $+25^\circ 4655$ in Figures V-25 and V-26 respectively, with $v_T = 0$ and with v_T equal to the value determined from the nitrogen lines. Quadratic Stark effect broadening has been included for some of the SiIII lines*. The abundances determined for silicon are

HZ 44	$\log(N_{Si}/\Sigma N_i)$	$= -4.3 \pm .3$
$+25^\circ 4655$	$\log(N_{Si}/\Sigma N_i)$	$= -3.6 \pm .3$
HD 127493	$\log(N_{Si}/\Sigma N_i)$	$= -4.6 \pm .3$

---

*Hardorp and Scholz (1969)

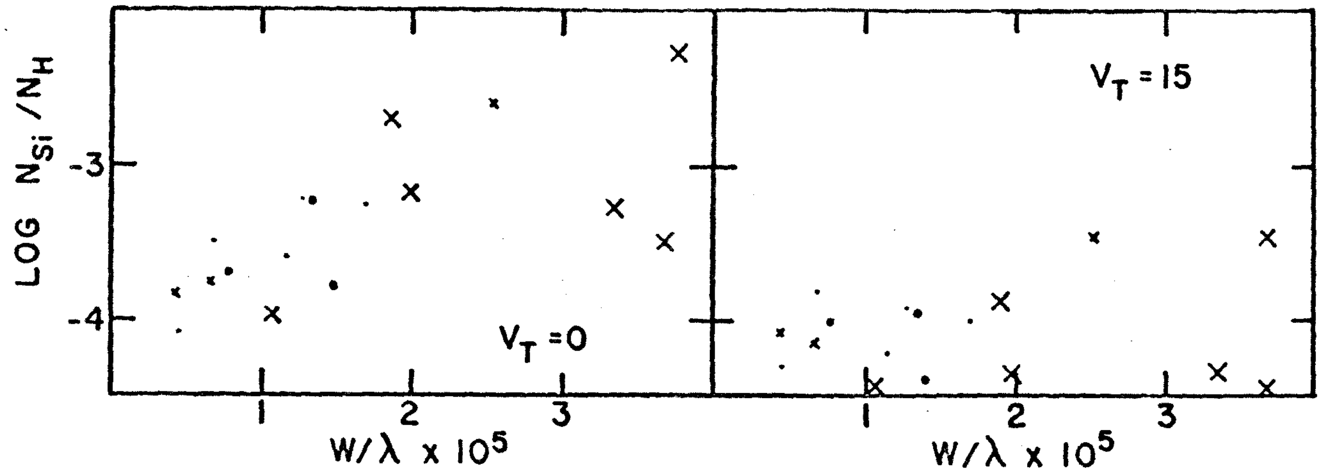

FIG. V-25 Derived abundance as a function of measured equivalent width for HZ 44; · SiIII; x SiIV

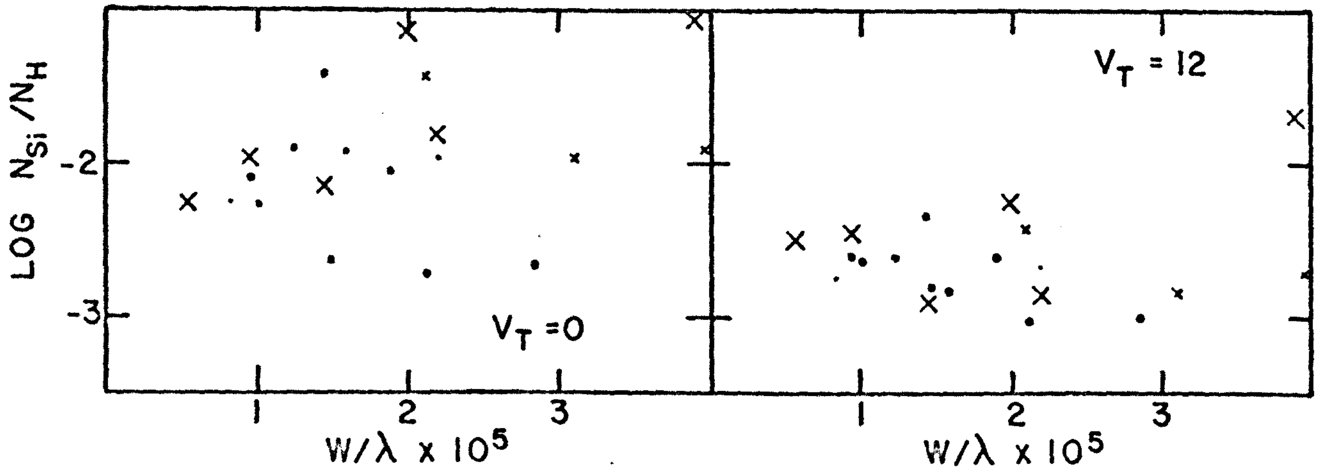

FIG. V-26 Derived abundance as a function of measured equivalent width for $+25^{o}4655$; · SiIII; x SiIV

The carbon and oxygen spectrum is very sparse. At solar abundances the CII doublet at λ4267 should be quite strong in HZ 44 and +25°4655 and there should be several moderately strong lines of CIII in HZ 44, +25°4655, and HD 127493. Similarly, there are normally many lines of OII and OIII found in the spectra of main sequence O stars. No measurable lines of carbon or oxygen have been found in HD 127493. Two weak lines of CIII (multiplet 1) have been measured in HZ 44 and in +25°4655. Table V-4 summarizes the carbon abundance information. Two very weak lines of oxygen have been measured in HZ 44 and several weak lines have been measured in +25°4655. Table V-5 summarizes the oxygen abundance data.

The abundances adopted for carbon and oxygen are

HZ 44	$\log(N_C/\Sigma N_i) = -4.9$
	$\log(N_O/\Sigma N_i) = -4.2$
+25°4655	$\log(N_C/\Sigma N_i) = -4.1$
	$\log(N_O/\Sigma N_i) = -3.5$
HD 127493	$\log(N_C/\Sigma N_i) < -4.8$
	$\log(N_O/\Sigma N_i) < -4.5$.

The neon abundance has been determined from the lines in the first multiplet of NeII. The logarithmic average abundances from these lines are

TABLE V-4 Carbon Abundance

	λ(A)	W(mA)	$\log(N_C/\Sigma N_i)$ $v_T=0$	v_T	$\log(N_C/\Sigma N_i)$
HZ 44					
CIII(1)	4647.42	38	-4.7	15	-4.9
	4650.25	58:	(-4.0)	15	(-4.4)
+25°4655					
CIII(1)	4647.42	48	-3.9	12	-4.1
	4650.25	37	-3.9	12	-4.1
HD 127493					
CIII(1)	4647.42	< 30	< -4.8	15	< -4.8
	4650.25	< 30	< -4.6	15	< -4.6

TABLE V-5 Oxygen Abundance

	λ(A)	W(mA)	$\log(N_O/\Sigma N_i)$ $v_T=0$	v_T	$\log(N_O/\Sigma N_i)$
HZ 44					
OII(1)	4649.14	23	-4.0	15	-4.2
OIII(2)	3759.87	25	-4.3	15	-4.5
+25°4655					
OII(1)	4649.14	42	-3.2	12	-3.5
OII(2)	4349.43	26	-3.4	12	-3.5
	4345.56	24	-3.1	12	-3.2
OII(3)	3749.49	37	-3.2	12	-3.4
OII(5)	4414.91	33	-3.3	12	-3.5
OII(6)	3973.26	27	-3.4	12	-3.5
OII(10)	4075.87	31	-3.5	12	-3.7
	4072.16	33	-3.3	12	-3.5
	4069.90	38	-3.2	12	-3.4
OII(15)	4590.97	27	-3.2	12	-3.4
OII(25)	4505.35	26	-3.3	12	-3.4
OII(2)	3759.87	33	-3.4	12	-3.7
HD 127493					
OIII(2)	3759.87	< 30	< -4.3	15	< -4.5

HZ 44 $\log(N_{Ne}/\Sigma\, N_i) = \begin{cases} -\ 3.3\ ;\ v_T = 0 \\ -\ 3.7\ ;\ v_T = 15 \end{cases}$

+25°4655 $\log(N_{Ne}/\Sigma\, N_i) = \begin{cases} -\ 2.7\ ;\ v_T = 0 \\ -\ 3.1\ ;\ v_T = 12 \end{cases}$.

Lines of ionized neon from multiplets 5, 52, 56, and 57 are also observed. The two lines measured from multiplet 5 appear to give abundances consistent with the abundance determined from multiplet 1. However, the lines from multiplets 52 and 56 give very discrepant abundances, more than a factor of 10 larger. All the f-values are from the compilation by Wiese et al (1966) and all are classified in class "D", that is, with errors up to 50 percent. Stark broadening parameters are available for the first seven multiplets only, so the lines from higher multiplets have been computed without damping due to the Stark effect. However, the arbitrary introduction of a Stark effect constant C_4 equal in value to the constant for multiplet 1, makes very little difference and the large discrepancy remains. It may be noted that Hardrop and Scholz (1969) also derive systematically high abundances from multiplets 52 and 56.

The magnesium abundance is derived from the only magnesium line identified in the hot subdwarf spectra - the MgII doublet at λ4481, which is blended with the red wing of the strong HeI line at λ4472. The results from this line are

	W(mA)	$\log(N_{Mg}/\Sigma N_i)$ $v_T=0$	v_T	$\log(N_{Mg}/\Sigma N_i)$
HZ 44	103	-3.6	15	-4.0
+25°4655	95	-3.7	12	-3.8
HD 127493	47		15	-4.3 .

Several lines of AlIII have been identified and measured in HZ 44 and +25°4655. The abundance has been determined from 2 lines in multiplet 3.

HZ 44 $$\log(N_{Al}/\Sigma N_i) = \begin{cases} -4.8 \; ; \; v_T = 0 \\ -5.1 \; ; \; v_T = 15 \end{cases}$$

+25°4655 $$\log(N_{Al}/\Sigma N_i) = \begin{cases} -4.2 \; ; \; v_T = 0 \\ -4.5 \; ; \; v_T = 12 \end{cases}$$

The sulfur abundance has been determined from several fairly weak lines.

HZ 44 $\log(N_S/\Sigma N_i) = \begin{cases} -4.1 \;;\; v_T = 0 \\ -4.5 \;;\; v_T = 15 \end{cases}$

+25°4655 $\log(N_S/\Sigma N_i) = \begin{cases} -3.9 \;;\; v_T = 0 \\ -4.5 \;;\; v_T = 12 \end{cases}$

Several high excitation lines of FeIII have been identified in these hot subdwarfs. The abundance determined from those lines for which f-values are available are

HZ 44 $\log(N_{Fe}/\Sigma N_i) = -3.6$

+25°4655 $\log(N_{Fe}/\Sigma N_i) = -3.5$

In Table V-6 is a summary of the abundance determinations for HZ 44, +25°4655, and HD 127493. For comparison the solar abundances as determined by Lambert and Warner (1969) are given also. The abundances, originally given in the form $\log \epsilon_i = 12.00 + \log(N_i/N_H)$, have been translated into mass fractions for more meaningful comparison. The helium abundance given for the sun is $\log \epsilon_{He} = 10.80$, and for all the stars the assumption is made that $\Sigma \mu_i N_i = \mu_H N_H + \mu_{He} N_{He} = 1$, where μ_i is the atomic weight of the element i.

Systematic errors in the abundance determinations

TABLE V-6 Chemical Abundances

	⊙	HZ 44	+25°4655	HD 127493
	$\log(\mu_i N_i/\Sigma\mu_i N_i)$	$\log(\mu_i N_i/\Sigma\mu_i N_i)$	$\log(\mu_i N_i/\Sigma\mu_i N_i)$	$\log(\mu_i N_i/\Sigma\mu_i N_i)$
H	-0.10	-0.54	-1.62	-0.70
He	-0.67	-0.15	-0.01	-0.10
C	-2.44	-4.2	-3.6	<-4.1
N	-3.00	-2.1	-1.8	-2.4
O	-2.10	-3.3	-2.8	<-3.7
Ne	-2.90	-2.7	-2.4	
Mg	-3.20	-3.0	-3.0	-3.3
Al	-4.25	-4.0	-3.7	
Si	-3.07	-3.2	-2.7	-3.5
S	-3.36	-3.3	-3.3	
Fe	-3.82	-2.1	-2.3	
CNO	-1.90	-2.05	-1.73	-2.3

are difficult to assess. The abundances are systematically higher in +25°4655 than in HZ 44 and in the sun even when expressed as mass fractions, suggesting the possibility of an error in normalization. As noted in the Introduction, and as is qualitatively evident by simply looking at the spectra, the nitrogen abundance is high and the oxygen and carbon abundances are low as compared with solar values. The abundances of these elements should be accurate to about a factor of 2, with the exception of the carbon and oxygen in HD 127493 which were not observed at all. In HZ 44 the abundances of elements heavier than oxygen are consistent with the solar values to within a factor of 2, with the exception of iron which is extremely high. In their analysis of τ Sco and λ Lep, Hardorp and Scholz (1969) find that the iron abundance derived from FeIII lines is an order of magnitude larger than the solar abundance. They note that in an analysis of ι Her the abundance derived from the FeIII lines is also an order of magnitude larger than the abundance determined from FeII lines, and suggest that the discrepancy may be caused by the oscillator strengths. Recent measurements of f-values for neutral iron lines by Garz and Kock (1969) indicate that earlier values were too large by about .7 in the logarithm, in which case at least part of the iron abundance discrepancy can be traced to the solar value.

The abundances derived for +25°4655 are, on the average, a factor of two larger than the abundances of HZ 44. The abundances derived for HD 127493 tend to be a factor of two smaller than for HZ 44.

VI. CONCLUSIONS

It was anticipated that analysis of the spectra of hot subdwarfs would provide information about the composition, temperature, and luminosity of these stars, and that reasonable conjectures could be made about their relationship with other types of stars in the HR diagram.

The four stars whose spectra have been measured in some detail were originally chosen for the quality of plate material available. The appearance of the carbon, nitrogen, and oxygen spectra was later included as one of the characteristics defining the subgroup with which this investigation is particularly concerned. Among three other stars for which there is also some observational material available, two (HZ 1 and HZ 3) appear to fall into the defined subgroup and one (GD 298) does not by virtue of its very strong carbon lines. It is difficult to estimate how many of the stars described in the literature as hot subdwarfs belong to the subgroup with strong nitrogen lines and weak carbon and oxygen lines, since studies carried out at dispersions less than about 50 A/mm will be able to distinguish only the strong hydrogen and helium lines. Among hot subdwarfs studied at high enough dispersions to detect the narrow lines of heavier elements are HD 49798 (Jaschek and Jaschek 1963) and HD 113001 (Wallerstein and Spinrad 1960) which appear to belong to the subgroup being considered, and HD 128220 (Wallerstein et al, 1963) which does not belong by virtue of having strong lines of OIII.

There is no direct evidence for the masses or distances of the four stars investigated in this paper. The indirect evidence, most of which is subject to large statistical uncertainties, falls into several categories - properties of other hot subdwarfs, mass to luminosity ratio from the model atmospheres, proper motions and radial velocities, and interstellar absorption.

As mentioned in the Introduction, only a small number of objects classified as hot subdwarfs in the literature occur in known binary systems or in clusters. Of these only one or two belong to the subgroup considered here. The visual binary ADS 8734 (= HD 113001) described by Wallerstein and Spinrad (1960) and Sturch and Wallerstein (1962) appears to consist of a main sequence F star and an O9 subdwarf with lines of NIII, NeII, and SiIV, but no oxygen or carbon lines. From the estimated difference in magnitude of the two components and a spectroscopic parallax from the FV star, an absolute magnitude of +3.6 is determined for the O star. Sturch and Wallerstein estimate less than $1\mathcal{M}_{\odot}$

(0.36 $\pm$.36$\mathcal{M}_\odot$) for the mass of the hot subdwarf, but place an upper limit of 3.4$\mathcal{M}_\odot$.

The spectroscopic binary HD 128220 described by Wallerstein, Sturch, and Klemola (1963) and Wallerstein and Wolff (1966) has a subdwarf O star with absolute magnitude about zero and a mass of 2 or 3$\mathcal{M}_\odot$, but this star does not belong to the same subgroup.

The star GS 259-8 is described by Münch and Slettebak (1959). If it belongs to the expanding Lacerta association it has an absolute magnitude of +3.5 to +4.0. At 87A/mm a few lines of NIII and SiIV are observed in addition to the strong helium lines and weak hydrogen lines.

A star classified as an O subdwarf with an absolute magnitude of about +1.2 has been found in the globular cluster NGC 6397 by Searle and Rodgers (1966). At the dispersion of 85 A/mm only hydrogen and helium lines can be definitely identified.

From the surface gravity and effective temperature of the model atmosphere a mass to luminosity ratio can be determined for each star. Letting $[X] = \log(X_*/X_\odot)$ be the logarithm of the quantity X expressed in solar units, then

$$[\mathcal{M}/L] = [g] - 4\,[T_e] \quad .$$

The mass to luminosity ratio determined from the model atmospheres is given for HZ 44, +25°4655, and HD 127493 in Table VI-1. The solar values are taken from Allen (1963). Also given in Table VI-1 are the absolute visual magnitudes and distances for several assumed masses. The distances are derived from the distance modulus $m - M_V$ assuming no absorption.

The strength of the interstellar absorption lines is related to the distance of the star in a statistical manner. Münch (1968) shows the relation between the equivalent width of the interstellar K line and distance determined by spectroscopic parallaxes; a theoretical curve of growth based on a statistical cloud model is fitted to the observations. The relation for small distances ($r \lesssim 400$ pc) is approximately $r_K(\text{pc}) \approx 2.8 W_K$ (mA), with, however, a mean error of nearly 100 percent at 200 pc. The small observed equivalent widths for the interstellar absorption lines in HZ 44, +25°4655, and HD 127493 suggest that the stars are quite close. Table VI-2 summarizes the information from the interstellar lines for these stars. It must, of course, be remembered that the equivalent widths are accurate to less than 20 percent, and that the relation between distance and the strength of the K line is statistical with very large scatter at small equivalent widths.

TABLE VI-1

Mass to Luminosity Ratio from Models

	HZ 44		+25°4655		HD 127493	
[$\mathcal{M}$/L]	-2.1		-1.2		-2.2	
$\mathcal{M}$	M_V	r(pc)	M_V	r(pc)	M_V	r(pc)
0.5	4.1	330	6.6	42	4.0	130
1.0	3.3	470	5.8	59	3.2	180
2.0	2.6	660	5.1	83	2.5	260
10.0	0.8	1480	3.3	190	0.7	580

TABLE VI-2 Interstellar Absorption

	W_K(mA)	r_K(pc)
HZ 44	87	240
+25°4655	33	90
HD 127493	29	80
+75°325	< 30	< 90
10 Lac	180	500

The star 10 Lac with a distance of 460 pc is also included in the table. The equivalent width is a photoelectric measurement by Mihalas (1964) with an estimated error of ±20 mA. Its galactic latitude is about $-16°$ and its position in the sky is about 15° from +25°4655. A linear relation between W_K and distance would imply that the distance of +25°4655 is on the order of 80 pc. However, if the interstellar absorption lines are formed in clouds which statistically occur with a frequency of 8 kpc^{-1}, it is not really possible to assume a linear relation for distances much less than about 500 pc. It may be noted that the star +75°325 ($b^{II} \approx 30°$), for which no model was computed, also has a very small interstellar absorption. The interstellar calcium line in HZ 44 ($b^{II} \approx 78°$) is weaker than the interstellar lines in horizontal branch stars at high latitudes (Greenstein 1968) suggesting that HZ 44 lies within the absorbing layer of the galaxy despite its high latitude.

The number of objects is too small for a meaningful analysis of the kinematic properties of these stars. However, the radial velocity and proper motion data available will be included for completeness.

In Table VI-3 the radial velocities are resolved into the Π, Θ, and Z components. The radial velocity of

+75°325 was derived from 1 plate. The transverse velocities, computed from the proper motions for several assumed distances, are resolved into the Π , Θ , and Z components in Table VI-4. Only the proper motions of HZ 44 and +25°4655 can be considered statistically significant. The velocities in Tables VI-3 and VI-4 are with respect to the sun. Table VI-5 gives the total Π , Θ , and Z velocities with respect to the local standard of rest for HZ 44 and +25°4655 assuming the same distances as in Table VI-4. A solar peculiar motion of $\Pi_\odot$ = -9 km/sec, $\Theta_\odot$ = +12 km/sec, and $Z_\odot$ = +7 km/sec (Delhaye 1965) has been assumed.

From consideration of the radial velocities alone, these objects appear to belong to the Older Population I. In any case there is little to suggest Extreme Population II. The interstellar absorption and mass-luminosity ratio put a stronger limit on the distance of +25°4655 than does the proper motion data. In HZ 44 the Π component of the peculiar velocity becomes surprisingly large for the larger distances.

Consideration of the preceding points suggests that a mass of about $0.5\mathcal{M}_\odot$ and an absolute visual magnitude of about +4.0 is not unreasonable for the stars HZ 44 and HD 127493. Since the mass to luminosity ratio is proportional to the surface gravity, the ten times higher gravity

TABLE VI-3 Radial Velocities

	v_{rad} (km/sec)	Π_{rad} (km/sec)	Θ_{rad} (km/sec)	Z_{rad} (km/sec)
HZ 44	-12	0	-2	-11
+25°4655	-30	4	-28	12
HD 127493	-16	12	6	-9
+75°325	(-44)	(-29)	(-24)	(-23)

TABLE VI-4

Proper Motions and Transverse Velocities

		Π_{trans} (km/sec)	Θ_{trans} (km/sec)	Z_{trans} (km/sec)
HZ 44	μ_{total} = 0".069 ±.015			
	r = 100 pc	32	-6	1
	r = 250 pc	81	-15	4
	r = 500 pc	162	-31	7
+25°4655	μ_{total} = 0".044 ±.015			
	r = 100 pc	-15	-6	-8
	r = 250 pc	-36	-15	-20
	r = 500 pc	-72	-30	-40

TABLE VI-5 Total Peculiar Velocity

	Π (km/sec)	Θ (km/sec)	Z (km/sec)
HZ 44			
r = 100 pc	23	4	-3
r = 250 pc	72	-5	0
r = 500 pc	153	-21	3
+25°4655			
r = 100 pc	-20	-22	11
r = 250 pc	-41	-31	-1
r = 500 pc	-77	-46	-21

in the model for +25°4655 makes a difference of 2.5 magnitudes in the absolute magnitude. This would make +25°4655 nearly as faint as the brightest white dwarfs for an assumed mass of $0.5\mathcal{M}_{\odot}$. While this is not out of the question, there is also the possibility that the surface gravity of the star has been overestimated, or that the mass of +25°4655 is greater than that of HZ 44 and HD 127493. If +75°325 has the same mass as the other three stars, it is likely to be more luminous because of its higher temperature.

The most striking abundance characteristics of these hot subdwarfs are the high helium and nitrogen abundances and low carbon and oxygen abundances. This strongly suggests that the material now in the outer layers of these stars has been processed in the CNO cycle. Since such abundances are not normally observed in the atmospheres of main sequence stars, it is likely that the hot subdwarfs represent an advanced stage of evolution of a star with a prior history of hydrogen burning by the CNO cycle and subsequent mixing or loss of the hydrogen-rich envelope. Nuclear processing in the star has been suggested before by Münch (1956) and by Wallerstein and Wolff (1966) as an explanation for the abundance anomalies in hot subdwarfs.

As a consequence of the relative reaction rates of the various nuclear species involved in the CNO cycle, a strong enhancement of the nitrogen abundance at the expense of depleting carbon and oxygen, is predicted at equilibrium (Caughlin and Fowler 1962). Since the relative reaction rates are temperature dependent, the equilibrium abundances depend on the temperature at which the hydrogen burning takes place. Table VI-6 gives the equilibrium abundance ratios (by number) predicted for several temperatures. At temperatures less than 16×10^6 °K, oxygen is not burned and its abundance should be unaffected. At temperatures greater than 26×10^6 °K the equilibrium abundances for carbon become greater than for oxygen.

Table VI-7 gives the observed carbon, nitrogen, and oxygen ratios for the sun, HZ 44, +25°4655, and HD 127493. The excellent agreement of the observed C, N, and O ratios in HZ 44 with the ratios predicted for $T_6 = 17$, must be considered somewhat fortuitous, since a single temperature does not describe the burning of hydrogen in an actual star, and in any case the abundance determinations are not that accurate. In addition, the process responsible for causing the nitrogen-enriched material to appear at the surface of the star is likely to affect the relative abundances.

If these stars have indeed burned hydrogen in the CNO cycle, then they must have belonged initially to the

TABLE VI-6

Predicted Carbon, Nitrogen, and Oxygen
Abundance Ratios for Equilibrium in the CNO Cycle -
Data Comes from Table 5, Caughlin and Fowler (1962)

	T_6=16	T_6=17	T_6=18	T_6=19	T_6=20
log(C/N)	-2.15	-2.11	-2.06	-2.02	-1.97
log(O/N)	-1.15	-1.31	-1.42	-1.51	-1.57
log(C/O)	-1.00	-0.80	-0.63	-0.51	-0.41

TABLE VI-7

Observed Carbon, Nitrogen, and Oxygen Ratios

	$\odot$	HZ 44	+25°4655	HD 127493
log(C/N)	+0.62	-2.0	-1.8	<-1.7
log(O/N)	+0.84	-1.3	-1.1	<-1.4
log(C/O)	-0.22	-0.7	-0.7	

upper main sequence with initial masses $1.9\mathcal{M}_\odot$ or greater, since for stars of approximately solar composition the dominant mode of hydrogen burning in that mass range is by the CNO cycle (Iben 1967). (Note that if the subdwarf in the binary system HD 113001 has as a companion an F star still on the main sequence, then the evolved subdwarf must have had an initial mass greater than that of the F star.) It is not possible to make detailed comparisons with the theoretical evolutionary models. Iben's models begin with hydrogen burning on the main sequence, continue through the red giant stage and stop at the end of core helium burning. No mass loss is considered in the evolutionary models. Cox and Giuli (1961) construct a series of static helium models making up a helium main sequence, and Cox and Salpeter (1961) consider helium models with hydrogen-rich envelopes. In the latter paper a $0.5\mathcal{M}_\odot$ model is fitted to HZ 44, but of course the static helium models shed no light on the prior history of such a star.

In Iben's evolutionary models for $3\mathcal{M}_\odot$, $5\mathcal{M}_\odot$, and $9\mathcal{M}_\odot$ stars (Iben 1965, 1966a, 1966b) hydrogen is exhausted for a mass fraction $\mathcal{M}/\mathcal{M}_* \lesssim 0.2$ at the point where the models terminate. The helium-exhausted core is somewhat smaller. At an earlier stage on the red giant branch when the luminosity source is a hydrogen burning shell, the hydrogen-exhausted core encompasses a smaller fraction of the mass, and helium burning has not yet started. Between this point and a hot subdwarf which displays surface abundances expected from a helium core, there is a large theoretical gap, which at this time can only be filled by conjecture.

Both mixing and mass loss are possible mechanisms for bringing the processed material to the surface. Iben's models indicate that during the giant phase a deep convection zone develops in the extended envelope. This region can extend as far as the hydrogen burning shell and thus bring nitrogen-enriched material to the surface. However, because of the very much larger mass of the envelope, the nitrogen to carbon ratio is enhanced by only a factor of about three as compared with the enhancement by more than a factor of a hundred in the hot subdwarfs. A large amount of mass loss is thus a necessary sequel to Iben's models if they are to represent the early history of the hot subdwarfs. Of course, it has been realized for some time that mass loss must be important at some phase in the evolution of most stars of mass greater than $1\mathcal{M}_\odot$. However, if the mass loss does not occur in the red giant phase or soon after, it is possible that helium burning in a shell source would eventually deplete the helium core.

The very low rotational velocities (vsini $\lesssim$ 20 km/sec) tend to favor mass loss. It is likely that the rotational velocities on the main sequence were fairly high. With the surface gravity up by a factor of fifty, the radius must be smaller by at least a factor of seven. If each mass shell were to conserve angular momentum, then an increase by a factor of seven in the rotational velocity would be implied. A large angular momentum loss is probably required in order to explain the observed low velocities.

The helium abundances derived for HZ 44, +25°4655, and HD 127493 are $Y \approx 0.4$, $Y \approx 0.9$, and $Y \approx 0.5$ respectively. There are several possible explanations for the intermediate values of the helium abundance. Mixing with varying amounts of hydrogen-rich envelope material may have occurred. The star may have begun on the main sequence with a mass in the range $1.1\mathcal{M}_\odot < \mathcal{M}_* < 1.9\mathcal{M}_\odot$ in which case hydrogen is burned both in the p-p chain and in the CNO cycle. Alternatively hydrogen burning in the CNO cycle may have been interrupted before going to completion. Calculations by Caughlin (1965) describe the approach to equilibrium of the CNO cycle and detailed tables are presented for $T_6 = 20$. A helium to CNO abundance of log (He/CNO) $\approx$ 2.5 as has been determined for HZ 44 occurs at a point where the CNO elements are already essentially in equilibrium. For initial CNO ratios of approximately solar composition, the predicted ratios are such that the C/N ratio equals the equilibrium value, the O/N ratio is somewhat greater than the equilibrium value, and the C/O ratio is somewhat less.

The chemical compositions observed in the hot subdwarfs investigated in this paper can thus be well explained by theoretical calculations based on hydrogen burning in the CNO cycle. From the main sequence masses involved, from the total heavy element abundance, and more weakly from the radial velocities, it seems likely that these stars are older Population I objects. It is clear that the preceding discussion cannot apply to such objects as the hot subdwarf in the globular cluster NGC 6397 described by Searle and Rodgers (1966). There may be Population II analogues of the stars described. If so, the nuclear history will have been quite different and it is likely that at high enough dispersion the spectra would be distinguishable.

Appendix MODEL ATMOSPHERE DATA

The models used in line profile and abundance calculations are presented here. Tables A-1, A-2, and A-3 give the model data as a function of optical depth for the stars HZ 44, $+25^{\circ}4655$, and HD 127493 respectively. The first column gives the optical depth at the standard wavelength 912 A, the second column gives the temperature, the third column the total gas pressure, the fourth column the electron pressure, and the fifth column the optical depth at 4000 A. Table A-4 gives the same data for the model (43 000, 6.7, 0.9, M), which is the same as the model given in Table A-2 except that opacity due to carbon, nitrogen, oxygen, and neon has been included. Figures A-1, A-2, A-3, and A-4 show the flux errors as a function of the standard depth for the four models. Figures A-5, A-6, A-7, and A-8 show the flux derivatives for the four models.

TABLE A-1 Model (40 000, 5.7, 0.4) for HZ 44

Te = 40 000	log g = 5.7	Y = 0.4

log τ_{912}	T	log P	log P_e	log τ_{4000}
-5.000	29890	1.32	1.08	-4.98
-4.833	29340	1.57	1.31	-4.81
-4.667	30010	1.70	1.44	-4.63
-4.500	29390	1.84	1.57	-4.45
-4.333	29310	2.02	1.74	-4.27
-4.167	29210	2.20	1.92	-4.09
-4.000	29130	2.37	2.08	-3.89
-3.833	29090	2.55	2.25	-3.69
-3.667	29080	2.72	2.42	-3.47
-3.500	29120	2.89	2.59	-3.25
-3.333	29200	3.06	2.77	-3.01
-3.167	29340	3.22	2.92	-2.76
-3.000	29570	3.38	3.08	-2.51
-2.833	29880	3.53	3.23	-2.25
-2.667	30270	3.67	3.37	-2.00
-2.500	30740	3.81	3.52	-1.74
-2.333	31290	3.95	3.66	-1.50
-2.167	31920	4.09	3.78	-1.26
-2.000	32670	4.21	3.91	-1.03
-1.833	33560	4.34	4.04	-0.80
-1.667	34570	4.46	4.16	-0.58
-1.500	35570	4.57	4.28	-0.37
-1.333	36420	4.68	4.39	-0.16
-1.167	39600	4.79	4.51	+0.03
-1.000	41520	4.88	4.61	0.22
-0.833	43260	4.96	4.71	0.41
-0.667	45000	5.05	4.79	0.59
-0.500	46920	5.14	4.89	0.77
-0.333	49160	5.23	4.99	0.96
-0.167	51850	5.33	5.09	1.15
0.000	55070	5.43	5.19	1.33
0.167	58820	5.54	5.31	1.52
0.333	63080	5.66	5.43	1.72
0.500	67800	5.78	5.55	1.91
0.667	72940	5.91	5.67	2.10
0.833	78420	6.03	5.79	2.29
1.000	84210	6.16	5.93	2.49
1.167	90580	6.29	6.05	2.68
1.333	98160	6.41	6.17	2.87

TABLE A-2 Model (43 000, 6.7, 0.9) for +25° 4655

Te = 43 000 log g = 6.7 Y = 0.9

log τ_{912}	T	log P	log P_e	log τ_{4000}
-5.000	30310	2.56	2.29	-4.72
-4.833	28440	2.81	2.51	-4.52
-4.667	28540	2.95	2.64	-4.31
-4.500	28500	3.09	2.79	-4.08
-4.333	28500	3.25	2.95	-3.83
-4.167	28580	3.41	3.11	-3.58
-4.000	28740	3.56	3.26	-3.32
-3.833	28980	3.71	3.41	-3.06
-3.667	29300	3.85	3.55	-2.81
-3.500	39700	3.98	3.68	-2.57
-3.333	30170	4.11	3.81	-2.33
-3.167	30690	4.24	3.94	-2.10
-3.000	31240	4.36	4.05	-1.88
-2.833	31810	4.47	4.17	-1.66
-2.667	32380	4.59	4.29	-1.45
-2.500	32970	4.70	4.40	-1.24
-2.333	33580	4.81	4.50	-1.04
-2.167	34242	4.91	4.61	-0.84
-2.000	34980	5.02	4.72	-0.65
-1.833	35820	5.12	4.82	-0.46
-1.667	36710	5.22	4.92	-0.27
-1.500	37490	5.32	5.02	-0.08
-1.333	37010	5.42	5.13	+0.10
-1.167	39660	5.52	5.23	0.28
-1.000	43080	5.60	5.33	0.45
-0.833	45150	5.67	5.41	0.61
-0.667	47050	5.73	5.49	0.76
-0.500	49160	5.80	5.58	0.92
-0.333	51780	5.87	5.65	1.09
-0.167	54820	5.94	5.74	1.26
0.000	58300	6.02	5.83	1.43
0.167	62170	6.11	5.92	1.61
0.333	66420	6.21	6.02	1.80
0.500	71010	6.32	6.13	1.99
0.667	76180	6.43	6.25	2.18
0.833	82010	6.55	6.36	2.37
1.000	88510	6.67	6.49	2.56
1.167	95620	6.80	6.61	2.75
1.333	103360	6.92	6.73	2.94

TABLE A-3 Model (43 000, 5.7, 0.6) for HD 127493

Te = 43 000 log g = 6.7 Y = 0.6

log τ_{912}	T	log P	log P_e	log τ_{4000}
-5.000	33100	1.34	1.13	-4.97
-4.833	32680	1.58	1.36	-4.80
-4.667	33360	1.71	1.49	-4.63
-4.500	33140	1.84	1.63	-4.45
-4.333	32900	2.01	1.79	-4.26
-4.167	32910	2.18	1.96	-4.07
-4.000	32700	2.35	2.12	-3.87
-3.833	32530	2.53	2.28	-3.66
-3.667	32300	2.71	2.45	-3.44
-3.500	32110	2.89	2.62	-3.21
-3.333	32020	3.06	2.80	-2.98
-3.167	32030	3.24	2.96	-2.73
-3.000	32170	3.41	3.13	-2.48
-2.833	32450	3.57	3.28	-2.22
-2.667	32870	3.72	3.44	-1.97
-2.500	33390	3.87	3.58	-1.71
-2.333	34000	4.00	3.72	-1.47
-2.167	34690	4.14	3.85	-1.23
-2.000	35470	4.26	3.98	-1.00
-1.833	36360	4.38	4.09	-0.78
-1.667	37400	4.49	4.21	-0.56
-1.500	38600	4.59	4.32	-0.36
-1.333	40070	4.68	4.42	-0.16
-1.167	41790	4.77	4.52	+0.03
-1.000	43580	4.86	4.62	0.22
-0.833	45280	4.94	4.71	0.41
-0.667	47130	5.03	4.80	0.60
-0.500	49220	5.12	4.90	0.78
-0.333	51640	5.22	5.00	0.97
-0.167	54460	5.32	5.11	1.16
0.000	57780	5.43	5.21	1.35
0.167	61560	5.54	5.33	1.55
0.333	65770	5.66	5.45	1.74
0.500	70270	5.78	5.58	1.93
0.667	75140	5.91	5.70	2.13
0.833	80630	6.03	5.82	2.32
1.000	86890	6.16	5.95	2.51
1.167	94150	6.28	6.07	2.71
1.333	102660	6.41	6.20	2.90

TABLE A-4 Model (43 000, 6.7, 0.9, M) for +25° 4655 including Opacity due to C, N, O, Ne

Te = 43 000 log g = 6.7 Y = 0.9

log τ_{912}	T	log P	log P_e
-5.000	27850	2.63	2.33
-4.833	27890	2.87	2.57
-4.667	27920	2.99	2.69
-4.500	27940	3.12	2.82
-4.333	28030	3.27	2.97
-4.167	28160	3.42	3.12
-4.000	28370	3.57	3.27
-3.833	28650	3.71	3.41
-3.667	29000	3.85	3.55
-3.500	29420	3.98	3.68
-3.333	29900	4.11	3.81
-3.167	30410	4.23	3.93
-3.000	30960	4.35	4.05
-2.833	31510	4.47	4.17
-2.667	32070	4.58	4.29
-2.500	32650	4.69	4.39
-2.333	33250	4.80	4.50
-2.167	33890	4.91	4.61
-2.000	34620	5.02	4.72
-1.833	35440	5.12	4.82
-1.667	36310	5.22	4.93
-1.500	37210	5.32	5.03
-1.333	37690	5.42	5.13
-1.167	39990	5.51	5.23
-1.000	42273	5.60	5.33
-0.833	44510	5.67	5.42
-0.667	47220	5.74	5.50
-0.500	50020	5.80	5.59
-0.333	52663	5.87	5.66
-0.167	55190	5.94	5.74
0.000	57700	6.02	5.82
0.167	60280	6.11	5.92
0.333	62960	6.20	6.01
0.500	65800	6.30	6.12
0.667	68800	6.40	6.22
0.833	72010	6.51	6.32
1.000	75450	6.62	6.43
1.167	79120	6.73	6.54
1.333	83100	6.83	6.65

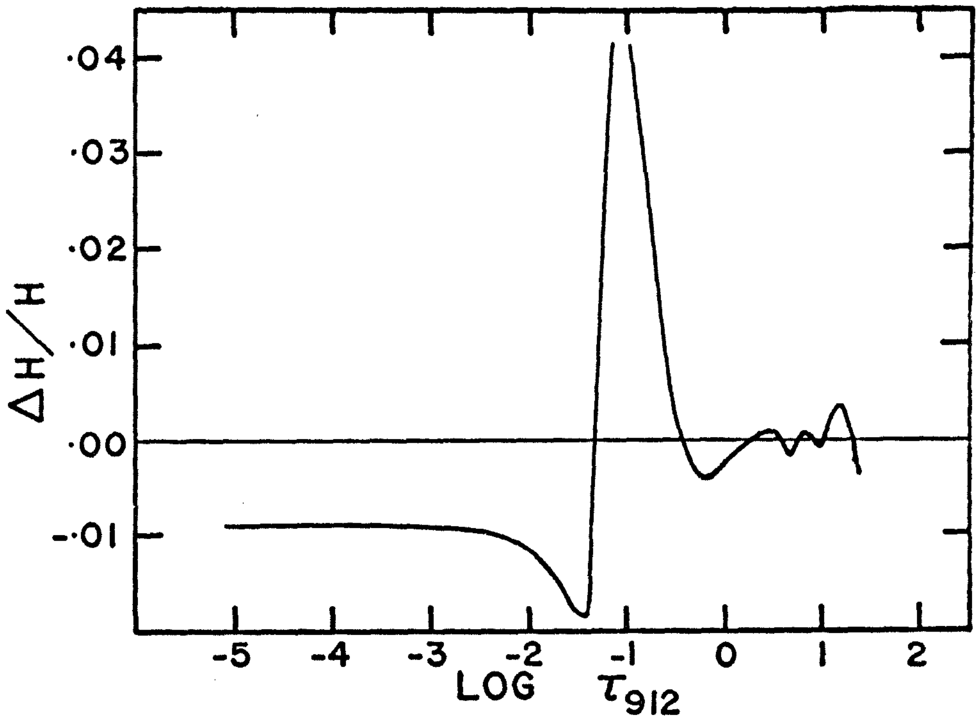

FIG. A-1 Flux error for model (40 000, 5.7, 0.4)

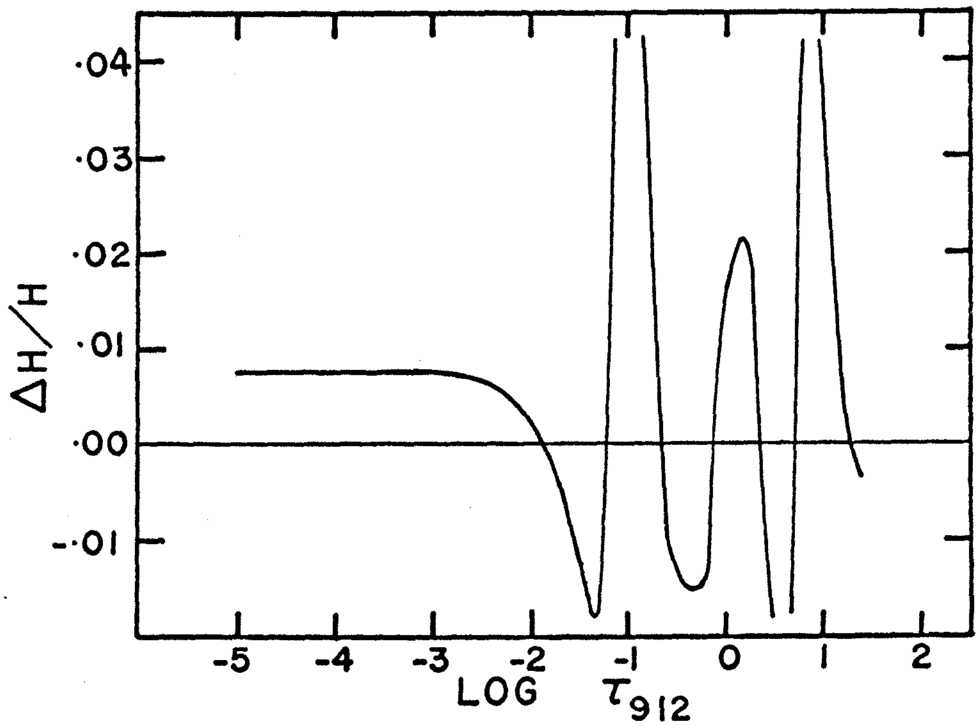

FIG. A-2 Flux error for model (43 000, 6.7, 0.9)

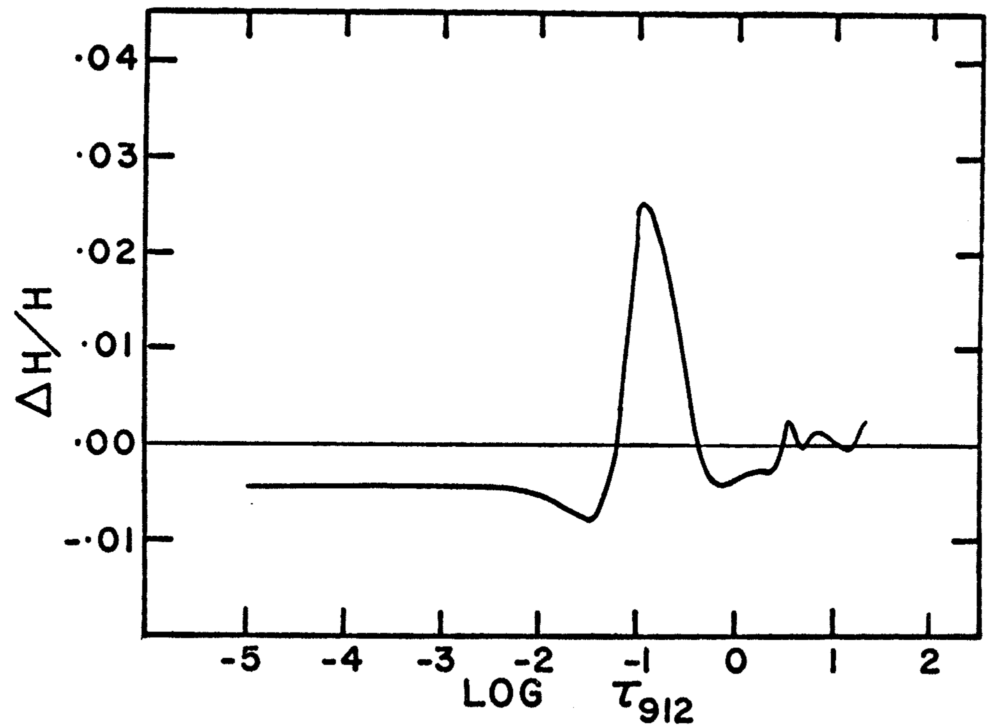

FIG. A-3 Flux error for model (43 000, 5.7, 0.6)

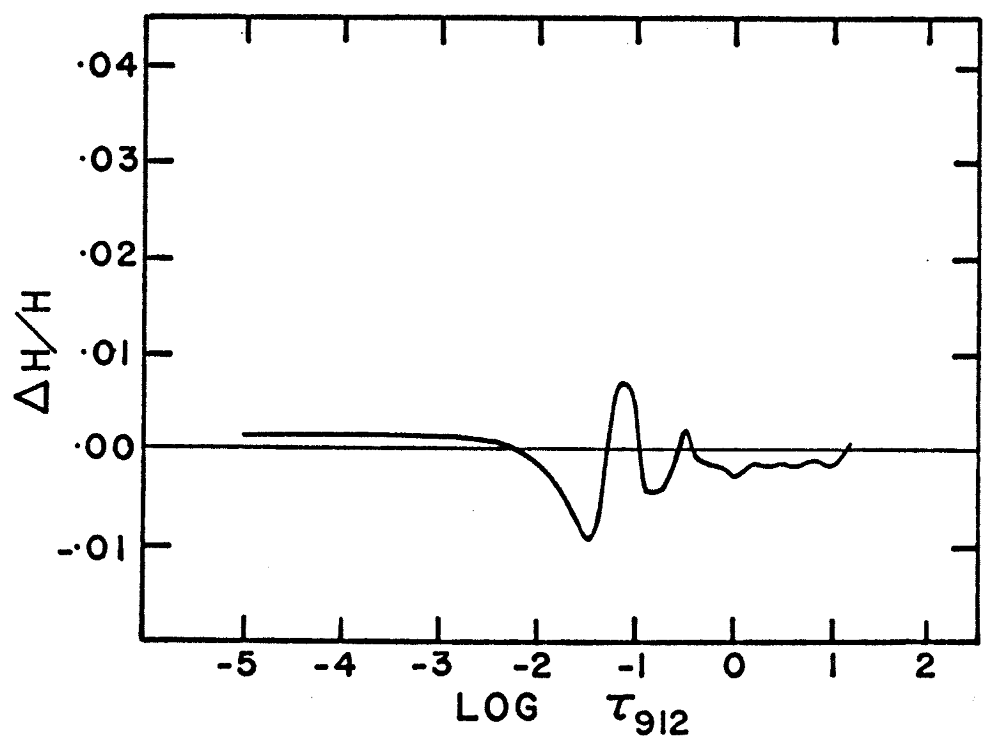

FIG. A-4 Flux error for model (43 000, 6.7, 0.9, M)

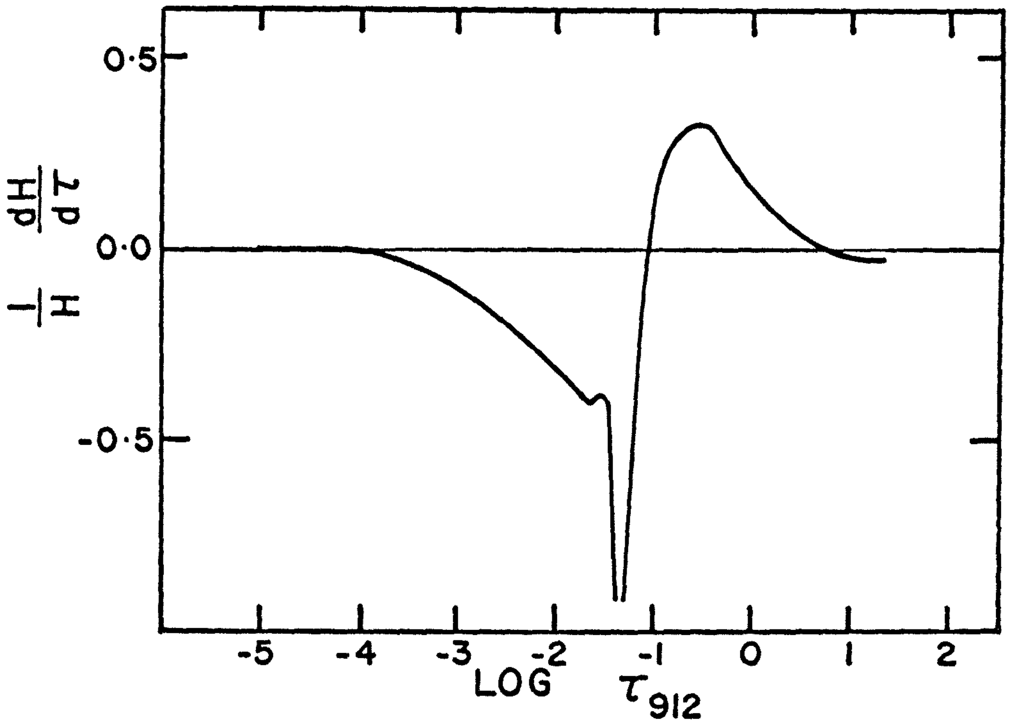

FIG. A-5 Flux derivative for (40 000, 5.7, 0.4)

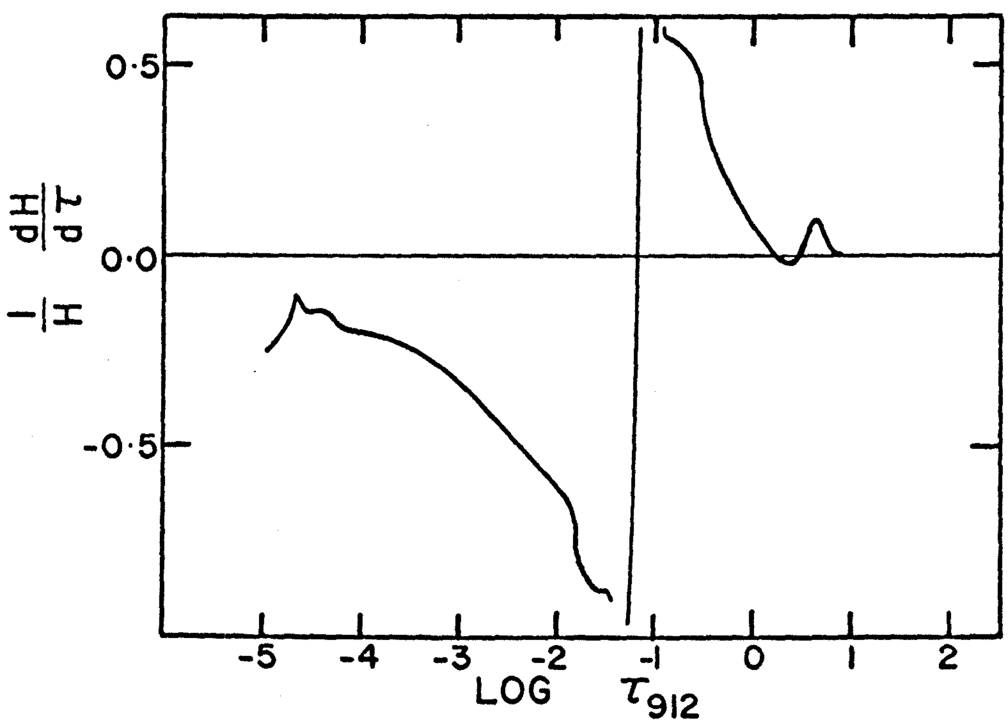

FIG. A-6 Flux derivative for (43 000, 6.7, 0.9)

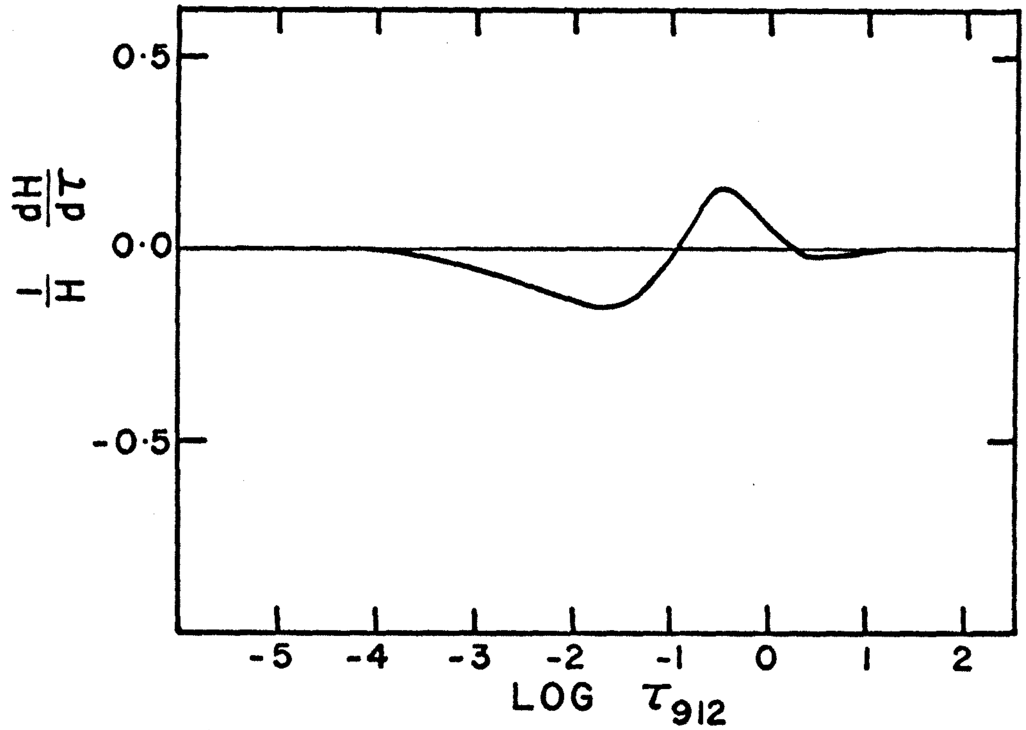

FIG. A-7 Flux derivative for (43 000, 5.7, 0.6)

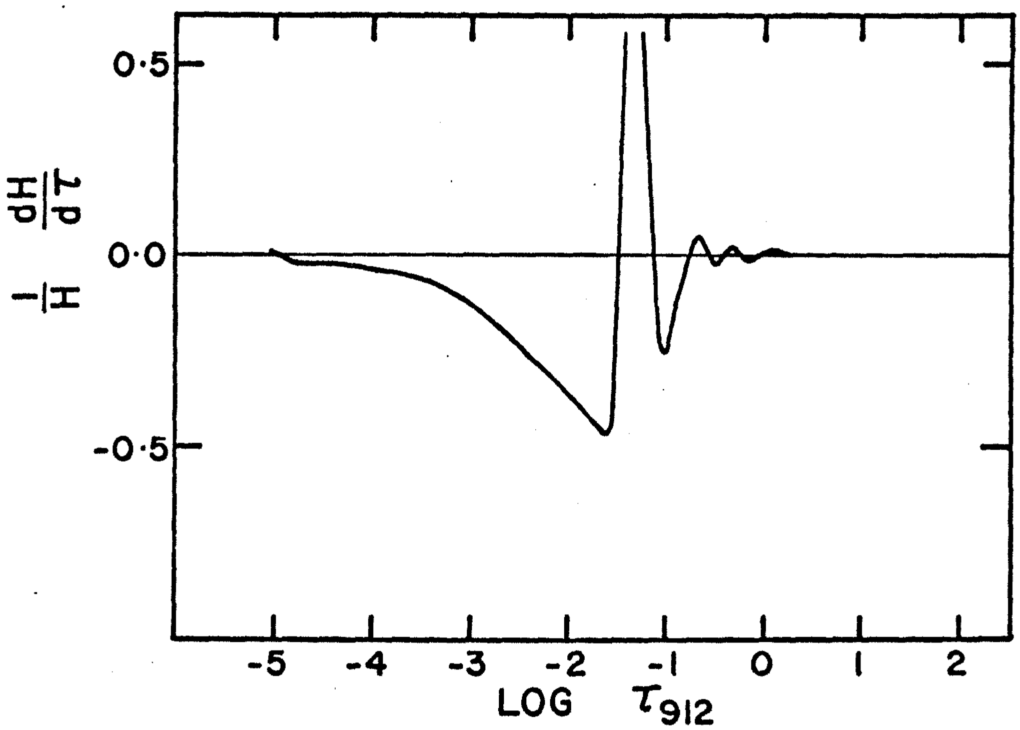

FIG. A-8 Flux derivative for (43 000, 6.7, 0.9, M)

REFERENCES

Allen, C. W. 1963, *Astrophysical Quantities*, (London: Athlone Press).

Aller, L. H. 1960, *Stellar Atmospheres*, ed. J. L. Greenstein (Chicago: U. of Chicago Press), p. 156.

Baschek, B., Holweger, H., and Traving, G. 1966, *Abhandl. Hamburger Sternw.*, **8**, 26: errata Peytremann et al. 1967, part E.

Backasten, K. 1955, *Ark. f. Fys.*, **9**, 457.

——————. 1956, *ibid.*, **10**, 567.

Börgstrom, A. 1968, *Ark. f. Fys.*, **38**, 243.

Caughlin, G. R. 1965, *Ap. J.*, **141**, 688.

Caughlin, G. R., and Fowler, W. A. 1962, *Ap. J.*, **136**, 453.

Cox, J. P., and Giuli, R. T. 1961, *Ap. J.*, **133**, 755.

Cox, J. P., and Salpeter, E. E. 1961, *Ap. J.*, **133**, 764.

Delhaye, J. 1965, *Galactic Structure*, ed. A. Blaauw and M. Schmidt (Chicago: U. of Chicago Press), p. 61.

Edmonds, F. N., Schlüter, H., and Wells, D. C. 1967, *Mem. R. A. S.*, **71**, 271.

Elvius, T., and Sinnerstad, U. 1958, *Ark. f. Astr.*, **2**, 189.

Eriksson, K. B. S. 1958, *Ark. f. Fys.*, **13**, 303.

Garz, T., and Kock, M. 1969, *Astron. and Astroph.*, **2**, 274.

Glad, S. 1954, *Ark. f. Fys.*, **7**, 7.

Glad, S. 1956, Ark. f. Fys., 10, 291.

Gould, N. L., Herbig, G. H., and Morgan, W. W. 1957, Pub. A. S. P., 69, 242.

Greenstein, J. L. 1968, Ap. J., 152, 431.

Greenstein, J. L. and Eggen, O. J. 1966, Vistas in Astronomy Vol. 8, ed. A. Beer (New York: Pergammon Press) p. 63.

Greenstein, J. L., and Münch, G. 1955, Carnegie Institution of Washington Yearbook, Vol. 54, 11.

————————. 1967, private communication.

Griem, H. R. 1962, Ap. J., 136, 422.

————————. 1964, Plasma Spectroscopy (New York: McGraw-Hill).

————————. 1967, Ap. J., 147, 1092.

————————. 1968, ibid., 154, 1111.

Griem, H. R., and Shen, K. Y. 1961, Phys. Rev., 122, 1490.

Hallin, R. 1966a, Ark. f. Fys., 32, 201.

————————. 1966b, ibid., 31, 511.

Hardorp, J., and Scholz, M. 1969, Ap. J. Suppl., to be published.

Iben, I. 1965, Ap. J., 142, 1447.

————————. 1966a, ibid., 143, 483.

————————. 1966b, ibid., p. 505

————————. 1966c, ibid., p. 516

————————. 1967, Science, 155, 785.

Isberg, B. 1968, Ark. f. Fys., 35, 551.

Jaschek, M., and Jaschek, C. 1963, Pub. A. S. P., 75, 365.

Kepple, P., and Griem, H. R. 1968, Phys. Rev., 173, 317.

Kurucz, R. L. 1969, Ap. J., 156, 235.

Lambert, D., and Warner, B. 1969, to be published.

Luyten, W. J., ed. 1964, First Conference on Faint Blue Stars (The Observatory, University of Minnesota), p. 122.

Messerschmidt, D., Scholz, M., and Traving G. 1967, Zs. f. Ap., 66, 246.

Mihalas, D. 1964, Ap. J., 140, 885.

Minnhagen, L. 1963 - 1964, Ark. f. Fys., 25, 203.

Moore, C. E. 1959, A Multiplet Table of Astrophysical Interest, Rev. ed., N. B. S. Technical Note 36 (Washington, D. C.: U. S. Gov't Printing Office).

__________. 1965, Selected Tables of Atomic Spectra - SiII, SiIII, SiIV, NSRDS-NBS 3, Sect. 1 (Washington, D. C.: U. S. Gov't Printing Office).

Münch, G. 1956, Carnegie Institution of Washington Yearbook Vol. 55, 41.

__________. 1958, Ap. J., 127, 642.

__________. 1968, Nebulae and Interstellar Matter, ed. B. M. Middlehurst and L. H. Aller (Chicago: U. of Chicago Press), p. 365.

Münch, G., and Slettebak, A. 1959, Ap. J., **129**, 852.

Oke, J. B. 1969, private communication.

Persson, W., and Minnhagen, L. 1968, Ark. f. Fys., **37**, 273.

Peterson, B. A. 1968, private communication.

Peterson, D. M. 1969, private communication.

Peytremann, E., Baschek, B., Holweger, H., and Traving, G. 1967, Un Programme Fortran d'Analyse Quantative de Spectres Stellaires, Observ., Genève.

Pfennig, H. 1966, Z. Naturforsch., **21a**, 1648.

Pfennig, H. and Trefftz, E. 1966, Z. Naturforsch., **21a**, 697.

Risberg, G. 1955, Ark. f. Fys., **9**, 483.

Sargent, W. L. W., and Searle, L. 1968, Ap. J., **152**, 443.

Scholz, M. 1967, Zs. f. Ap., **65**, 1.

―――――――. 1968, private communication.

Searle, L., and Rodgers, A. W. 1966, Ap. J., **143**, 809.

Smithsonian Astrophysical Observatory Star Catalog 1966, (Washington, D. C.: U. S. Gov't Printing Office).

Strom, S. E., and Avrett, E. H. 1964, Ap. J., **140**, 1381.

―――――――. 1965, Ap. J. Suppl., **12**, 1.

Sturch, C., and Wallerstein, G. 1962, Pub. A. S. P., **74**, 325.

Torresson, Y. G. 1960, Ark. f. Fys., **17**, 179.

―――――――. 1960 - 1961, ibid., **18**, 389.

Underhill, A. B. 1968, B. A. N., **19**, 500.

Wallerstein, G., and Spinrad, H. 1960, Pub. A. S. P., **72**, 486.

Wallerstein, G., Sturch, C., and Klemola, A. R. 1963, *Pub. A. S. P.*, **75**, 61.

Wallerstein, G., and Wolff, S. C. 1966, *Pub. A. S. P.*, **78**, 390.

Wiese, W. L., Smith, M. W. and Glennon, B. M. 1966, *Atomic Transition Probabilities, Hydrogen Through Neon*, NSRDS - NBS 4 (Washington, D. C.: U. S. Gov't Printing Office).

Wrubel, M. H. 1949, *Ap. J.*, **109**, 66.